Bulletin of the Geological Society of Denmark

VOLUME 60 | DECEMBER 2012 | COPENHAGEN

DGF

Bulletin of the Geological Society of Denmark

is published by the Geological Society of Denmark (DGF, Dansk Geologisk Forening), founded in 1893

The *Bulletin* publishes contributions of international interest in all fields of geological sciences, with a natural emphasis on results of new work on material from Denmark, the Faroes and Greenland. Contributions based on foreign material may also be submitted to the Bulletin in cases where the author is a member of the Society. The rate of publishing is one volume per year. All articles are published as pdf-files immediately after acceptance and technical production. A paper edition of each volume is issued at the end of the year and is circulated to libraries only.

Scientific editing and reviewing is done on unpaid collegial basis and technical production expenses are covered by the membership fees.

The bulletin is freely accessible on the web page of the Geological Society of Denmark: http://2dgf.dk/publikationer/bulletin/index.html.

Instructions to authors:

See inside the back cover and also: http://2dgf.dk/publikationer/bulletin/vejledning.html

Cover: The Faxe limestone quarry is a famous fossil-hunter locality which over the years has yielded thousands of well-preserved fossils from the coral and bryozoan mound complexes exposed there. Faxe has now given name to a new geological formation, the Faxe Formation (see this volume pp 47–60: Lauridsen, B.W., Bjerager, M. & Surlyk, F: The middle Danian Faxe Formation – new lithostratigraphic unit and a rare taphonomic window into the Danian of Denmark). A particular facies within the mounds is described as the Baunekule faces which presents exceptionally well-preserved fossils. However, the localities with the Baunekule facies have now all been quarried away. The picture shows the quarry in 2012, viewed from NW; the locality called 'Ravns næse', shown on p 50 in a photo from 1908, was located approximately between the two limestone heaps in the right background, and the locality 'Stationsvej' was situated about in the middle of the present lake in the right foreground. Photo: Jesper Milàn, Geomuseum Faxe.

The petrology and provenance of coal artifacts from Thule settlements in north-eastern Greenland

WOLFGANG KALKREUTH, CLAUS ANDREASEN, HENRIK I. PETERSEN & LARS STEMMERIK

Kalkreuth, W., Andreasen, C., Petersen, H.I. & Stemmerik, L., 2012. The petrology and provenance of coal artifacts from Thule settlements in north-eastern Greenland © 2012 by Bulletin of the Geological Society of Denmark, Vol. 60, pp. 1–13. ISSN 0011–6297. (www.2dgf.dk/publikationer/bulletin)

Coal petrographic techniques have been used to trace the origin of coal used to produce artifacts by the Thule people in north-eastern Greenland. The coal artifacts were collected from the north-east coast settlements between 76°55'–80°18'N and date back to the 15th century A.D. The petrographic data suggest that they have a common source, the Middle Jurassic coals outcropping south of 75°15' in north-eastern Greenland. It is thus evident that the Thule people used local material rather than bringing the coal from the known "mines" in Arctic Canada. It also implies that contemporaneous Thule people groups along the east coast of Greenland were in contact and traded.

Received 3 May 2010
Accepted in revised form
7 December 2011
Published online
24 February 2012

Keywords: coal artifacts, coal petrology, Thule Culture, north-eastern Greenland

Wolfgang Kalkreuth [wolfgang.kalkreuth@ufrgs.br], Universidade Federal do Rio Grande do Sul, Porto Alegre, Brazil. Claus Andreasen [claus.andreasen47@gmail.com], Greenland National Museum and Archives, P.O. Box 145, DK-3900 Nuuk, Greenland. Henrik I. Petersen [hip@geus.dk], Geological Survey of Denmark and Greenland, Øster Voldgade 10, DK-1350 Copenhagen K, Denmark. Lars Stemmerik [Lars.Stemmerik@snm.ku.dk], Department of Geography and Geology, University of Copenhagen, Øster Voldgade 10, DK-1350 Copenhagen K, Denmark (Presently Natural History Museum of Denmark, Øster Voldgade 5-7, DK-1350 Copenhagen K, Denmark).

Coal petrographic techniques have over the past years successfully been used to identify the provenance of coal artifacts excavated by archaeologists. Teichmüller (1992) studied coal ornaments from Roman and Celtic grave sites and was able to trace some of the materials to sources in southern Germany, Bohemia and the Czech Republic. Smith (1996, 1997) studied coal relics collected from Roman sites in Britain and found that nearly all the specimens originated from the nearest outcrops of coal seams.

In the Canadian Arctic, Alaska and Greenland, coal artifacts are occasionally found in excavated winter house ruins from the Thule culture period (McCullough 1989; Steffian 1992; Kalkreuth *et al*. 1993), representing an early phase of Inuit occupation. Previous examinations of coal artifacts from the Bache Peninsula region of eastern Ellesmere Island and Axel Heiberg Island in Arctic Canada, including the analysis of beads and a possible labret (lip piercing piece), showed that the artifacts consisted of a variety of coal and organic-rich shale types (lignite, boghead coal, cannel shale), some of which could be traced to nearby outcrops (Kalkreuth *et al*. 1993; Kalkreuth & Sutherland 1998). Boghead coal appears to have been particularly suitable for making delicate ornaments and carvings; however, the origin of the boghead coal used for some of the coal artifacts from Ellesmere Island and Axel Heiberg Island is still uncertain.

The Thule culture came to Greenland from the northern part of the Bering Strait. The timing of the arrival is heavily debated and ranges from the early 12th century A.D. to the late 13th century A.D. (McCullough 1989; McGhee 2000; Schledermann & McCullough 2003; Friesen & Arnold 2008; Jensen 2009). They settled in the Thule area in northwest Greenland and later some Thule culture groups migrated eastwards to north-eastern Greenland while others moved southward along the west coast of Greenland (Fig. 1). The migration into north-eastern Greenland went along the north coast and south into J.P. Koch Fjord and eastwards through Wandel Dal and Midsommersøer in southern Peary Land (Fig. 2; Grønnow & Jensen 2003). Migration must have been fast since there are no winter houses known between Hall Land (ca. 81°N/60°W) and Amdrup Land (Fig. 2), where the northernmost winter houses on the northeast coast of

Greenland occur (Grønnow & Jensen 2003). The Thule people settled and established a small-scale whale-hunting society at the Northeast Water Polynia, which offered access to marine hunting of whales, walrus, narwhale and seals with some possibilities of hunting musk ox and caribou. Six to seven settlements are known around the polynia (Andreasen 1997), but so far only few excavations have been undertaken. The migration continued southwards along the east coast, where we see many settlements in the Dove Bugt area (Grønnow & Jensen 2003) and from ca. A.D.1400 there was also substantial settlement at and around Clavering Ø (Sørensen 2010).

When the migrants came to north-eastern Greenland they brought along tools, clothes and raw material from the Thule area. Objects of coal are not known from the Thule area. In north-eastern Greenland, large pieces of coal have recently been found at three North-east Water sites: Sophus Müller Næs, Eskimonæs, and the southern of the small islands Henrik Krøyer Holme (Fig. 2). Farther south, in Dove Bugt, objects of coal are known from the large Rypefjeldet site (Fig. 2), and in addition a few very small coal pieces were excavated by members of the Danmarks Ekspeditionen in 1906–08 (Thostrup 1911): L3059 from Grave 321 at Stormbugt Øst, L3060 from Snenæs House, and seven beads, L3064, from grave 529 at Rypefjeldet (Thomsen 1917), and later two beads were found in ruin group II, house 2 at Dødemandsbugten on Clavering Ø (Larsen 1934).

The present study focuses on the petrographic examination of five coal artifacts collected from Thule settlements in north-eastern Greenland (Fig. 2), believed to date back to the 15th century A.D. The results are compared with existing data from coal seams outcropping in north-eastern Greenland in order to determine if these coal seams may be the sources for the artifacts.

Table 1. Information on sample location, sample identification, and sample type

Location	Coordinates		Sample id.	Sample type
Eskimonæs, Holm Land	80°25´11˝N	15°41´21˝W	KNK 2071x1	coal, female figurine
Henrik Krøyer Holme	80°36´23˝N	13°58´19˝W	KNK 2073x47	coal, preform to a figurine
Henrik Krøyer Holme	80°36´23˝N	13°58´19˝W	KNK 2073x52	lump of coal
Sophus Müller Næs, Amdrup Land	*c.* 80°47´N	*c.* 14°10´W	L1 5696	coal, drop-like shape (amulet?)
Rypefjeldet, Dove Bugt	*c.* 76°11´N	*c.* 20°20´W	L1 5794	lump of coal

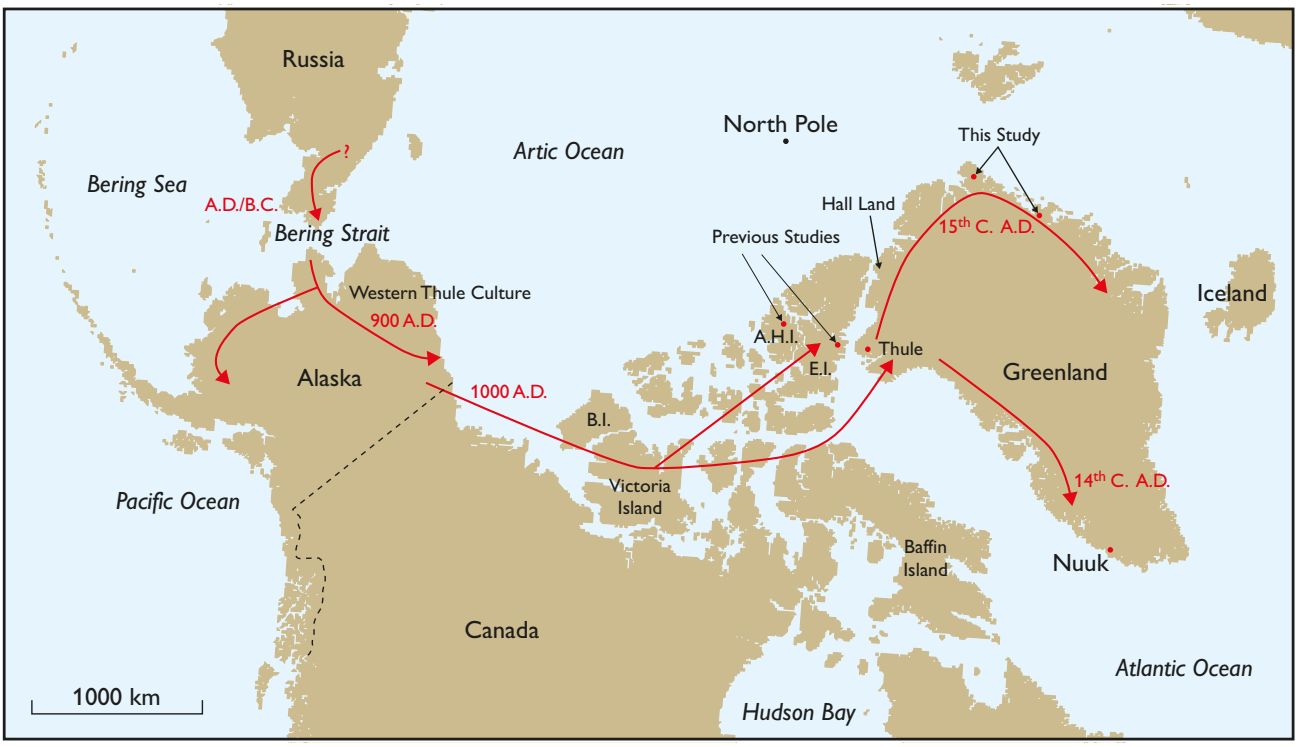

Fig. 1. Map showing migration routes of the early Thule Culture and the locations of previous and the present coal artifact studies. See text for discussion of migration. B.I.= Banks Island, E.I.= Ellesmere Island, A.H.I.= Axel Heiberg Island.

Sampling, sample preparation and analytical methods

Sampling

The coal artifacts examined in this study all come from north-eastern Greenland (Fig.2; Table 1).

Sample KNK 2071x1 was found on the surface at Eskimonæs on Holm Land (Fig. 2) in 1996 and most likely represents the same settlement phase as the excavated features, i.e. around A.D. 1400 (Andreasen 1997). Coal artifacts KNK 2073x47 and KNK 2073x52 were collected in 1993 as surface samples from Henrik Krøyer Holme (Fig. 2). Material from this location has not been dated, but it is, however, most likely that they have the same age as the material found at Eskimonæs. Coal artifact L1 5696 was excavated in a house ruin at Sophus Müller Næs, Amdrup Land (Grønnow & Jensen 2003), whereas coal artifact L1 5794 was collected much farther to the south at Rypefjeldet, Dove Bugt (Fig. 2).

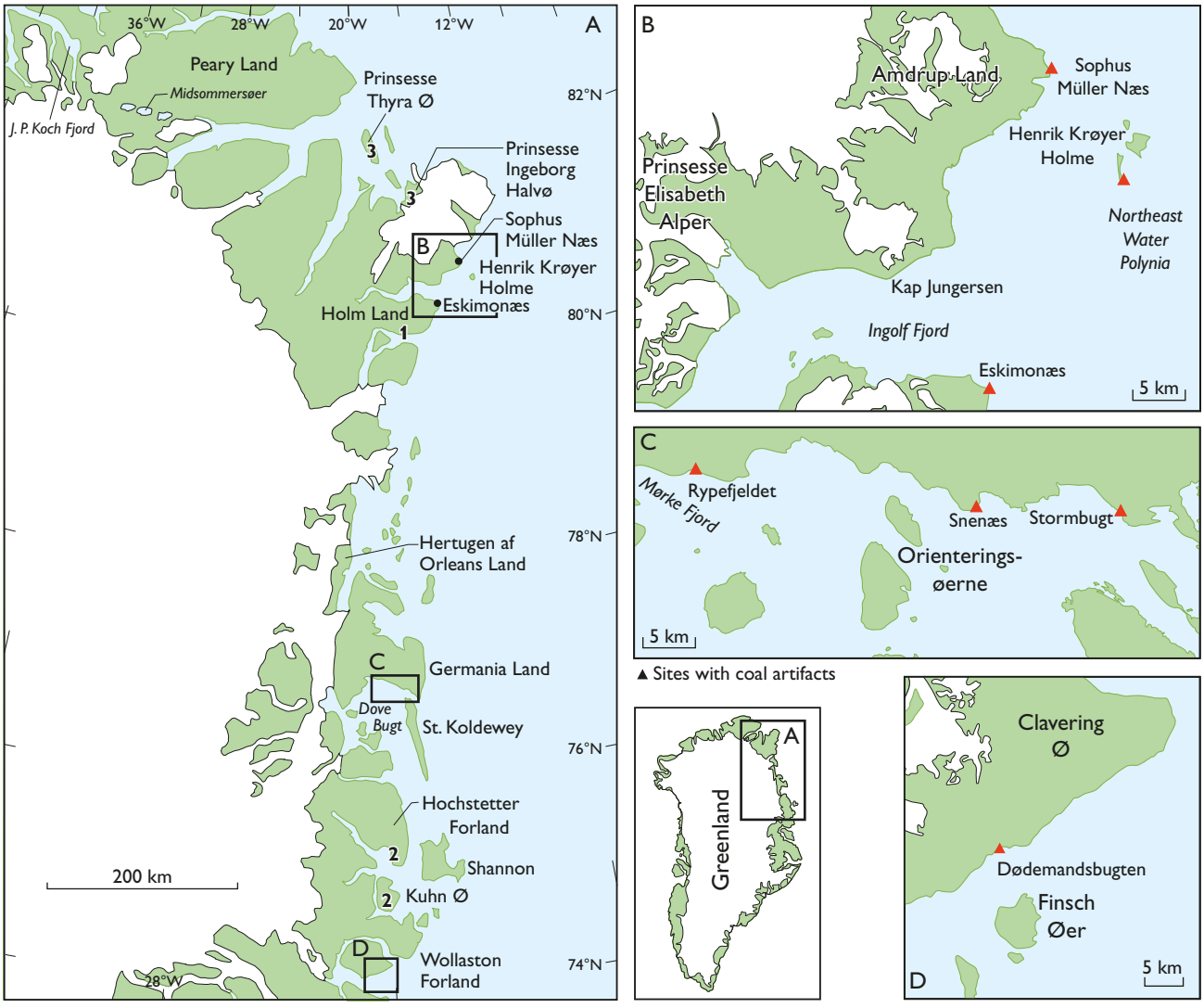

Fig. 2. Maps of north-eastern Greenland. The coal artifacts were collected at Eskimonæs (KNK2071x1), Henrik Krøyer Holme (KNK 2073x47, KNK 2073x52), Sophus Müller Næs, (L1 5696) and at Rypefjeldet, Dove Bugt (L1 5794). Numbers in A indicate outcrops of coal-bearing strata: (1) in the Lower Carboniferous Sortebakker Formation on southern Holm Land, (2) in the Middle Jurassic Muslingebjerg Formation at Hochstetter Forland and Kuhn Ø - erratic blocks of the Middle Jurassic Muslingebjerg Formation are known also from Germania Land and Hertugen af Orleans Land -, and (3) in the Palaeogene (?) Thyra Ø Formation on Prinsesse Thyra Ø and on Prinsesse Ingeborg Halvø.

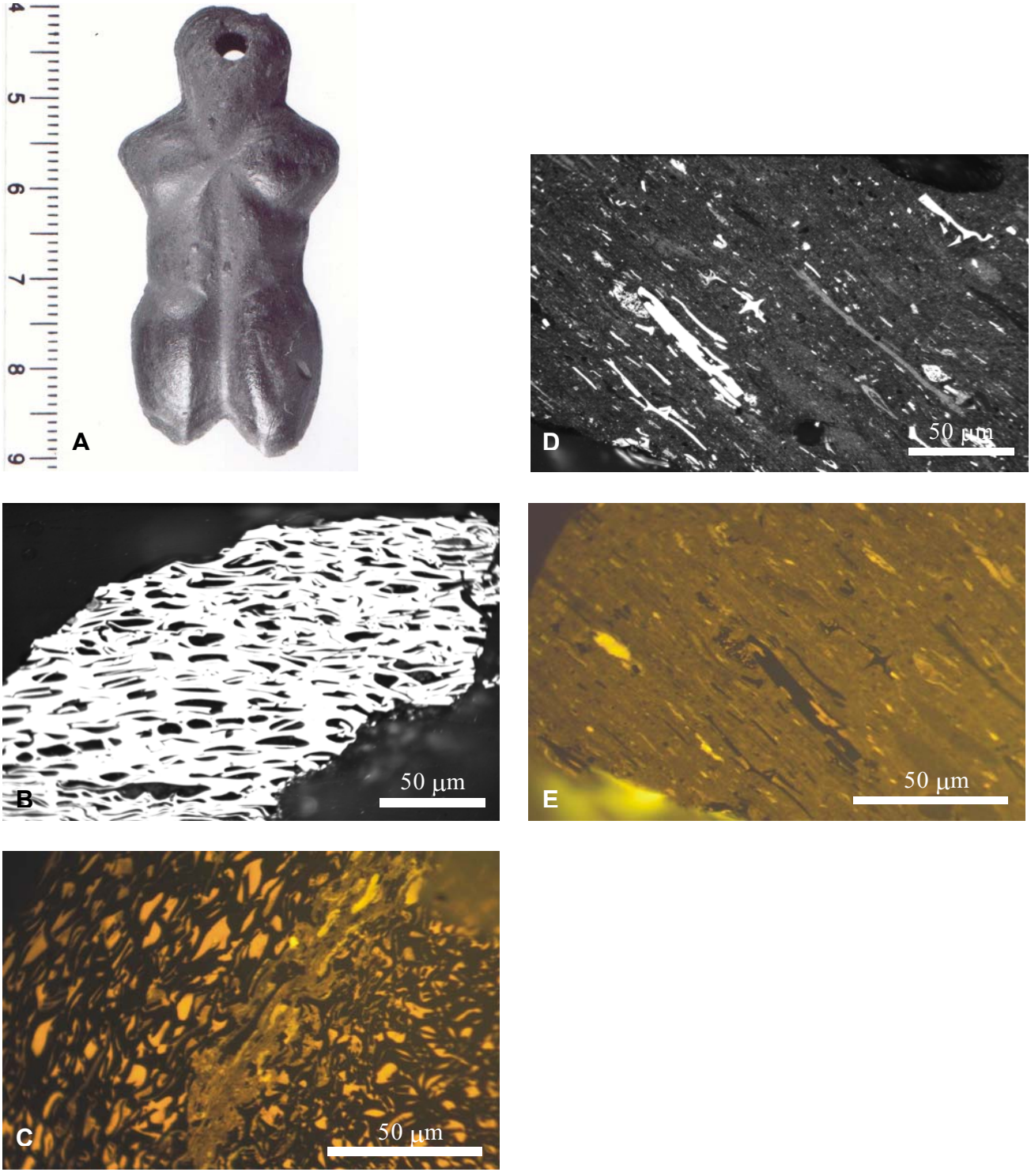

Fig. 3. **A**, coal artifact KNK 2071x1, Eskimonæs, Holm Land. Specimen has been carved in the shape of a female figurine. For details see text. **B–E**, photomicrographs in oil immersion of coal artifact KNK 2071x1; B and D shown in white reflected light, C and E shown in fluorescence-inducing blue light illumination. **B,** fusinite with well-preserved botanical cell-structure. **C**, yellowish fluorescing exsudatinite filling cell lumen of fusinite. Centre of image shows fluorescing groundmass associated with sporinite. **D,** fine-grained clay mineral matrix associated with inertodetrinite. **E**, fluorescing groundmass associated with sporinite and non-fluorescing inertinite.

Sample preparation and analytical methods

Due to the precious nature of the coal artifacts, sample material was obtained by carefully scraping small fragments off the original specimen. The material was mounted in epoxy resin, and grinding and polishing procedures were applied as routinely used for coal and other organic material (Bustin *et al*. 1989).

Analytical methods applied include microscopical examination of the sample material in reflected white- and fluorescence-inducing blue light to study the petrographic characteristics using the nomenclature of the International Committee for Coal and Organic Petrology (ICCP) (1963, 1971, 1998, 2001). Vitrinite (huminite) reflectances were measured in random mode to determine the thermal maturity (rank) of the organic material by standard petrographic routines (Bustin *et al*. 1989).

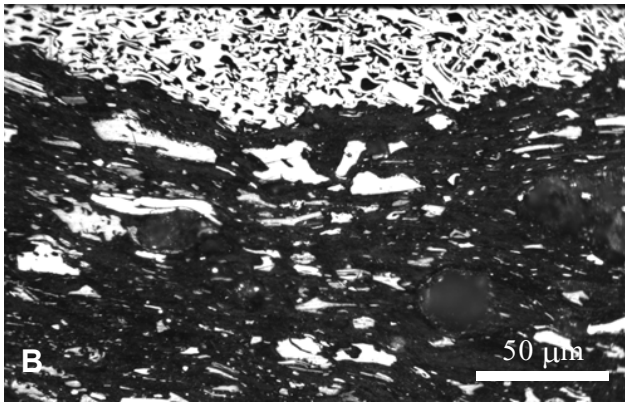

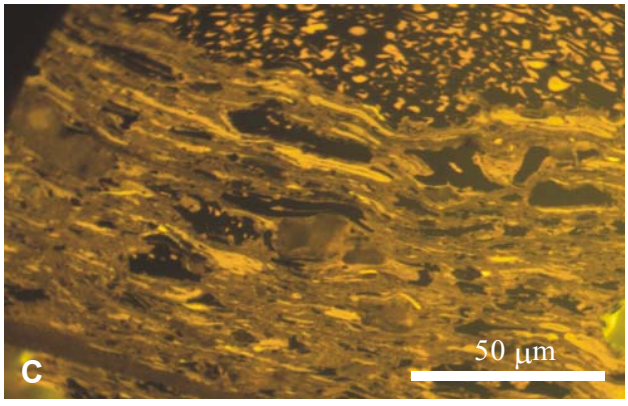

Results

Petrographic analyses

Coal artifact KNK 2071x1

This artifact is a polished piece of stratified coal that has been carved in the shape of a female figurine (Fig. 3A), measuring 50×25×10 mm.

Petrograhic analysis shows the predominance of fusinite and sporinite macerals associated with a fluorescing groundmass of clay minerals. The fusinite particles are characterized by a well-preserved botanical cell-structure (Fig. 3B). When applying blue-light excitation it becomes apparent that almost all open cell luminae of the fusinite particles are filled with yellowish fluorescing exsudatinite (Fig. 3C). Sporinite macerals are enriched in the fluorescing groundmass (Fig. 3D, E).

Vitrinite (huminite) reflectance measurements (Table 2) indicate a mean value of 0.31 $\%R_{random}$. In terms of coal rank this corresponds to lignite.

Fig. 4. **A**, coal artifact KNK 2073x47, Henrik Krøyer Holme. Specimen has been carved and may present a preform to a figurine. For details see text. **B** and **C**, photomicrographs in oil immersion of coal artifact KNK 2073x47; B shown in white reflected light, C shown in fluorescence-inducing blue light illumination. **B,** fusinite showing typical "Bogen" structure (top of image) and mineral matrix (clay minerals and quartz) associated with inertodetrinite in centre and lower part of image. **C**, yellowish fluorescing exsudatinite filing cell lumen of fusinite associated with fluorescing groundmass enriched in sporinite.

Coal artifact KNK 2073x47
This artifact is a piece of stratified coal that has been carved and may represent a pre-form to a figurine (Fig. 4A), measuring 40×20×10 mm.

Petrographic analysis in white light shows the predominance of fusinite and inertodetrinite macerals associated with clay minerals and quartz (Fig. 4B). Blue light excitation shows enrichment of sporinite in the fluorescing groundmass (Fig. 4C), and exsudatinite filling the cell lumen of fusinite.

Vitrinite reflectance measurements indicate a mean value of 0.40 $\%R_{random}$ (Table 2), corresponding to subbituminous rank.

Coal artifact KNK 2073x52
This artifact is a piece of stratified coal (Fig. 5A), measuring 70×50×20 mm. One plane parallel to bedding has macroscopically identifiable remnants of fusain. Fusain is principally considered to be derived from forest fires (Scott 1989; Scott & Jones 1994) near or at the site of organic matter accumulation. Microscopic analysis in white light shows the predominance of fusinite and inertodetrinite macerals (Fig. 5B) associated with quartz and clay minerals. Blue light excitation shows exsudatinite filling the cell lumen of fusinite (Fig. 5C) and enrichment of sporinite in the fluorescing groundmass (Fig. 5D).

Vitrinite (huminite) reflectance measurements indicate the existence of two reflectance populations (Table 2), with means of 0.29 and 0.53 $\%R_{random}$ respectively. These values correspond to a rank of lignite and subbituminous A, respectively.

Coal artifact L1 5696
This artifact is a piece of polished coal that has been carved into a drop-like shape, possibly representing an amulet (Fig. 6A), measuring 35×20×10 mm.

Petrographic analysis shows that the organic matter is dominated by sporinite and vitrinite macerals (Fig. 6B, C). Inertinite macerals as shown in Fig. 6B are rare.

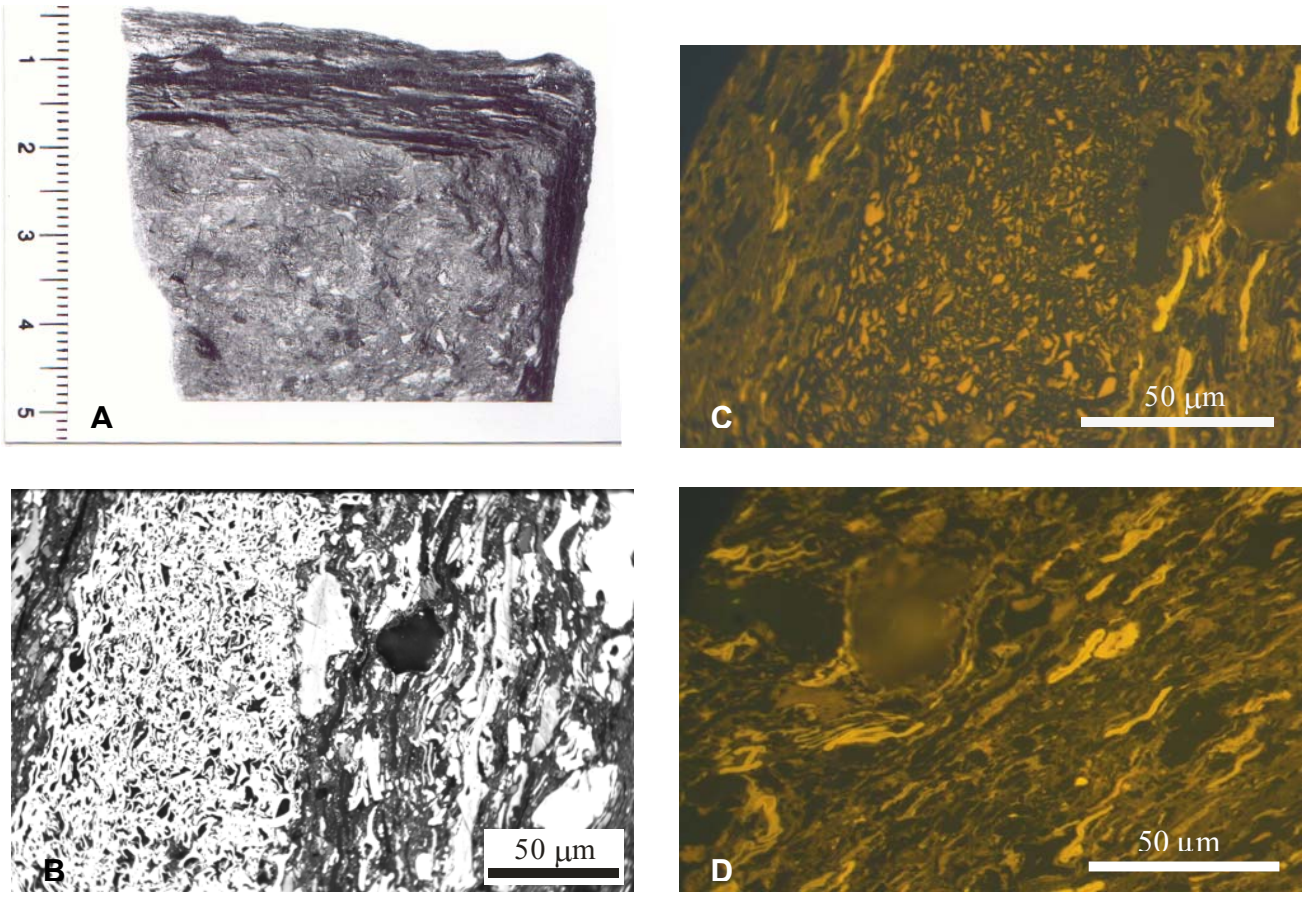

Fig. 5. **A**, coal artifact KNK 2073x52, Henrik Krøyer Holme. Specimen represents a lump of coal, for details see text. **B–D**, photomicrographs in oil immersion of coal artifact KNK 2073x52; B shown in white reflected light, C and D shown in fluorescence-inducing blue light illumination. **B**, enrichment of fusinite and inertodetrinite macerals with sporinite (dark elongated stringers). **C**, yellowish fluorescing exsudatinite filling cell lumen of fusinite (centre of image) associated with fluorescing groundmass containing brightly fluorescing sporinite. **D**, fluorescing groundmass showing enrichment of sporinite.

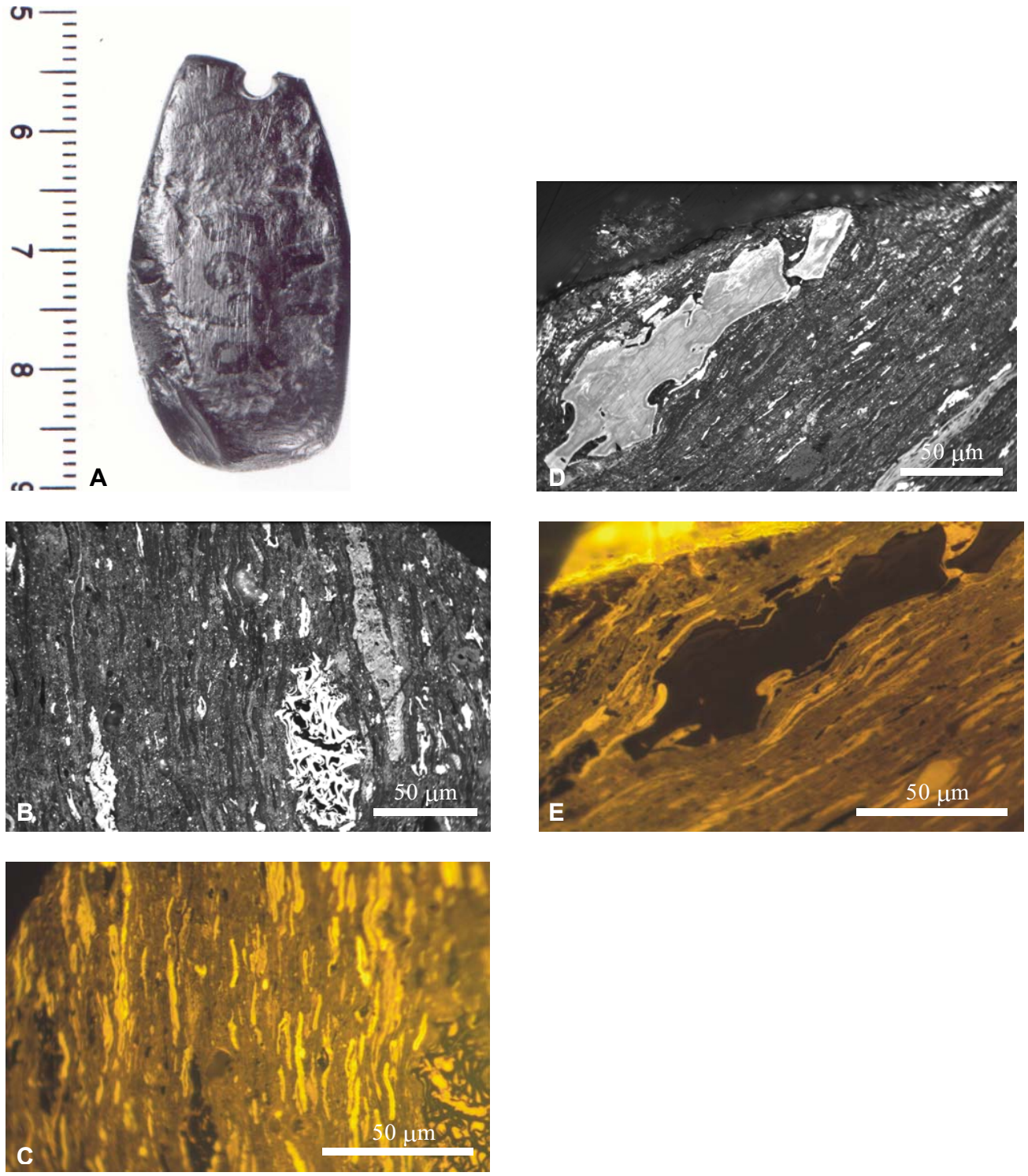

Fig. 6. **A**, coal artifact L1 5696, Sophus Müllers Næs, Amdrup Land. This piece has been carved into a drop-like shape and possibly represents an amulet; for details see text. **B–E**, photomicrographs in oil immersion of coal artifact L1 5696. B and D shown in white reflected light, C and E shown in fluorescence-inducing blue light illumination. **B**, fine-grained mineral matrix with inclusions of fusinite, inertidetrinite, vitrinite and sporinite (elongated dark stringers). **C**, fluorescing groundmass with abundant occurrences of strongly fluorescing sporinite. Exsudatinite fills cell lumen of fusinite (right base of image). **D**, relict of fish bone/tooth (?) associated with fine grained mineral matrix containing inertodetrinite and sporinite (dark elongated stringers). **E**, fish bone/tooth (?) in fluorescing matrix associated with abundant sporinite.


A

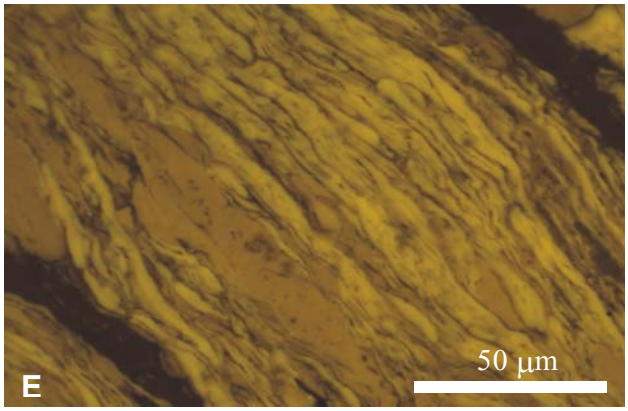
50 µm
E

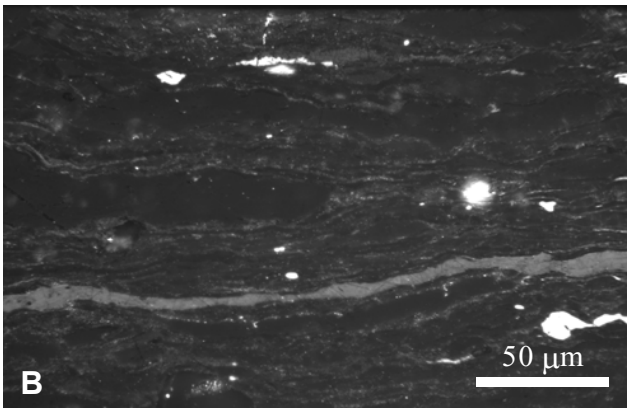
50 µm
B

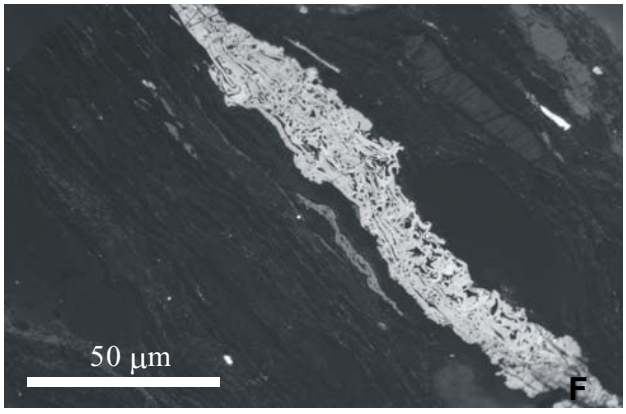
50 µm
F

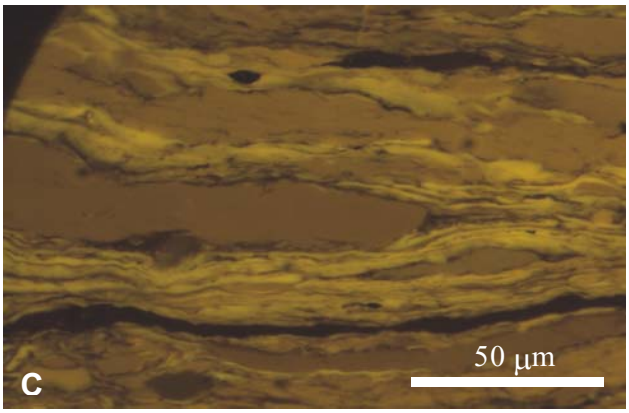
50 µm
C

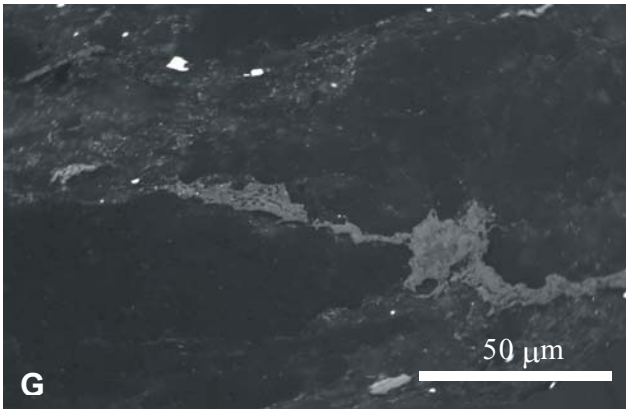
50 µm
G

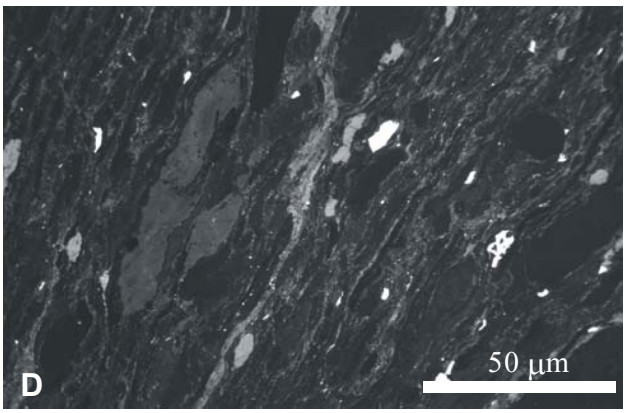
50 µm
D

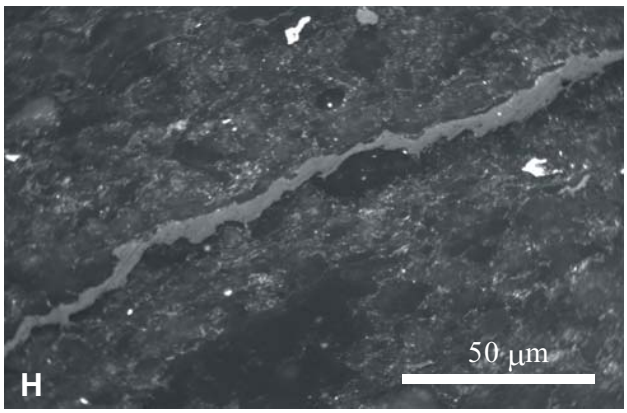
50 µm
H

Table 2. Summary of petrographical characteristics of the coal artifacts

Sample id.	Comments on petrographic composition	$\%R_{random}$	Std.	N
KNK 2071x1	fluorescing groundmass, rich in sporinite, fusinite, exsudatinite filling cell lumen of fusinite	0.31	0.02, 0.08	14, 6
KNK 2073x47	fluorescing groundmass, rich in sporinite and inertinite with exsudatinite in cell lumens of fusinite	0.40	0.03	5
KNK 2073x52	fluorescing groundmass, rich in liptinite and inertinite with exsudatinite in cell lumens of fusinite	0.29, 0.53	0.03, 0.12	6, 8
L1 5696	rich in liptinite (sporinite) and vitrinite, rare inertinite, fragment of fish bone/tooth (?) associated with sporinite	0.33	0.03	10
L1 5794	extremely rich in liptinite (resinite, cutinite, liptodetrinite), rare inertinite	0.25	0.03	20

$\%R_{random}$: mean random vitrinite reflectance
Std.: standard deviation
N: number of measurements

Figure 6D and 6E show sporinite macerals associated with a large fragment of fish bone (?).

The mean vitrinite (huminite) reflectance value is 0.33 $\%R_{random}$ (Table 2), corresponding to a rank of lignite.

Coal artifact L1 5794

This artifact is a piece of coal of irregular shape, measuring 50×50×25 mm (Fig. 7A).

Petrographic analysis shows that the sample is enriched in liptinite macerals. The most abundant component is resinite (Fig. 7B, C, D, E), followed by sporinite and cutinite. Inertinite macerals such as fusinite (Fig. 7F) are rare, whereas the vitrinite content is moderate (Figs 7F and 7G). Petrographic characteristics of this specimen also include the occurrence of vitrinized (?) medium gray elongated stringers with morphological characteristics of sporinite or cutinite (Fig. 7H).

The mean value of vitrinite (huminite) reflectance is 0.25 $\%R_{random}$ (Table 2), corresponding to a rank of lignite.

Summary of the petrographic characteristics of the coal artifacts

From a coal petrographic point of view the artifacts form two distinct groups:

The first group consists of samples collected at Eskimonæs (KNK 2071x1) and Henrik Krøyer Holme (KNK 2073x47 and KNK 2073x52). These artifacts are all characterized by the relative high amounts of inertinite (fusinite, inertodetrinite) associated with sporinite. Typically the open spaces of fusinite particles are filled with exsudatinite, considered to be a secondary maceral (Teichmüller 1974a,b; Kalkreuth & Macauley 1987), believed to be formed during the bituminization process, filling pores and fractures in coal. The high amount of exsudatinite observed in the coal artifacts from Greenland is, however, rather unusual. Macroscopic similarities such as stratification, dimensions and thicknesses of the specimens as well as very similar petrographic characteristics suggest that coal artifact KNK 2073x52 and the carved coal artifact KNK 2073x47 were derived from the same coal piece.

The second group of samples consists of the artifacts collected at Sophus Müller Næs (L1 5696) and Rypefjeldet (L1 5794), which are characterized by the dominance of sporinite and resinite respectively, whereas inertinite macerals are rare.

The vitrinite (huminite) reflectances determined in the coal artifacts range from 0.25 to 0.53 $\%R_{random}$, corresponding to coal ranks ranging from lignite to high volatile A bituminous coal. However, all specimen are enriched in liptinite macerals, and it is well known that vitrinite reflectances may be considerably lowered by the presence of liptinite macerals (Kalkreuth 1982; Petersen & Vosgerau 1999), and may thus not indicate the 'true' level of coal rank.

◀ Fig. 7. **A**, coal artifact L1 5794, Rypefjeldet, Dove Bugt. This specimen is an irregular coal lump; for details see text. **B**–**F**, photomicrographs in oil immersion of coal artifact L1 5794. B, D and F–H shown in white reflected light, C and E shown in fluorescence-inducing blue light illumination. **B**, vitrinite stringer associated with liptinite (resinite, liptodetrinite). **C**, large bodies of brownish-orange fluorescing resinite associated with cutinite and sporinite macerals. **D**, vitrinite and inertodetrinite associated with resinite and cutinite. **E**, enrichment of yellowish fluorescing cutinite and resinite. **F**, occurrence of rare fusinite with well-preserved botanical cell-structure associated with sporinite and resinite. **G**, vitrinite associated with resinite. **H**, elongated medium grey particle with morphological characteristics typical of sporinite or cutinite (vitrinized ?).

Coal occurrences in north-eastern Greenland

Palaeogene, Middle Jurassic and Lower Carboniferous coal-bearing strata are exposed in localised areas along the coast in north-eastern Greenland from Kuhn Ø at ~74°43'N, 20°15'W to Prinsesse Thyra Ø at 82°05'N, 19°16'W (Fig. 2). The Middle Jurassic coals have been thoroughly investigated by the Geological Survey of Denmark and Greenland, whereas the knowledge about the Lower Carboniferous and Palaeogene coals is less detailed.

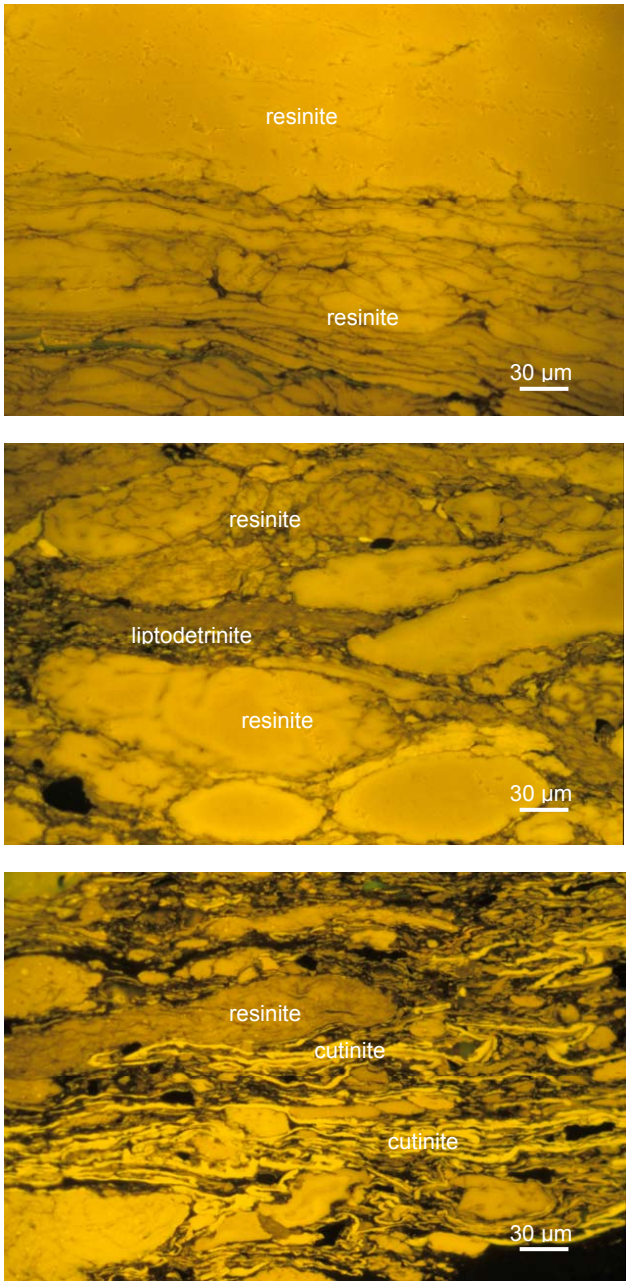

Fig. 8. Photomicrographs of liptinite-rich coals from the Muslingebjerg Formation at Payer Dal, Kuhn Ø. The coals are extraordinarily rich in resinite, but also cutinite and liptodetrinite (reflected light microscopy, blue light excitation).

Palaeogene coal occurrences

Palaeogene coal occurs in the Upper Paleocene to ?lowermost Eocene Thyra Ø Formation at Prinsesse Thyra Ø and Prinsesse Ingeborg Halvø (Fig. 2) in the vicinity of Station Nord (~81°30'–82°05'N, 16°48'–19°16'W; Lyck & Stemmerik 2000). The formation consists of interbedded fine-grained sandstones, siltstones and coal, but generally the formation is poorly exposed with most information provided by isolated outcrops along rivers on southern Prinsesse Thyra Ø and Prinsesse Ingeborg Halvø. A coal from the Thyra Ø Formation is characterised by a dominance of huminite, some liptinite and minor amounts of inertinite. The liptinite appears mainly to be composed of liptodetrinite, sporinite and thin cutinite, whereas resinite is largely absent. The vitrinite reflectance is 0.51 $\%R_{random}$, corresponding to subbituminous A rank.

Middle Jurassic coal occurrences

Middle Jurassic coal beds of the Muslingebjerg Formation are known from outcrops on Kuhn Ø and the southern coast of Hochstetter Forland in north-eastern Greenland (~74°43'–75°14'N, 20°00'–20°15'W), and erratic blocks are known farther north from Germania Land to Hertugen af Orleans Land at *c.* 78°N, 21°W (Fig. 2). Vitrinite reflectance values of 0.49–0.53 $\%R_{random}$ show that the coals are of subbituminous A rank (Petersen & Vosgerau 1999). In Bastian Dal on Kuhn Ø, the Muslingebjerg Formation is up to 11 m thick and contains three 1–2 m thick coal beds interbedded with fluvial sediments (Alsgaard *et al*. 2003). The coals are mineral-poor and on a mineral matter free basis (mmf) composed of 42–98 vol.% huminite, 2–55 vol.% inertinite and 0–31 vol.% liptinite, although the majority contain less than 7 vol.% liptinite (Petersen *et al*. 2002). In Payer Dal on Kuhn Ø samples from a 15 cm thick coal bed are dominated by liptinite (Fig. 8). On a mineral matter free basis these coals contain 53–87 vol.% liptinite, which principally is composed of resinite (32–70 vol.%, mmf) followed by liptodetrinite and cutinite (Petersen & Vosgerau 1999). The composition is comparable to that of the dull coal facies in the Muslingebjerg Formation in the coastal cliff at Kulhus, Hochstetter Forland approximately 40–50 km north of Kuhn Ø (Fig. 2). At Kulhus, the coal-bearing succession is *c.* 20 m thick. Due to faulting the succession is repeated along the coast. It consists of a sandstone-dominated 'shoreface facies association' and a 'coastal plain facies association' containing silt- and sandstones and four coal beds of which only

three, 1.15–3.45 m thick, are exposed (Clemmensen & Surlyk 1976; Bojesen-Koefoed *et al*. 1996; Petersen *et al*. 1998). Each coal bed consists of three coal facies (dulling-upward) cycles recording increasing flooding of the precursor mires and thus repeated outpacing of peat formation by the rising water table. The dull coals towards the top of the coal beds are extraordinarily enriched in liptinite, particularly resinite, due to selectively removal of huminitic organic matter during flooding (Petersen *et al*. 1998). They contain (mmf) generally 35–60 vol.% huminite, less than 20 vol.% inertinite, and more than 35 vol.% liptinite. The liptinite is dominated by resinite, up to more than 50 vol.% (mmf) of the maceral composition, followed by liptodetrinite and cutinite. The bright and banded coals, characteristic of the lower and middle parts of the coal facies cycles, consist generally of more than 60 vol.% huminite, less than 20% vol.% inertinite and less than 30 vol.% liptinite on a mineral matter free basis.

The liptinite-enriched coals from both Kulhus and Payer Dal have strongly suppressed vitrinite reflectance values, yielding reflectances down to 0.30 $\%R_{random}$ corresponding to reflectance suppression of up to 0.23 $\%R_{random}$ (Petersen & Vosgerau 1999).

Lower Carboniferous coal occurrences

Coal beds occur in the non-marine Lower Carboniferous Sortebakker Formation at Sortebakker, southern Holm Land (~80°09'N, 17°44'W; Fig. 2) (Dalhoff *et al*. 2000). The formation is estimated to be about 1 km thick and is mainly composed of fluvial sediments forming stacked fining-upward cycles of sandstones and shales (Dalhoff & Stemmerik 2000). The coal occurs in mud-dominated coal and coaly shale beds, usually <1 m thick. Sparse rootlets have been observed and the coal is described as black to brownish (Dalhoff & Stemmerik 2000). A coal sample from the Sortebakker Formation has a T_{max} value of 572°C, corresponding to a vitrinite reflectance of above 3 $\%R_{random}$ and thus anthracite rank. This high thermal maturity agrees with the assumption that the Sortebakker Formation was exhumed and that up to 2 km of sediments have been removed by erosion.

Discussion: origin of the coal artifacts

Palaeogene coal source ?

The Palaeogene coals exposed at Prinsesse Thyra Ø and Prinsesse Ingeborg Halvø (Fig. 2) occur relatively close to the artifacts collected at Eskimonæs and Henrik Krøyer Holme (KNK 2071x1, KNK 2073x47, KNK 2073x52) and could potentially be the source for the artifacts. Although the vitrinite reflectance reported for the Palaeogene coals (0.51 $\%R_{random}$) is comparable to the reflectance (0.53 $\%R_{random}$) from coal artifact KNK 2073x52, the maceral composition of the Palaeogene coal is dominated by huminite macerals, and the coal does not show the fluorescing groundmass, abundance of inertinite and exsudatinite as observed in coal artifact KNK 2073x52 and in the other artifacts. It appears unlikely that the Palaeogene coals were the source for the artifacts.

Middle Jurassic coal source ?

The petrographic composition and the vitrinite reflectance values of the liptinite-enriched dull coal layers from Kulhus on Hochstetter Forland and Payer Dal on Kuhn Ø (Petersen *et al*. 1998; Petersen & Vosgerau 1999) are comparable to that of the coal artifact L1 5794 collected at Rypefjeldet, Dove Bugt. Petrographically, sample L1 5794 is essentially composed of resinite, cutinite and liptodetrinite, with rare occurrences of vitrinite and inertinite (Fig. 7), which is strikingly similar to the liptinite composition (Fig. 8) of the dull coal layers from Kulhus and Payer Dal (Petersen & Vosgerau 1999). Coal with liptinite-enriched maceral composition and extraordinary amounts of resinite and exsudatinite is highly unusual, not only in Greenland but also elsewhere around the world, suggesting that coal artifact L1 5794 could have been collected from Middle Jurassic coals at Kulhus, Payer Dal or perhaps at other outcrops in north-eastern Greenland. In addition, the vitrinite reflectance of 0.25 $\%R_{random}$ obtained from coal artifact L1 5794 is close to the suppressed values reported for the liptinite-enriched coal layers at Kulhus and Payer Dal, which are also located relatively close to Rypefjeldet, Dove Bugt, where coal artifact L1 5794 was found. However, there need not have been any visits at all to the outcrops. Loose blocks of liptinite-rich coals such as those found at Kulhus and Payer Dal have been reported far from the outcrops, for instance in Germania Land and on Store Koldewey (Bojesen-Koefoed *et al*. 1996). These loose blocks may represent particularly robust parts of coals suited for carving, and such coal pieces will naturally catch the eye in a region otherwise dominated by basement rocks.

The coals from Bastian Dal, Payer Dal and Kulhus can also be rather rich in inertinite and/or sporinite, which may agree with the abundant inertinite macerals (fusinite, inertinite) and sporinite observed in the coal artifacts (KNK 2071x1, KNK 2073x47, KNK 2073x52 and L1 5696). This group of coal artifacts is characterized by depressed vitrinite reflectances typical for liptinite rich coals as they have been reported

for the Middle Jurassic coals in north-eastern Greenland (Bojesen-Koefoed *et al*. 1996; Petersen *et al*. 1998; Petersen & Vosgerau 1999).

Considering the above discussion it is suggested that the coal artifacts have a common source in the Middle Jurassic coals in north-eastern Greenland.

Lower Carboniferous coal source ?

Lower Carboniferous coals from the Sortebakker Formation are anthracites, and because of this they are excluded as the source of the coal artifacts, since these are all characterized by significantly lower rank levels.

Conclusions

Based on petrographic characteristics it is evident that the coal outcropping closest to the Thule settlements around the Northeast Water Polynia, the Palaeogene coal at Prinsesse Thyra Ø and Prinsesse Ingeborg Halvø and the Carboniferous coal at southern Holm Land, are unlikely as a source for the coal artifacts. The investigated Thule culture coal artifacts are suggested to have a common source which is the Middle Jurassic coals found at Kulhus, Hochstetter Forland, on Kuhn Ø, and as loose blocks other places in north-eastern Greenland (Fig. 2). There are some Thule settlements in this area, but the main settlements are to the east and south on Shannon, Clavering Ø and Wollaston Forland (Sørensen 2010). The Thule people migrated from the north down the east coast of Greenland, so the presence of Jurassic coal from south of 75°15'N in the settlements at Dove Bugt and the Northeast Water Polynia (located between 76°55'N and 80°18'N) suggests that a group of people might have been moving northwards again from the 'coal area' or that contemporaneous groups in the north and south were in contact and traded. If the coal was collected from Middle Jurassic coal beds in north-eastern Greenland, this study presents the first indication that a local raw material in north-eastern Greenland was moved by Thule people from south to north against the main migration direction in prehistoric time. Alternatively, loose blocks found farther north were the source of the artifacts. In either case, the more precise nature of this movement of material and/or carvings or ideas in north-eastern Greenland in the 15th century A.D. remains to be explored in an archaeological context.

Acknowledgements

The authors thank J.A. Bojesen-Koefoed (GEUS) and an anonymous reviewer for their constructive comments on an earlier version of the article. J. Halskov (GEUS) is thanked for figure drafting.

References

Alsgaard, P.C., Felt, V.L., Vosgerau, H. & Surlyk, F. 2003: The Jurassic of Kuhn Ø, North-East Greenland. In: Ineson, J.R. & Surlyk, F. (eds), The Jurassic of Denmark and Greenland. Geological Survey of Denmark and Greenland Bulletin 1, 865–892.

Andreasen, C. 1997: The prehistory of the coastal areas of Amdrup Land and Holm Land adjacent to the Northeast Water Polynya: an archaeological perspective. Journal of Marine Systems 10, 41–46.

Bojesen-Koefoed, J.A., Christiansen, F.G., Petersen, H.I., Piasecki, S., Stemmerik, L. & Nytoft, H.P. 1996: Resinite-rich coals of northeast Greenland – a hitherto unrecognized, highly oil-prone Jurassic source rock. Bulletin of Canadian Petroleum Geology 44, 458–473.

Bustin, R., Cameron, A., Grieve, D. & Kalkreuth, W. 1989: Coal petrology - Its principles, methods and applications. Geological Association of Canada, Short Course Notes, Volume 3, 3rd edition, 278 pp.

Clemmensen, L.B. & Surlyk, F. 1976: Upper Jurassic coal-bearing shoreline deposits, Hochstetter Forland, East Greenland. Sedimentary Geology 15, 193–211.

Dalhoff, F. & Stemmerik, L. 2000: Depositional history of the fluvial Lower Carboniferous Sortebakker Formation, Wandel Sea Basin, eastern North Greenland. Geology of Greenland Survey Bulletin 187, 65–77.

Dalhoff, F., Vigran, J.O. & Stemmerik, L. 2000: Stratigraphy and palynology of the Lower Carboniferous Sortebakker Formation, Wandel Sea Basin, eastern North Greenland. Geology of Greenland Survey Bulletin 187, 51–63.

Friesen, T.M. & Arnold, C.D. 2008: The timing of the Thule migration: new dates from the western Canadian Arctic. American Antiquity 73, 527–538.

Grønnow, B. & Jensen, J.F. 2003: The northernmost ruins of the Globe. Eigil Knuth's archaeological investigations in Peary Land and adjacent areas of high arctic Greenland. Meddelelser om Grønland, Man & Society 29, 403 pp. København.

ICCP 1963: International Committee for Coal and Organic Petrology. International handbook of coal petrography. Centre National de la Recherche Scientifique, Paris.

ICCP 1971: International Committee for Coal and Organic Petrology. International handbook of coal petrography, 1st supplement to 2nd edition. Centre National de la Recherche Scientifique, Paris.

ICCP 1998: International Committee for Coal and Organic

Petrology. The new vitrinite classification (ICCP System 1994). Fuel 77, 349–358.

ICCP 2001: International Committee for Coal and Organic Petrology. The new inertinite classification (ICCP System 1994). Fuel 80, 459–471.

Jensen, A.M. 2009: Radiocarbon dates from recent excavations at Nuvuk, Point Barrow, Alaska, and their implications for neoeskimo prehistory. In: Grønnow, B (ed.), On the track of the Thule Culture from Bering Strait to East Greenland. Proceedings of the SILA Conference "The Thule Culture – New Perspectives in Inuit Prehistory." Publications from the National Museum. Studies in Archaeology & History 15, 45–62. Copenhagen.

Kalkreuth, W. 1982: Rank and petrographic composition of selected Jurassic–Lower Cretaceous coals of British Columbia, Canada. Bulletin of Canadian Petroleum Geology 30, 112–139.

Kalkreuth, W. & Macauley, G. 1987: Organic petrology and geochemical (Rock Eval) studies on oil shales and coals from the Pictou and Antigonish areas, Nova Scotia, Canada. Bulletin of Canadian Petroleum Geology 35, 263–295.

Kalkreuth, W., McCullough, K. & Richardson, R. 1993: Geological, archaeological and historical occurrences of coal, east-central Ellesmere Island, Arctic Canada. Arctic and Alpine Research 25, 277–307.

Kalkreuth, W. & Sutherland, P. 1998: The archeology and petrology of coal artifacts from a Thule settlement on Axel Heiberg Island, Arctic Canada. Arctic 51, 345–349.

Larsen, H. 1934: Dødemandsbugten. An Eskimo settlement on Clavering Island. Meddelelser om Grønland 102(1), 186 pp.

Lyck, J.M. & Stemmerik, L. 2000: Palynology and depositional history of the Paleocene? Thyra Ø Formation, Wandel Sea Basin, eastern North Greenland. Geology of Greenland Survey Bulletin 187, 21–49.

McCullough, K. 1989: The ruin islanders – early Thule Culture pioneers in the eastern high Arctic. Archaeological Survey of Canada, Mercury Series Paper 141, Canadian Museum of Civilization, 347 pp.

McGhee, R. 2000: Radiocarbon dating and the timing of the Thule migration. Identities and cultural contacts in the Arctic. Proceedings of a Conference at the Danish National Museum, Copenhagen. The Danish National Museum and Danish Polar Center 2000, 181–191.

Petersen, H.I. & Vosgerau, H. 1999: Composition and organic maturity of Middle Jurassic coals, North-East Greenland: evidence for liptinite-induced suppression of huminite reflectance. International Journal of Coal Geology 41, 257–274.

Petersen, H.I., Bojesen-Koefoed, J.A., Nytoft, H.P., Surlyk, F., Therkelsen, J. & Vosgerau, H. 1998: Relative sea-level changes recorded by paralic liptinite-enriched coal facies cycles, Middle Jurassic Muslingebjerg Formation, Hochstetter Forland, Northeast Greenland. International Journal of Coal Geology 36, 1–30.

Petersen, H.I., Bojesen-Koefoed, J.A. & Nytoft, H.P. 2002: Source rock evaluation of Middle Jurassic coals, northeast Greenland, by artificial maturation: aspects of petroleum generation from coal. American Association of Petroleum Geologists Bulletin 86, 233–256.

Schledermann, P. & McCullough K.M. 2003: Late Thule Culture developments on the central east coast of Ellesmere Island. Danish Polar Center Publication 12, 203 pp. Copenhagen.

Scott, A.C. 1989: Observations on the nature and origin of fusain. International Journal of Coal Geology 12, 443–475.

Scott, A.C. & Jones, T. 1994: The nature and influence of fire in Carboniferous ecosystems. Palaeogeography, Palaeoclimatology, Palaeoecology 106, 91–112.

Smith, A.H. 1996: Provenance of coals from Roman sites in U.K. Counties bordering River Severn and its estuary and including Wiltshire. Journal of Archaeological Science 23, 373–389 .

Smith, A.H. 1997: Provenance of coals from Roman sites in England and Wales. Britannia, XXVIII, 297–324.

Sørensen, M. 2010: Inuit landscape use and responses to climate change in the Wollaston Forland – Clavering Ø region, Northeast Greenland. Danish Journal of Geography 110, 155–174.

Steffian, A. 1992: Archaeological coal in the Gulf of Alaska: A view from Kodiak Island. Arctic Anthropology 29, 111–129.

Teichmüller, M. 1974a: Entstehung und Veränderung bituminöser Substanzen in Kohlen in Beziehung zur Entstehung und Umwandlung des Erdöls. Fortschritte in der Geologie von Rheinland und Westfalen 24, 65–112.

Teichmüller, M. 1974b: Über neue Macerale der Liptinitgruppe und die Entstehung von Micrinit. Fortschritte in der Geologie von Rheinland und Westfalen 24, 37–64.

Teichmüller, M. 1992: Organic petrology in the service of archaeology. International Journal of Coal Geology 20, 1–21.

Thomsen Th. 1917: Implements and artefacts of the North-East Greenlanders. Finds from graves and settlements. Meddelelser om Grønland 44(5), 357–496.

Thostrup, C. B. 1911: Ethnographic description of the Eskimo settlements and stone remains in North-East Greenland. Meddelelser om Grønland 44(4), 177–355.

Rare finds of the coiled cephalopod *Discoceras* from the Upper Ordovician of Bornholm, Denmark

JAN AUDUN RASMUSSEN & FINN SURLYK

Rasmussen, J.A. & Surlyk, F. 2012. Rare finds of the coiled cephalopod Discoceras from the Upper Ordovician of Bornholm, Denmark. © 2012 by Bulletin of the Geological Society of Denmark, Vol. 60, pp. 15–22. ISSN 0011–6297 (www.2dgf.dk/publikationer/bulletin).

Coiled nautiloid cephalopods of the genus *Discoceras* are locally common in the Middle and Upper Ordovician of Baltica, for example in the Oslo Graben, but are exceedingly rare in contemporaneous strata from the Danish island of Bornholm. The two new species of *Discoceras* described here, *D. costatum* n. sp. and *D. vasegaardense* n. sp., occur in shales of the Upper Ordovician Lindegård Formation. The nautiloids are preserved as external molds in laminated siliciclastic mudstones. The very rare occurrence of cephalopods, combined with the apparently endemic nature of the *Discoceras* fauna, may be explained by the location of Bornholm distally on the Baltoscandian shelf combined with the influence of relatively cold ocean currents from the adjacent Rheic Ocean.

Received 29 June 2011
Accepted in revised form
17 January 2012
Published online
20 March 2012

Keywords: Nautiloid cephalopod, *Discoceras*, Lindegård Formation, Upper Ordovician, Bornholm, Denmark.

Jan Audun Rasmussen [janr@snm.ku.dk], Natural History Museum of Denmark, University of Copenhagen, Øster Voldgade 5–7, DK-1350 Copenhagen K, Denmark.
Finn Surlyk [finns@geo.ku.dk], Department of Geography and Geology, University of Copenhagen, Øster Voldgade 10, DK-1350 Copenhagen K, Denmark.

Coiled nautiloid cephalopods are exceptionally rare in the Lower Palaeozoic shales of the island of Bornholm, Denmark, located in the Baltic Sea south of Sweden. They have not been described or figured earlier, but the tarphycerid genus *Discoceras* was noted to occur within the Upper Ordovician Lindegård Formation, formerly referred to as the *Tretaspis* shale (C. Poulsen 1964; V. Poulsen 1966). In contrast they are relatively common in the Middle and Upper Ordovician of Baltica, for example in the Oslo Graben in Norway and in Estonia (e.g. Sweet 1958). A loose specimen here referred to the genus *Discoceras* was recently found on the beach at Sose Bugt east of Sose Odde on the south coast of Bornholm (Fig. 1). Together with two coiled nautiloids from the collections in the Natural History Museum of Denmark (SNM) it makes up a total of three specimens of coiled nautiloids from the Upper Ordovician succession of Denmark known so far. Slabs of the lower Upper Ordovician *Dicellograptus* shale are very common on the beach at Sose Bugt and contain abundant specimens of diplograptid graptolites. Pieces of the upper Upper Ordovician Lindegård Formation occur as well, but less commonly. Most likely, the major part of the Lindegård Formation slabs originates from the area between Sose Bugt and the rivulet Øleå some 10 km towards the southeast. The aim of this paper is to describe the tarphycerid nautiloids from Bornholm and to place them into the context of other finds of *Discoceras* from correlative successions elsewhere on Baltica.

Stratigraphy

The Upper Ordovician succession of Bornholm comprises the *c.* 21 m thick *Dicellograptus* shale (Pedersen 1989; Schovsbo *et al.* 2011) and the overlying more than 20 m thick Lindegård Formation (Pedersen 1989, fig. 12), the latter unit including the Jerrestad Formation and Tommarp Mudstone of Pedersen (1989) (Fig. 2). The *Dicellograptus* shale consists of black and dark grey, organic-rich, graptolite-bearing laminated mudstone usually showing a distinct shaly parting (Pedersen 1989), whereas the Lindegård Formation typically consists of more massive, grey or brownish

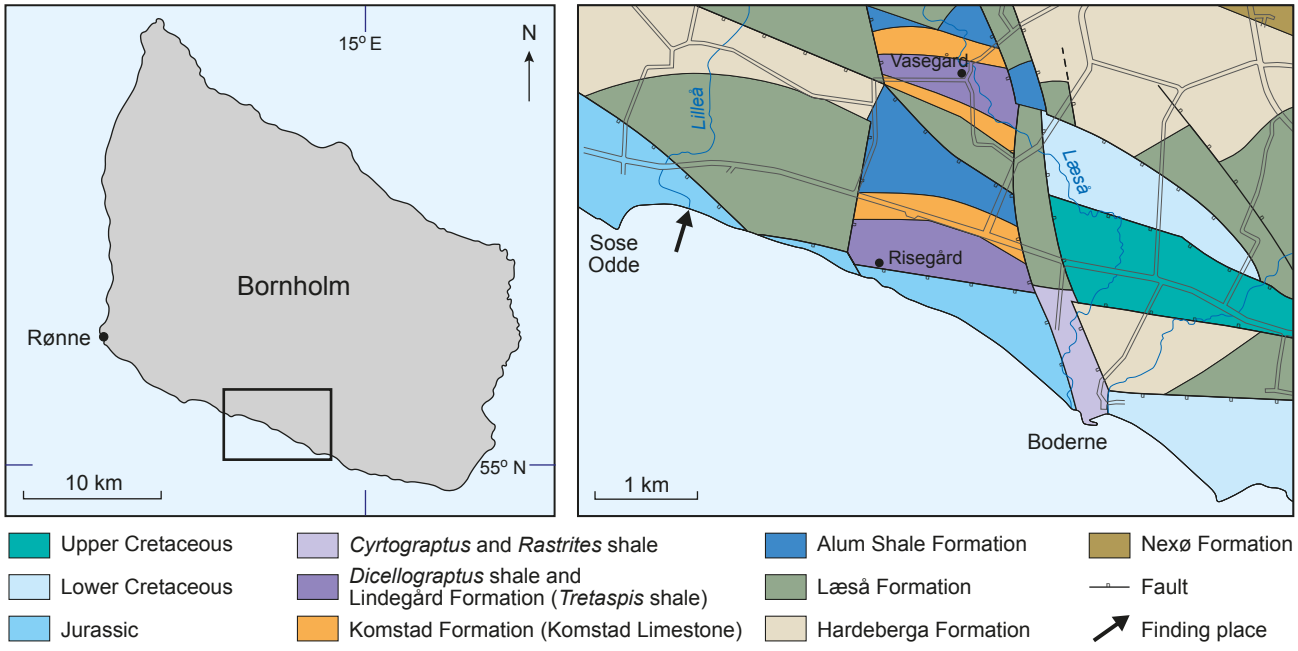

Fig. 1. Geological sketch map showing the two Bornholm localities where *Discoceras vasegaardense* n. sp. and *D. costatum* n. sp. were found. The arrow east of Sose Odde indicates where the *D. vasegaardense* n. sp. specimen (MGUH 29286) from Sose Bugt was found loose on the beach. *D. costatum* n. sp. (MGUH 29285) and most likely also the holotype of *D. vasegaardense* (MGUH 29287) were collected next to Vasegård (also spelled Vasegaard). The map is modified from H. Gry after Poulsen (1969), including the lithostratigraphic revisions by Nielsen & Schovsbo (2007).

mudstone and occasionally siltstone containing a benthic fauna, including trilobites and brachiopods (Ravn 1899; Kielan 1959).

The *Dicellograptus* shale has been correlated with parts of the Sularp, Skagen, Mossen and Fjäcka Formations in Sweden (e.g. Bergström *et al*. 1999; Pålsson 2001), but these subdivisions cannot easily be recognised on Bornholm. Accordingly, the old, informal name is maintained here, awaiting a lithostratigraphical revision of the unit. The upper 10 m of the *Dicellograptus* shale of Bornholm crops out at the Læså and Risebæk rivulets, where it comprises the *Diplograptus foliaceus*, *Dicranograptus clingani* and *Pleurograptus linearis* graptolite zones (Bruvo & Nielsen 2004). At the Risebæk locality, which is situated next to the farm Risegård (Fig. 1), conodonts from a limestone nodule 3 m below the top of the *Dicellograptus* shale belong to the upper part of the *Amorphognathus superbus* conodont Zone (Stouge & Rasmussen 1996). The overlying Lindegård Formation, established by Glimberg (1961) in Skåne, Sweden, corresponds to the *Trinucleus* shale (Gry 1948; C. Poulsen 1936), the *Tretaspis* shale (V. Poulsen 1966, 1968, 1969), and the Jerrestad Formation and Tommarp Mudstone (Bergström 1982; Pedersen 1989; Schovsbo *et al*. 2011). The lowermost part of the Lindegård Formation correlates with the Upper Ordovician *Dicellograptus complanatus* graptolite Zone and the overlying part includes the Upper Ordovician *Staurocephalus clavifrons*, *Eodindymene pulchra*, *Dalmanitina olini*, *Dalmanitina mucronata* and *Brongniartella platynota* trilobite zones (V. Poulsen 1966), which correlate with the *Dicellograptus anceps*, *Normalograptus extraordinarius* and *N. persculptus* graptolite zones (see Chen *et al*. 2006).

Chronostratigraphy			Graptolite zones	Litho-stratigraphy Bornholm
System	Global stages	British Series		
Bergström *et al*. (2009)			Chen *et al*. (2006) Bruvo & Nielsen (2004)	Schovsbo *et al*. (2011)
Upper Ordovician	Hirnantian	Ashgill	*N. persculptus*	Lindegård Fm.
			N. extraordinarius	
	Katian		*D. anceps*	
			D. complanatus	
		Caradoc	*P. linearis*	*Dicellograptus* shale
			D. clingani	
	Sandbian		*D. foliaceus*	
			N. gracilis	

Fig. 2. Stratigraphy of the Upper Ordovician strata from the island of Bornholm, Denmark. Grey filling represents depositional hiatus.

Two of the three nautiloid-bearing shale samples contain additional benthic fossils. A brachiopod belonging to the superfamily Plectambonitoidea of the order Strophomenida was observed in the shale slab containing cephalopod specimen MGUH 29286 (determined by David A.T. Harper, 2011), whereas the slab containing specimen MGUH 29287 shows two imprints of the trilobite *Tretaspis* (determined by Arne T. Nielsen, 2011). These findings together with the lithological characteristics of the three slabs indicate that they all originate from the Lindegård Formation rather than the *Dicellograptus* shale.

Palaeobiogeographic significance

The two new species of *Discoceras* from Bornholm are not known with certainty from other regions. *Discoceras antiquissimum*, which resembles *D. costatum* n. sp. is known from several Baltoscandian localities, including the Upper Ordovician Nabala, Vormsi and Pirgu Stages (formerly "Lyckholm-Stufe") of northern Estonia (Eichwald 1842; Teichert 1930) and the Upper Ordovician Husbergøya Formation (formerly 5a) of the Oslo Region, Norway (Strand 1933). In addition it has been described from probably Upper Ordovician erratic boulders of Zawidowice, southern Poland (Roemer 1861; Dzik 1984).

Discoceras vasegaardense n. sp. is similar to, but not identical with, a Darriwilian to lower Sandbian species of *Discoceras*, which commonly has been named *Discoceras arcuatum* (Lossen), but this name is regarded as a *nomen nudum* herein (see Systematic palaeontology below). "*D. arcuatum*" is known from the uppermost part of the Elnes Formation in the Oslo Region, Norway (Lossen 1860; Sweet 1958). Hence, the two Bornholm species are undoubtedly related to relatively shallow water species of *Discoceras* that are common in more proximal parts of the Baltic platform, but are different from these at the species level.

The very rare occurrence and the apparently endemic nature of the Late Ordovician *Discoceras* fauna from Bornholm may probably be explained by the distal shelf palaeoenvironment on the southern margin of Baltica combined with influence of temperate to boreal ocean currents from the adjacent Rheic Ocean (Dzik 1983; Christiansen & Stouge 1999).

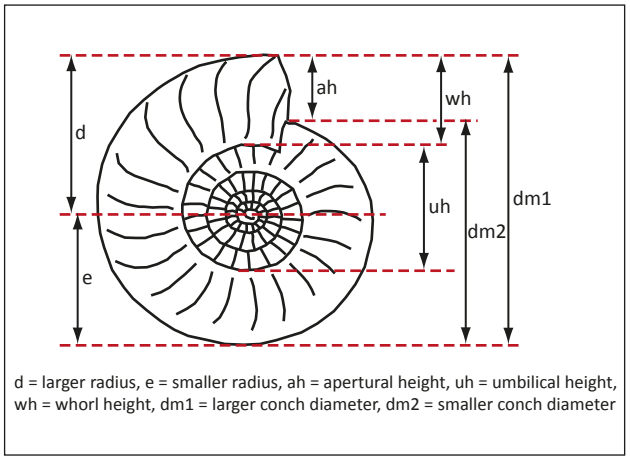

Fig. 3. Principal descriptive conch characters used in the present study (modified from Korn & Klug 2003).

Systematic palaeontology

Class Cephalopoda Cuvier, 1797
Subclass Nautiloidea Agassiz, 1847
Order Tarphycerida Flower & Kummel, 1950
Family Discoceratidae Dzik, 1984
Genus *Discoceras* Barrande, 1867

Type species: *Clymenia antiquissima* Eichwald, 1842, from the Katian Stage, Upper Ordovician, Estonia.

Diagnosis (after Furnish & Glenister 1964, p. K360): Gradually expanded ribbed or smooth forms characterized by slight to moderate impression and subquadrate whorl section; siphuncle central in initial half-volution, marginodorsal in succeeding 1.5–2 whorls, subdorsal at maturity; connecting rings thick, layered. Upper Ordovician, Llandeilo–Ashgill.

Remarks: *Schroederoceras* Hyatt, 1894 is regarded as a junior synonym of *Discoceras* (Strand 1933; Furnish & Glenister 1964). All figured specimens are housed in the type collections of the Natural History Museum of Denmark (Geological Museum; MGUH).

Characters and indices related to the shape of the shell (Fig. 3) have been described according to the suggestions by Korn & Klug (2003) used for description of coiled ammonoids.

Discoceras costatum n. sp.

Fig. 4A–B
aff. 1842 *Clymenia antiquissima* Eichwald – Eichwald, pp. 33–35, pl. 3, figs 16, 17.
aff. 1861 *Lituites antiquissimus* (Eichwald) – Roemer, pp. 62–65, pl. 6, fig. 2f (*partim*), not pl. 6, figs 2a–2e, 2g.
aff. 1925 *Discoceras antiquissimum* (Eichwald) – Foerste, pp. 58–59, pl. 18, figs 1A, 1B [copy of holotype figured by Eichwald (1842)].
aff. 1933 *Discoceras antiquissimum* (Eichwald) – Strand, pp. 33–36, pl. 2, figs 4, 11; pl. 4, figs 2, 3; pl. 13, fig. 9 (with additional synonymy).

aff. 1953 *Discoceras antiquissimum* (Eichwald) – Balashov, pp. 265–266, pl. 4, figs 2a, 2b; pl. 9, fig. 3; pl. 12, fig. 1a, b [copy of holotype figured by Eichwald (1842)].
aff. 1958 *Discoceras antiquissimum* (Eichwald) – Sweet, pl. 11, figs 1, 2.
aff. 1984 *Discoceras antiquissimum* (Eichwald) – Dzik, text-fig. 9c–d, pl. 7, fig. 1a–b.

Holotype: The holotype is a fragmented, external mold (MGUH 29285) kept in the Palaeozoic collections of the Natural History Museum of Denmark.

Type locality: The holotype MGUH 29285 was collected from shale exposures at the farm Vasegård, Åkirkeby, Bornholm (UTM zone 33U, 492789E 6100883N, datum WGS 84).

Type stratum: Lower part of the Lindegård Formation, upper Katian, Upper Ordovician.

Derivation of name: The species name *costatum* refers to the characteristic transverse ribs (from Latin: costae).

Material: One specimen (accession number 1984.455; MGUH 29285) from the Palaeozoic collections of the Natural History Museum of Denmark collected at the farm Vasegård, Bornholm.

Diagnosis: A moderately expanding *Discoceras* with a sculpture consisting of transverse, prominent ribs, usually irregularly spaced. Approximately 30 ribs are visible in the outer whorl. Whorl expansion rate (WER = $(dm1/dm2)^2$) is 2.14. Between five and fifteen secondary, transverse lirae are situated between the ribs.

Description: The holotype (Fig. 4, MGUH 29285) is a fragmented, flattened, coiled, convolute phragmocone with a diameter of 79 mm and almost 2½ volutions preserved. The living chamber is missing. The height of the last whorl (wh) is 25 mm, and the umbilical height (uh) is 35 mm (see Fig. 3 for explanation). The whorl expansion rate (WER) is 2.14, meaning that the conch is moderately expanding (see Fig. 3). Cross section of conch and internal characters are not preserved, but the imprint zone, which is the difference between wh and the apertural height (ah), is narrow as judged from the side view. Ornamentation consists of approximately 30 transverse, oblique, sharp, prominent ribs per whorl, usually irregularly spaced. Ribs form a distinct hyponomic sinus. Between 5 and 15 (on average *c.* 10) secondary, transverse lirae (growth lines) are situated between the ribs. Bifurcated lirae occur sporadically. The overall morphology of the shell is characterised as mimosphinctid according to the scheme of Korn & Klug (2003, fig. 3).

Remarks: *Discoceras costatum* n. sp. shares characters with one of the earliest species of *Discoceras*, the upper Darriwilian to Sandbian *D. boreale* Sweet, 1958, and two younger species, the Katian *D. antiquissimum* (Eichwald, 1840), and the Hirnantian *D. siljanense* Kröger, Ebbestad, Högström & Frisk, 2011. The three species are characterised by prominent transverse ribs and distinct lirae similar to those of *D. costatum*. The latter specimen differs, however, from *D. siljanense* in having fewer ribs per whorl (*c.* 30 instead of *c.* 40), and a higher whorl expansion rate (WER 2.14 instead of 1.82). It differs from *D. boreale* Sweet in having significantly fewer ribs (*D. boreale* has more than 50 per whorl; see holotype figured by Sweet 1958, pl. 9, fig 1).

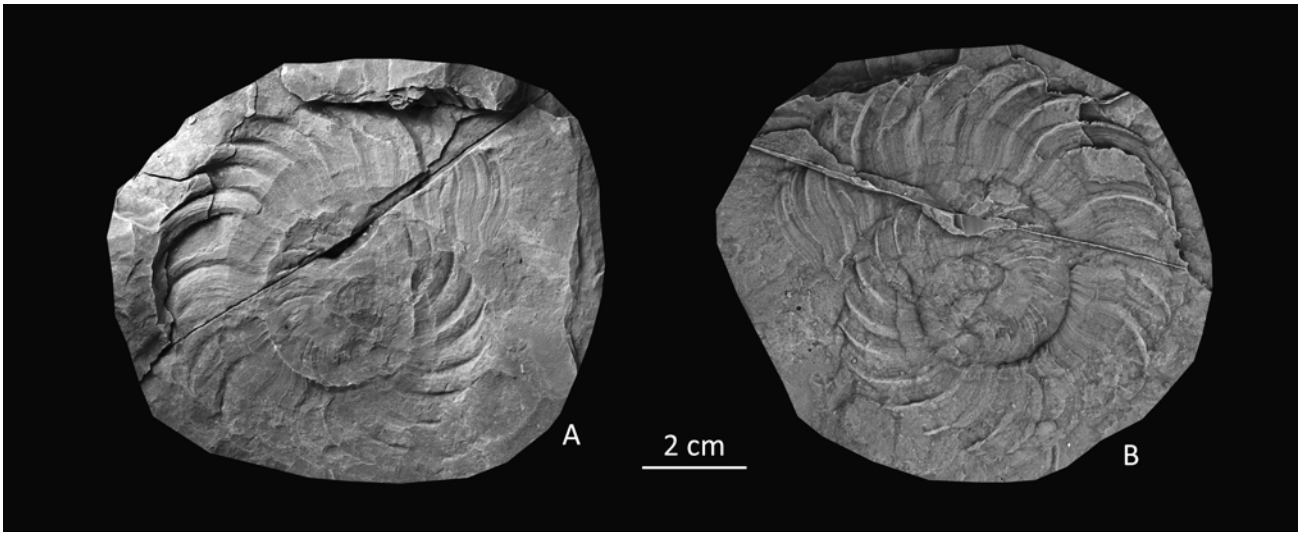

Fig. 4. *Discoceras costatum* n. sp. from the Lindegård Formation of Vasegaard, Bornholm. **A**, lateral view of specimen MGUH 29285. **B**, latex cast of A.

D. antiquissimum is characterised by almost the same number of ribs per whorl as *D. costatum* (*c.* 30–38 *vs. c.* 30), but the ribs are generally less curved and characterised by a more shallow hyponomic sinus (see description by Strand, 1933). The whorl expansion rate (WER) is higher in *D. costatum* (2.14) than in *D. antiquissimum* (between 1.65 and 2.07; 1.65 in the holotype).

Occurrence: *D. costatum* n. sp. is only known from the Upper Ordovician Lindegård Formation of Bornholm. The closely related species *Discoceras antiquissimum* is known from Katian (Upper Ordovician) strata in northern Estonia, the Oslo Region in Norway, and Sweden.

Discoceras vasegaardense n. sp.

Fig. 5A–D

aff. 1860 *Lituites arcuatus* n. sp. – Lossen, pp. 25 [*nomen nudum*].

aff. 1861 *Lituites antiquissimus* (Eichwald) – Roemer, pp. 62–65, pl. 6, figs 2b, c (*partim*).

aff. 1933 *Discoceras angulatum* (Saemann) – Strand, pp. 37–38, pl. 2, fig. 3; pl. 4, fig. 4 (picture and description of the holotype figured by Saemann 1852).

aff. 1953 *Schroederoceras angulatum* (Saemann) – Balashov, pp. 263–264, pl. 13, figs 1a, 1b, 2a, 2b.

aff. 1953 *Schroederoceras spongistratum* n. sp. – Balashov, pp. 254–255, pl. 7, fig. 8; pl. 8, figs 1, 2; pl. 9, fig. 3.

aff. 1958 *Discoceras arctuatum* [sic] (Lossen) – Sweet, pp. 103–104; textfig. 13J; pl. 12, fig. 4, ?pl. 8, fig. 7.

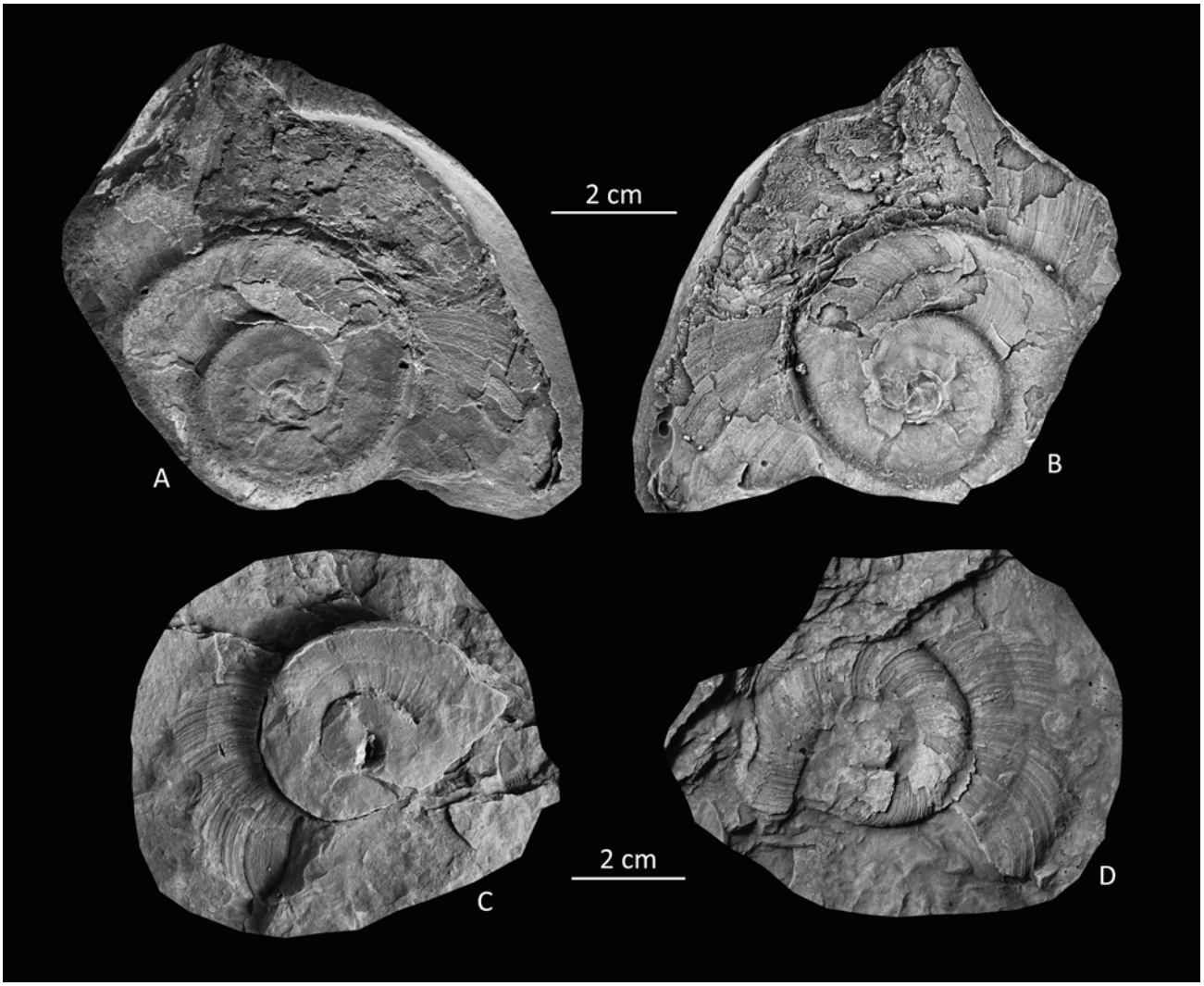

Fig. 5. *Discoceras vasegaardense* n.sp. from the Lindegård Formation of Bornholm. **A**, lateral view of specimen MGUH 29286 from a loose slab from the beach at Sose Bugt. **B**, latex cast of A. **C**, lateral view of specimen MGUH 29287, presumably found close to the farm Vasegård near the town Åkirkeby, Bornholm. **D**, latex cast of C.

Comments on the synonymy: *Lituites arcuatus* Lossen, 1860 was originally established on the basis of two specimens from the uppermost part of the Elnes Formation (previously named the Cephalopod shale) of Toten in the northern part of the Oslo Region, Norway, which has been dated as lower Sandbian (*N. gracilis* Zone). One specimen was from the village Billerud. Lossen did not illustrate the specimens and they were probably lost during the Second World War. According to Sweet (1958) one of the specimens was illustrated and described by Strand (unpublished notes, Oslo University) during a visit to Museum für Naturkunde, Berlin, before the war. Sweet (1958) diagnosed, described and illustrated the species based on the notes by Strand but he did not select a neotype for *Lituites arcuatus*. Accordingly, "*Lituites arcuatus*" is recognized as a *nomen nudum*.

Holotype: The holotype is a fragmented, external mold (MGUH 29287) kept in the Palaeozoic collections of the Natural History Museum of Denmark.

Type locality: The original label associated with the holotype MGUH 29287 says "Vasegaard?", indicating that the specimen likely originates from exposures next to the farm Vasegård near Åkirkeby, Bornholm (UTM zone 33U, 492789E 6100883N, datum WGS 84).

Type stratum: Lindegård Formation, upper Katian, Upper Ordovician.

Derivation of name: The specific name *vasegaardense* refers to the type locality, which presumably is situated near the farm Vasegård, Bornholm.

Material: Two specimens. MGUH 29286 is from an erratic shale slab found by Tom Christensen on the beach at Sose Bugt, Bornholm (approximately at UTM 489690E/6099554N), surrounded by numerous pieces of loose Upper Ordovician shales. MGUH 29287 (holotype) is from the Palaeozoic collections of the Natural History Museum of Denmark. The finder is unknown, but according to the label the specimen originates from the *Tretaspis* shale (Lindegård Formation) presumably at the farm Vasegård, Bornholm.

Diagnosis: Moderately to strongly expanding *Discoceras* with a smooth surface except for distinct, closely spaced, transverse lirae (growth lines). The whorl expansion rate (WER) varies between 2.39 and 2.43 and the umbilical width index UWI = uh/dm1 is between 0.46 and 0.50 (see Fig. 3 for explanation of the individual characters).

Description: The two specimens are both fragmented and flattened. The conch consists of coiled, convolute phragmocones with diameters of *c.* 85 mm in MGUH 29286 (Fig. 5A–B) and 55 mm in MGUH 29287 (Fig. 5C–D). Almost 2½ volutions are preserved in both specimens, and the living chamber is missing. The height of the last whorl (wh) is 18 mm in MGUH 29286 and 12 mm in MGUH 29287, and the umbilical heights (uh) are 40 mm and 30 mm, respectively. The conch is moderately to strongly expanding. The whorl expansion rate (WER) varies between 2.39 and 2.43 and the umbilical width index (UWI) varies between 0.46 and 0.50 judging from the most well-preserved parts of the phragmocone (see Fig. 3 for explanation of the individual characters).

Cross section of conch and internal characters are not preserved. The outer surface of the conch is almost smooth except for distinct, closely packed, slightly curved lirae (growth lines) that are occasionally bifurcated. A longitudinal, narrow, centrally placed impressed zone is seen in the second and third volutions. The overall morphology of the shell may be characterised as transitional between mimosphinctid and convoluticeratid according to the scheme of Korn & Klug (2003, fig. 3).

Remarks: *Discoceras vasegaardense* resembles "*Discoceras arcuatum* (Lossen)" (*nomen nudum*) in many aspects, but its whorl expansion rate (WER) is clearly higher. In *D. vasegaardense* it varies between 2.39 and 2.43, while it is 1.90–2.25 in "*D. arcuatum*". In "*D. arcuatum*" figured by Sweet (1958, pl. 12, fig. 4), which is a photograph of one of the two original, now lost, specimens described by Lossen (1860), WER is 2.2. Measurements of WER in specimens of *Discoceras angulatum* figured by Strand (1933, pl. 4, fig. 4; holotype) and Balashov (1953, pl. 13, fig. 1) show that also this species is characterised by a clearly lower WER than *D. vasegaardense* (1.9 *vs.* 2.39–2.43) despite the overall similarity. The same tendency is seen in *D. spongistratum* (Balashov, 1953) where WER = 2.1 (see Balashov 1953, pl. 8, fig. 1).

The holotype of *D. vasegaardense* (MGUH 29287) was identified as a *Discoceras* species in a lecture by Christian Poulsen in 1963 (Poulsen 1964), but he never described or figured the specimen.

Occurrence: *Discoceras vasegaardense* has only been documented from the Upper Ordovician shales of the Lindegård Formation on Bornholm. The closely related species "*Discoceras arcuatum* (Lossen)" (*nomen nudum*) resembles *Discoceras vasegaardense* and may be a possible ancestor to this. "*D. arcuatum*" is known from upper Middle and lowermost Upper Ordovician strata in the Oslo Region, Norway (Lossen 1860, Sweet 1958).

Acknowledgements

Specimen MGUH 29286 of *Discoceras vasegaardense* n. sp. was found by amateur palaeontologist Tom Christensen. It was donated to Jens Kofoed from Natur-Bornholm who forwarded it to FS. Björn Kröger and Per Ahlberg are sincerely thanked for reviewing the manuscript and offering many helpful suggestions. We are thankful to Sten Lennart Jacobsen who made latex casts and photographed the specimens, and to Jette Halskov for drafting. Arne T. Nielsen is thanked for discussion and valuable comments on an earlier draft of the manuscript. We are grateful for trilobite and brachiopod identifications by Arne T. Nielsen and David Harper. Funding by the Carlsberg Foundation to JAR in support of Ordovician cephalopod studies is gratefully acknowledged.

Dansk sammendrag

Spiralsnoede, nautiloide cephalopoder tilhørende slægten *Discoceras* er yderst sjældne i Mellem og Øvre Ordovicium på Bornholm, men er almindeligt forekommende på Balticakontinentet, fx i Oslo-området og i Estland. Til dato er kun tre eksemplarer kendt fra Danmark. De stammer alle fra Lindegård Formations skiferaflejringer fra Øvre Ordovicium på Bornholm og tilhører de to nye arter *Discoceras costatum* n. sp. og *Discoceras vasegaardense* n. sp. Nautiloiderne er bevaret som ydre aftryk. Den meget sjældne forekomst af nautiloide blæksprutter generelt og *Discoceras* især, skyldes formentlig den distale placering af Bornholm på den baltoskandiske kontinentalsokkel kombineret med påvirkninger af relativt kolde havstrømme fra det Rheiske Ocean igennem Sen Ordovicium.

References

Balashov, Z.G. 1953: Coiled and semicoiled Nautiloidea of the Ordovician of the Baltic area. Trudy Vsesoyuznogo Neftyanogo Nauchno-Issled Geologii-Razvedo Institute (VNIGRI) 78, 217–268 [In Russian].

Bergström, J. 1982: Scania. In: Bruton, D.L. & Williams, S.H. (eds): Field excursion guide. IV International Symposium on the Ordovician System. Palaeontological Contributions from the University of Oslo 279, 184–197.

Bergström, S.M., Huff, W.D., Koren, T., Larsson, K., Ahlberg, P. & Kolata, D.R. 1999: The 1997 core drilling through Ordovician and Silurian strata at Röstånga, S. Sweden: Preliminary stratigraphic assessment and regional comparison. GFF 121, 127–135.

Bergström, S.M., Chen, X., Gutiérrez-Marco, J.C. & Dronov, A. 2009: The new chronostratigraphic classification of the Ordovician System and its relations to major regional series and stages and to δ13C chemostratigraphy. Lethaia 42, 97–107.

Bruvo, M. & Nielsen , A T. 2004: The *Dicellograptus* Shale (Upper Ordovician) of Bornholm, Denmark. In: Hints, O. & Ainsaar, L. (eds): WOGOGOB-2004 Conference materials, p. 18.

Chen, X., Rong, J., Fan, J., Zhan, R., Mitchell, C.E., Harper, D.A.T, Melchin, M.J., Peng, P., Finney, S.C. and Wang, X. 2006: The Global Boundary Stratotype Section and Point (GSSP) for the base of the Hirnantian Stage (the uppermost of the Ordovician System). Episodes 29, 183–196.

Christiansen, J.L. & Stouge, S. 1999: Using Palaeo-oceanographical modelling in reconstructing Early Ordovocian palaeogeography. In: Kraft, P. & Fatka, O. (eds): Quo vadis Ordovician? Short papers of the 8th International Symposium on the Ordovician System. Acta Universitatis Carolinae: Geologica 43, 515–518.

Dzik, J. 1983: Early Ordovician conodonts from the Barrandian and Bohemian-Baltic faunal relationships. Acta Palaeontologica Polonica 28, 327–368.

Dzik, J. 1984: Phylogeny of the Nautiloidea. Acta Palaeontologica Polonica 45, 3–203.

Eichwald, E. 1842: Die Urwelt Russlands durch Abbildungen erlaeutert. Zweites Heft. Neuer Beitrag zur Geognosie Esthlands und Finlands. Akademie der Wissenschaften, St. Petersburg, pp. 1–138.

Foerste, A. 1925: Notes on cephalopod genera; chiefly coiled Silurian forms. Journal of Scientific Laboratories of Denison University 20, 1–69.

Furnish, W.M. & Glenister, B.F. 1964: Nautiloidea-Tarphycerida. In: Teichert, C. (ed.): Treatise on Invertebrate Paleontology, Part K, Mollusca 3, K343–K368. Geological Society of America and the University of Kansas Press. Boulder, Colorado.

Glimberg, C.F. 1961: Middle and Upper Ordovician strata at Lindegård in the Fågelsång district, Scania, S. Sweden. Geologiska Föreningens i Stockholm Förhandlingar 83, 79–85.

Gry, H. 1948: Bentoniten i Bornholms Ordovicium. Meddelelser fra Dansk Geologisk Forening 11, 364–386.

Kielan, Z. 1959: Upper Ordovician trilobites from Poland and some related forms from Bohemia and Scandinavia. Palaeontologica Polonica 11, 198 pp.

Korn, D. & Klug, C. 2003: Morphological pathways in the evolution of Early and Middle Devonian ammonoids. Paleobiology 29, 329–348.

Kröger, B., Ebbestad, J.O.R., Högström, A.E.S. & Frisk, Å.M. 2011: Mass concentration of Hirnantian cephalopods from the Siljan District, Sweden; taxonomy, palaeoecology and palaeobiogeographic relationships. Fossil Record 14, 35–53.

Lossen, C. 1860: Ueber einige Lituiten. Zeitschrift der Deutschen geologischen Gesellschaft 12, 15–28.

Nielsen, A.T. & Schovsbo, N.H. 2007: Cambrian to basal Ordovician lithostratigraphy in southern Scandinavia. Bulletin of the Geological Society of Denmark 53, 47–92.

Pedersen, G.K. 1989: The sedimentology of Lower Palaeozoic black shales from the shallow wells Skelbro 1 and Billegrav 1, Bornholm, Denmark. Bulletin of the Geological Society of Denmark 37, 151–173.

Poulsen, C. 1936: Übersicht über das Ordovizium von Bornholm. Meddelelser fra Dansk Geologisk Forening 9, 43–66.

Poulsen, C. 1964: Nogle bemærkninger om et fund af *Discoceras* i Tretaspisskiferen på Bornholm. Oversigt over Dansk Geologisk Forenings møder og ekskursioner i 1963. Meddelelser fra Dansk Geologisk Forening 15, 436.

Poulsen, V. 1966: Cambro–Silurian stratigraphy of Bornholm. Meddelelser fra Dansk Geologisk Forening 16, 117–137.
Poulsen, V. 1968: *Tretaspis* shale at Øleå, Bornholm. Meddelelser fra Dansk Geologisk Forening 18, 349–350.
Poulsen, V. 1969: Eokambrium og Palæozoikum. Geologi på Bornholm. Varv Ekskursionsfører Nr. 1, 23–41.
Pålsson, C. 2001: Graptolites from the Upper Ordovician *Dicranograptus clingani* Zone at Järrestad, Scania, southern Sweden. GFF 123, 217–224.
Ravn, J.P.J. 1899: Trilobitfaunaen i den bornholmske Trinucleus-skifer. Danmarks Geologiske Undersøgelse Serie 2, 10, 49–60.
Roemer, C.F. 1861: Die fossile Fauna der silurischen Diluvial-Geschiebe von Sadewitz bei Oels in Niederschlesien – Eine palaeontologische Monographie. Robert Nischkowsky, Breslau, 81 pp.
Saemann L. 1852: Über die Nautiliden. Palaeontographica 3, 121–167.
Schovsbo, N.H., Nielsen, A.T., Klitten, K., Mathiesen, A. & Rasmussen, P. 2011: Shale gas investigations in Denmark: Lower Palaeozoic shales on Bornholm. Geological Survey of Denmark and Greenland Bulletin 23, 9–12.
Stouge, S. & Rasmussen, J.A. 1996: Upper Ordovician conodonts from Bornholm and possible migration routes in the Palaeotethys Ocean. Bulletin of the Geological Society of Denmark 43, 54-67.
Strand, T. 1933: The Upper Ordovician cephalopods of the Oslo Area. Norsk geologisk Tidsskrift 14, 1–117.
Sweet, W.C. 1958: The Middle Ordovician of the Oslo region of Norway 10. Nautiloid cephalopods. Norsk Geologisk Tidsskrift 31, 1–178.
Teichert, C. 1930: Die Cephalopoden-Fauna der Lyckholm-Stufe des Ostbaltikums. Paläontologische Zeitschrift 12, 264–312.

Geochronological constraints on granitic magmatism, deformation, cooling and uplift on Bornholm, Denmark

TOD E. WAIGHT, DIRK FREI & MICHAEL STOREY

Waight, T.E., Frei, D. & Storey, M. 2012. Geochronological constraints on granitic magmatism, deformation, cooling and uplift on Bornholm, Denmark. © 2012 by Bulletin of the Geological Society of Denmark, Vol. 60, pp. 23–46. ISSN 0011–6297 (www.2dgf.dk/publikationer/bulletin).

U-Pb ages on zircon from 11 samples of granitoid and gneiss from the Danish island of Bornholm have been obtained using laser ablation - inductively coupled plasma mass spectrometry. These ages indicate that the felsic basement rocks were generated over a restricted period in the Mesoproterozoic at 1455 ± 10 Ma. No evidence has been found for the presence of 1.8 Ga basement gneisses as observed to the north in southern Sweden and as inferred in previous studies. No distinction in age can be made between relatively undeformed granitic lithologies and gneissic lithologies within the errors of the technique. This indicates that granitic magmatism, deformation and metamorphism all occurred within a relatively restricted and contemporaneous period. The granitic magmatism on Bornholm can thus be correlated to similar events at the same time in southern Sweden, Lithuania, and elsewhere in Baltica, and is therefore part of a larger magmatic event affecting the region. Argon and Rb-Sr ages on various minerals from a single sample of the Rønne Granite provide constraints on the cooling and uplift history of the basement in the region. Using recently published closure temperatures for each isotopic system a cooling curve is generated that illustrates a period of rapid cooling immediately after and/or during crystallisation. This likely represents the period of emplacement, crystallisation, and deformation of the felsic basement. The modelled rate of post-emplacement cooling is highly dependent on the choice of closure temperature for Ar isotopes in biotite. Use of recently published values of around 450°C defines a prolonged period of slower cooling (*c.* 4°C per million years) over nearly 100 million years down to *c.* 300°C and the closure temperature of Sr isotopes in biotite. Use of older and lower closure temperatures defines curves that are more consistent with theoretical models. The low closure temperature of Sr isotopes in biotite explains much of the wide variation in previous age determinations using various techniques on Bornholm. There is no evidence in the geochronological data for disturbance during later tectonic events in the region.

Keywords: Bornholm, geochronology, zircon, granitoid, gneiss, Danolopolian, Rb-Sr, ^{40}Ar-^{39}Ar.

Tod Waight [todw@geo.ku.dk], Department of Geography and Geology, University of Copenhagen, Øster Voldgade 10, DK-1350 Copenhagen K, Denmark. Dirk Frei, Geological Survey of Denmark and Greenland (GEUS), Øster Voldgade 10, DK-1350 Copenhagen K, Denmark; presently at Department of Earth Sciences, Corner Ryneveld and Merriman Streets, Stellenbosch, Private Bag X1, Matieland, 7602, South Africa. Michael Storey, QUADLAB, Department of Environmental, Social and Spatial Change, Roskilde University, Universitetsvej 1, DK-4000 Roskilde, Denmark.

Received 10 January 2012
Accepted in revised form
9 May 2012
Published online
15 June 2012

The only exposures of basement rocks in Denmark are found on Bornholm and comprise high-grade gneisses and intrusive granitoids (Callisen 1934; Micheelsen 1961; Berthelsen 1989). Bornholm is strategically important within the plate tectonic framework of Northern Europe, representing a link between the basement exposures of southern Sweden and the buried basement of northeast Poland and Lithuania. Structurally, Bornholm lies within the Tornquist zone, a complex large scale shear zone running between Sweden and Denmark and separating the old, thick cold crust of north-eastern Europe (Fennoscandia) from the hotter, thinner crust of the younger mobile belts of central and western Europe (e.g. Gorbatschev & Bogdanova 1993; Graversen 2009). Therefore, a better understanding of the geological evolution of this region is vital to a large-scale understanding of northern Europe.

Early studies proposed that all felsic basement lithologies on Bornholm (granites and gneisses) were chemically related, and therefore by inference

also contemporaneous (Callisen 1934). Micheelsen (1961) described a geological history beginning with a geosynclinal sequence of sediments and basalts that was progressively and variably granitised under granulitic then amphibolitic facies conditions (Rønne and Hammer stages respectively), simultaneous with the generation of foliations and both large and smaller scale folding. Post-kinematic granitisation resulted in formation of the Svaneke Granite although no specific time constraints were suggested for how the various granitisation episodes were related to each other. To the north of Bornholm, in the Blekinge Province of SE Sweden, geological and geochronological investigations identified a series of older (*c.* 1.8–1.7 Ga) basement gneiss lithologies (Tving granitoid and Västanå Formation) intruded by younger granitoids dated at around 1.45 Ga (Åberg 1988; Johansson & Larsen 1989; Kornfält 1993, 1996). Early K-Ar age determinations on Bornholm granites ranged between 1.4 and 1.25 Ga (Larsen 1971) and suggested a link between the granites on Bornholm and in SE Sweden. Based on these ages, and previous work, Berthelsen (1989) suggested two loosely constrained episodes of granitoid magmatism on Bornholm, an older phase at *c.* 1780–1650 Ma (e.g. gneiss and Rønne Granite) and a younger phase at *c.* 1400 Ma. More recent studies suggest that all the granitoids were emplaced over a relatively short time span (1470–1440 Ma) (Obst *et al.* 2004 and references therein; Zariņš & Johansson 2009), and no age distinction can be made between undeformed granitoids, deformed granitoids, and gneisses. These age ranges strongly suggest that the Bornholm granitoids can be correlated with rocks from the Blekinge Province in southern Sweden (Obst *et al.* 2004) and are part of a much larger province of intracratonic magmatism (e.g. Bogdanova *et al.* 2008).

In this study, we present new laser ablation - inductively coupled plasma mass spectrometry (LA-ICPMS) U-Pb zircon ages for 11 granitoids and gneisses from Bornholm. Several of these samples come from the same or similar localities dated using secondary ion mass spectrometry (SIMS) by Zariņš & Johansson (2009) and this provides an excellent opportunity to confirm these earlier results and to compare the two techniques. These authors also identified a number of older (inherited) zircons in several of their samples. In

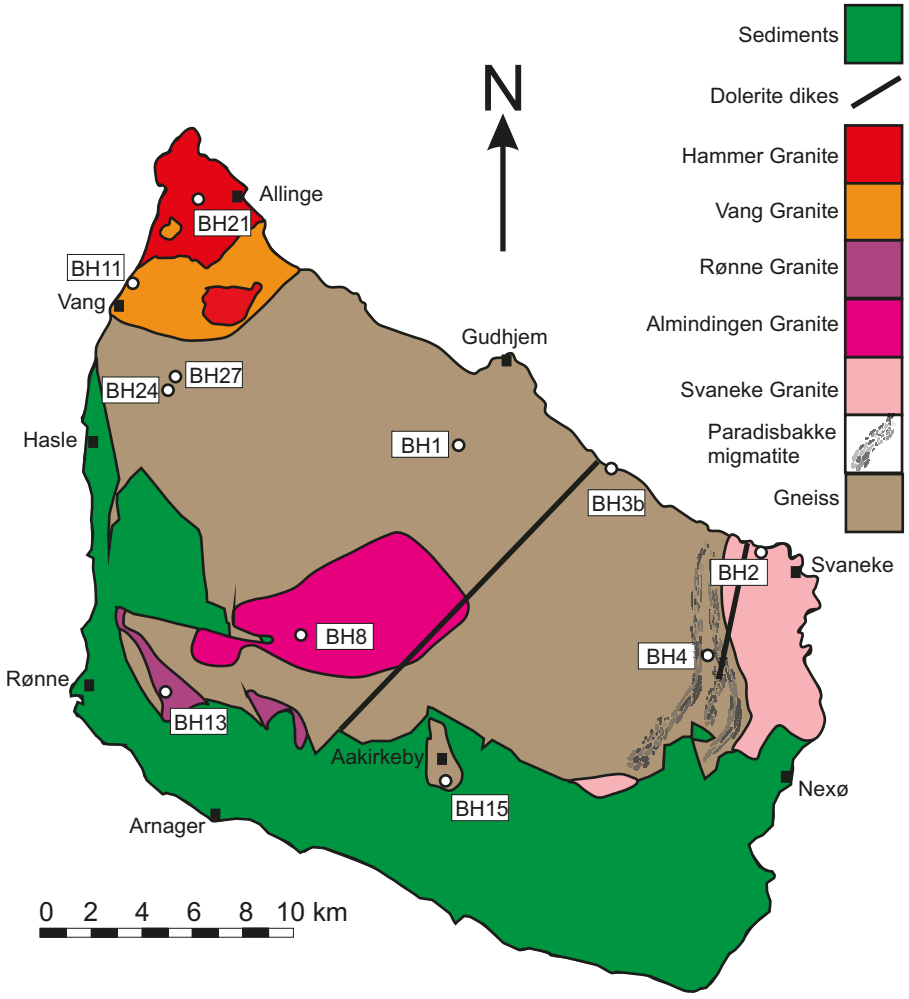

Fig 1: Location map, with sample localities and summary basement geology of Bornholm (modified from Berthelsen 1989). The Maegård Granite (sample BH24) is a small isolated outcrop and is not shown at the scale of this map.

light of this, we also analysed a larger population of zircons in several of the gneissic samples to more closely examine the inherited zircon population on Bornholm and provide constraints on potential source rocks and deeper crustal lithologies under Bornholm. Finally, we present a detailed geochronological study of a single sample, utilising a number of isotopic systems with distinct closure temperatures to attempt to establish a cooling path for the Bornholm basement.

Geological overview

The general geology of the granitoids of Bornholm was described in detail by Callisen (1934) and Micheelsen (1961); more recent detailed descriptions of the petrography and field relationships of the Bornholm granitoids and gneisses are summarised by Berthelsen (1989), Gravesen (1996), Obst *et al.* (2004), and Zariņš & Johansson (2009). Previous geochronological investigations on Bornholm have been succinctly summarised by Obst *et al.* (2004) and Zariņš & Johansson (2009). Berthelsen (1989) suggested that the gneissic basement on Bornholm was equivalent to the subduction-related 1.8 Ga gneisses exposed to the north in Sweden. These were then intruded by a series of older granitoids, and the entire sequence was subsequently deformed and folded. A series of younger granitoids were then emplaced and later deformed. In detail, at least six separate granitoid intrusions have been identified: Almindingen Granite, Hammer Granite, Maegård Granite, Rønne Granite, Svaneke Granite and Vang Granite (Fig. 1). The basement rocks on Bornholm are also intruded by a series of mafic dikes, which have recently been discussed in detail by Holm *et al.* (2010). Four distinct episodes of dike emplacement (1326 Ma, 1220 Ma, 950 Ma, and 300 Ma) are identified.

Zariņš & Johansson (2009) found no evidence for an older 1.8 Ga basement component on Bornholm, or two distinct granitic events. All units (both granitoid and gneiss) were found to have been emplaced in the Mesoproterozoic between 1.47 and 1.44 Ga. Of the gneissic basement that was previously considered to be 1.8 Ga, only two gneiss samples, together with the Paradisbakke Migmatite, yielded reliable U-Pb ages in the Zariņš & Johansson (2009) study. We therefore present ages for several new gneissic samples from different locations than those investigated by Zariņš & Johansson (2009). The small yet distinct Maegård intrusion has not been previously dated and therefore we also present an age for this unit. Table 1 gives details of the location and petrography of the samples investigated in this study.

Methods

Sample preparation and imaging

Samples were crushed and sieved and zircons were separated using conventional heavy liquid methods. The zircons were then handpicked and mounted in 1-inch round epoxy mounts, ground to approximately 60–75% of their thickness and polished to 1-micron grade. Prior to analysis the zircons were imaged in order to identify potential zoning, inherited cores, metamictization and other internal structures using backscattered electron (BSE) imaging on the JEOL JXA-8200 Superprobe at the Department of Geography and Geology, University of Copenhagen.

U-Pb geochronology

U-Pb dating was carried out by LA-ICPMS at GEUS in Copenhagen, using a double focusing Thermo-Finnigan Element2 SF mass spectrometer coupled to a NewWave UP213 frequency quintupled laser ablation system and analytical techniques described in detail by Gerdes & Zeh (2006) and Frei & Gerdes (2009). All analyses were obtained by single spot analysis with a spot diameter of 30 μm and a crater depth of approximately 15–20 μm. All analyses were pre-programmed and laser-induced elemental fractional and instrumental mass discrimination were corrected based on regular analyses of the reference zircon (GJ-1; Simon *et al.* 2004); two GJ-1 analyses were made for every ten sample zircon spots. For quality control the Plešovice zircon standard (Nasdala *et al.* 2008) was analysed regularly and yielded a concordia age of 338.8 ± 1.1 Ma (n = 28; MSWD of concordance and equivalence = 0.44), in good agreement with the published ID-TIMS $^{206}Pb/^{238}U$ age of 337.1 ± 0.4 Ma (Sláma *et al.* 2008). Calculation of concordia ages and plotting of concordia diagrams were carried out using Isoplot/Ex. 3.0 (Ludwig 2003). Unless stated otherwise, all ages are calculated using only those analyses that have the highest degree of concordance, i.e. are within the range of 97–103% concordant. A larger number of zircon analyses (*c.* 100) were made for several gneiss samples in order to asses the possibility of inheritance and the age of inherited populations. These data are presented as age probability diagrams constructed using AgeDisplay (Sircombe 2004).

Rb-Sr geochronology

Sr isotopic compositions and Rb and Sr concentrations were determined on biotite, feldspar (predominantly Na-rich plagioclase), and amphibole separates, and a whole rock powder from sample BH13 (Rønne

Granite). Mineral separates were produced using conventional heavy liquid and magnetic separations. The separates were hand-picked to remove impurities and then cleaned in MQ-water, weighed into Teflon beakers, and an appropriate amount of mixed ^{87}Rb-^{84}Sr tracer was added to each sample. Mineral and whole rock samples were then dissolved using standard HF-HCl-HNO_3 procedures and Rb and Sr were separated using techniques described by Waight *et al.* (2002a). Sr aliquots were loaded on single Ta filaments and analysed in multi-dynamic mode on the VG Sector 54 thermal ionisation mass spectrometer (TIMS) at the Department of Geography and Geology, University of Copenhagen. Rb was loaded in a similar fashion and run on the same instrument in static mode. Analysis of the SRM987 standard during the analytical session gave 0.71024 ± 1 (n=2) which is in perfect agreement with the long-term reproducibility in the laboratory.

^{40}Ar-^{39}Ar geochronology

^{40}Ar-^{39}Ar ages were determined at the Quaternary Dating Laboratory, Roskilde University, Denmark, on splits of the same biotite and amphibole separates analysed for Sr isotope composition. Samples were irradiated for 40 h in the CLICIT facility of the Oregon State University TRIGA reactor along with Fish Canyon sanidine (FCs-2; 28.172 Ma; Rivera *et al.*, 2011) as the neutron-fluence monitor mineral. The argon isotopic analyses were made on a fully automated Nu Instruments Noblesse multi-collector noble-gas mass spectrometer following protocols and corrections for interference isotopes detailed in Brumm *et al.* (2010) and Rivera *et al.* (2011). Step heating experiments were carried out using a 50-W Synrad CO_2 laser in conjunction with an integrator lens that delivered a *c.* 5 mm^2 square beam, with top hat energy profile, to the sample. The quoted uncertainties on the ^{40}Ar-^{39}Ar ages are experimental errors including the error on J (the neutron flux parameter), but do not include potential uncertainties on the ^{40}K decay constant.

Results

Zircon ages

Eleven samples were dated in this study; their locations and brief petrographic descriptions of the dated samples are given in Table 1. Analyses of representative concordant zircons are presented in Table 2 and the full data set is available as an electronic appendix at the web site http://2dgf.dk/publikationer/bulletin/192bull60.html or can be requested from the first author. Back-scattered electron images of representative zircons from each sample, together with concordia diagrams, are presented in Fig. 2 A–K.

BH1: Amphibole gneiss, Knarregård
This sample is typical of the grey, amphibole-bearing granitic orthogneisses that make up much of the basement exposures on Bornholm. In thin section the rock comprises anhedral to subhedral quartz up to *c.* 0.5

Table 1. Details of sample locations and brief sample descriptions

Sample	Unit[1]	Location	Description
BH1	Gneiss	Knarregård Quarry, 55°10′55.8″N, 14°56′17.8″E	Grey, medium-grained, foliated, equicrystalline hornblende-biotite orthogneiss
BH3b	Gneiss	Saltuna, 55°10′34.3″N, 15°1′21.3″E	Red, medium-grained, foliated, equicrystalline biotite gneiss
BH4	Paridisbakke migmatite	Præstebo Quarry, 55°6′13.1″N, 15°5′24.1″E	Grey, mesocratic, medium to coarse-grained, foliated hornblende-biotite gneiss/ migmatite with leucocratic veins
BH6	Svaneke Granite	Listed, Gulehald 55°8′42.2″N, 15°6′51.8″E	Red, coarse-grained, equicrystalline biotite granite
BH8	Almindingen Granite	Bjergebakke Quarry 55°7′8.1″N, 14°49′49.1″E	Red, leucocratic, medium-grained biotite granite
BH11	Vang Granite	Vang quarry 55°14′42.2″N, 14°44′5.5″E	Grey, mesocratic, medium-grained, equicrystalline biotite granite
BH13	Rønne Granite	Stubbegård quarry 55°6′11.4″N, 14°44′37.2″E	Grey, mesocratic, medium to coarse-grained equicrystalline biotite-hornblende granite
BH15	Gneiss	NaturBornholm 55°3′55.8″N, 14°55′2.0″E	White-pink, coarse-grained, equicrystalline biotite granite cut by numerous pegmatites displaying graphic intergrowths
BH21	Hammer Granite	Moseløkken quarry 55°16′24.4″N, 14°46′29.2″E	White-pink, leucocratic, medium-grained, equicrystalline biotite granite
BH24	Maegård Granite	Maegård 55°12′23.0″N, 14°45′17.0″E	Grey, mesocratic, fine-grained, porphyritic hornblende granite
BH27	Gneiss	Rutsker 55°12′41.2″N, 14°45′34.8″E	Red, leucocratic, medium-grained, equicrystalline, foliated biotite gneiss

1: unit names follow the terminology proposed by Berthelsen (1989).

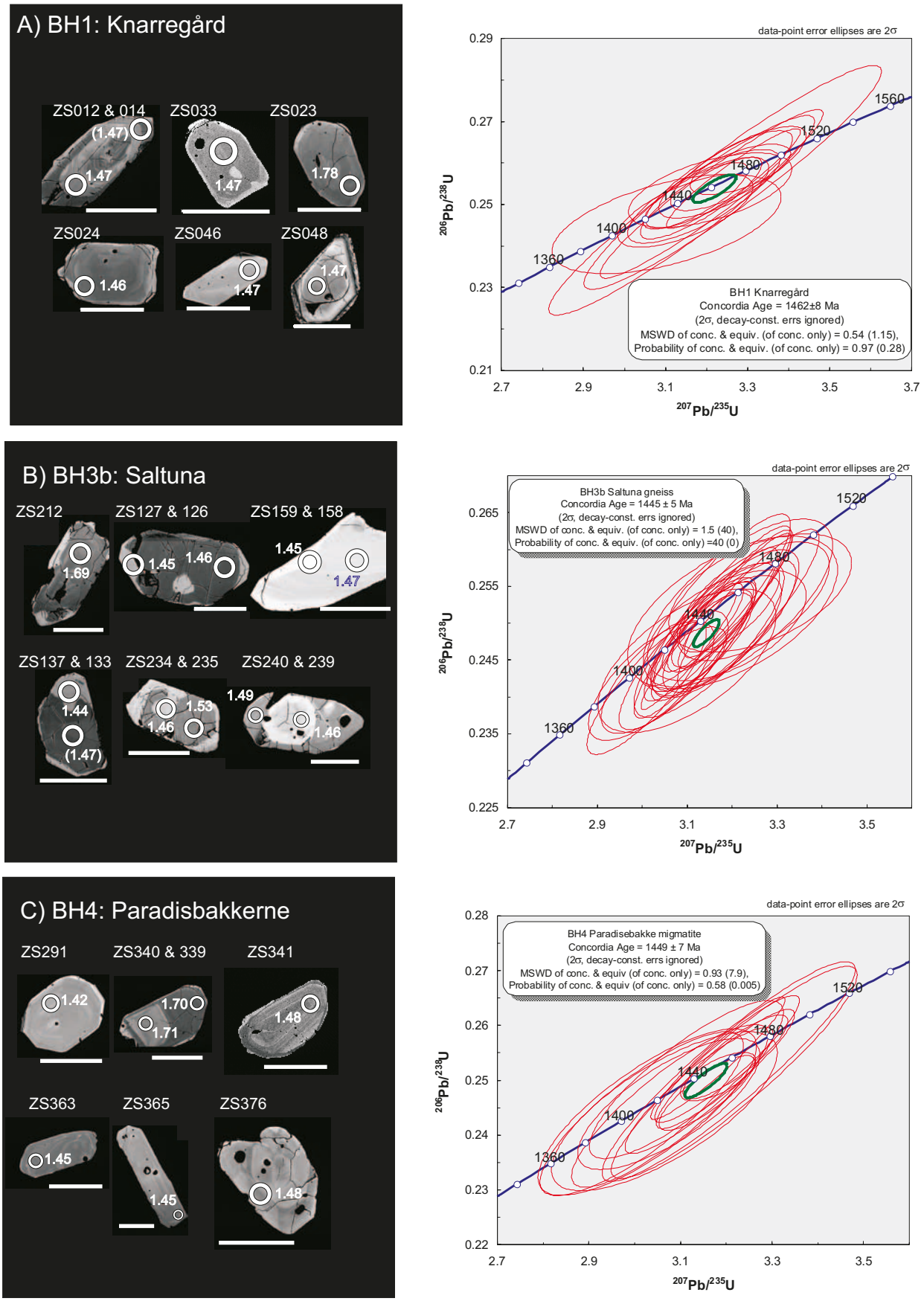
A) BH1: Knarregård
ZS012 & 014
ZS033
ZS023
ZS024
ZS046
ZS048
B) BH3b: Saltuna
ZS212
ZS127 & 126
ZS159 & 158
ZS137 & 133
ZS234 & 235
ZS240 & 239
C) BH4: Paradisbakkerne
ZS291
ZS340 & 339
ZS341
ZS363
ZS365
ZS376
data-point error ellipses are 2σ
BH1 Knarregård
Concordia Age = 1462±8 Ma
(2σ, decay-const. errs ignored)
MSWD of conc. & equiv. (of conc. only) = 0.54 (1.15),
Probability of conc. & equiv. (of conc. only) = 0.97 (0.28)
BH3b Saltuna gneiss
Concordia Age = 1445 ± 5 Ma
(2σ, decay-const. errs ignored)
MSWD of conc. & equiv. (of conc. only) = 1.5 (40),
Probability of conc. & equiv. (of conc. only) =40 (0)
BH4 Paradisebakke migmatite
Concordia Age = 1449 ± 7 Ma
(2σ, decay-const. errs ignored)
MSWD of conc. & equiv (of conc. only) = 0.93 (7.9),
Probability of conc. & equiv (of conc. only) = 0.58 (0.005)
206Pb/238U
207Pb/235U

Fig. 2 A-C.

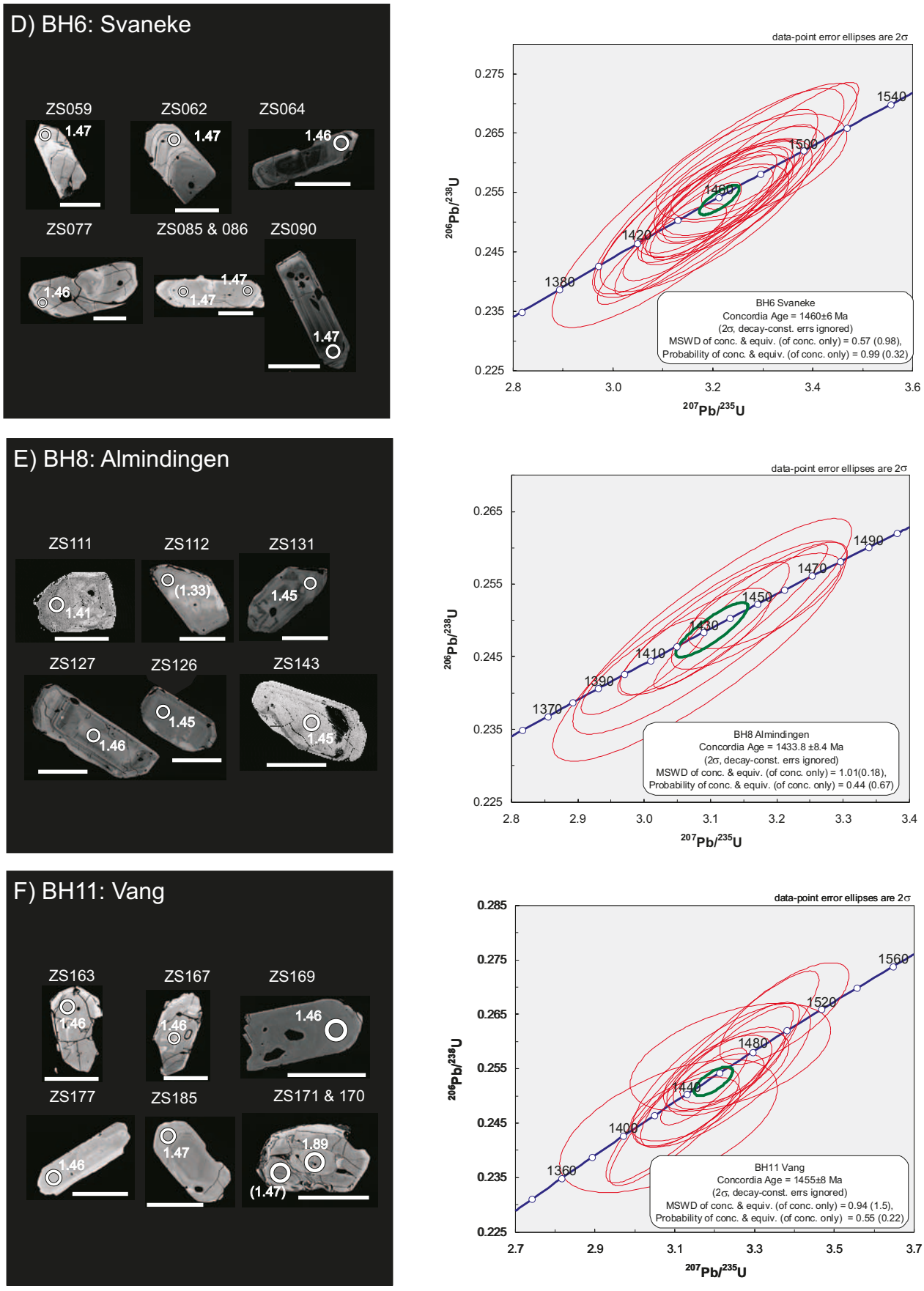
D) BH6: Svaneke
ZS059
ZS062
ZS064
ZS077
ZS085 & 086
ZS090
1.47
1.47
1.46
1.46
1.47
1.47
1.47
data-point error ellipses are 2σ
BH6 Svaneke
Concordia Age = 1460±6 Ma
(2σ, decay-const. errs ignored)
MSWD of conc. & equiv. (of conc. only) = 0.57 (0.98),
Probability of conc. & equiv. (of conc. only) = 0.99 (0.32)
E) BH8: Almindingen
ZS111
ZS112
ZS131
ZS127
ZS126
ZS143
1.41
(1.33)
1.45
1.46
1.45
1.45
data-point error ellipses are 2σ
BH8 Almindingen
Concordia Age = 1433.8 ±8.4 Ma
(2σ, decay-const. errs ignored)
MSWD of conc. & equiv. (of conc. only) = 1.01(0.18),
Probability of conc. & equiv. (of conc. only) = 0.44 (0.67)
F) BH11: Vang
ZS163
ZS167
ZS169
ZS177
ZS185
ZS171 & 170
1.46
1.46
1.46
1.46
1.47
1.89
(1.47)
data-point error ellipses are 2σ
BH11 Vang
Concordia Age = 1455±8 Ma
(2σ, decay-const. errs ignored)
MSWD of conc. & equiv. (of conc. only) = 0.94 (1.5),
Probability of conc. & equiv. (of conc. only) = 0.55 (0.22)

Fig. 2 D-F.

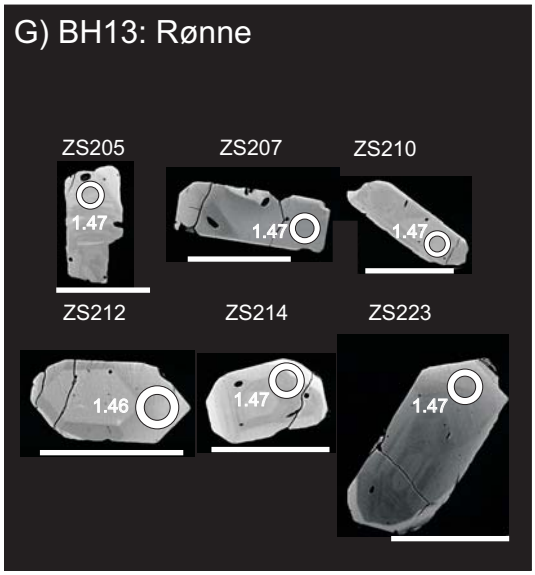
G) BH13: Rønne
ZS205
ZS207
ZS210
1.47
1.47
1.47
ZS212
ZS214
ZS223
1.46
1.47
1.47

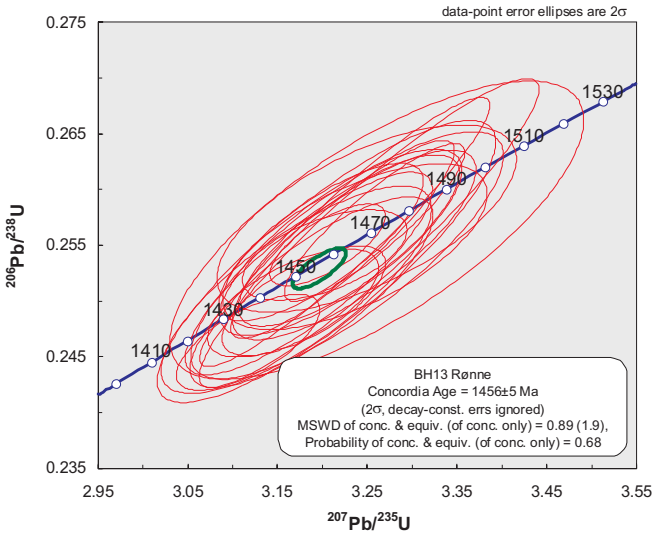
data-point error ellipses are 2σ
BH13 Rønne
Concordia Age = 1456±5 Ma
(2σ, decay-const. errs ignored)
MSWD of conc. & equiv. (of conc. only) = 0.89 (1.9),
Probability of conc. & equiv. (of conc. only) = 0.68
206Pb/238U
207Pb/235U

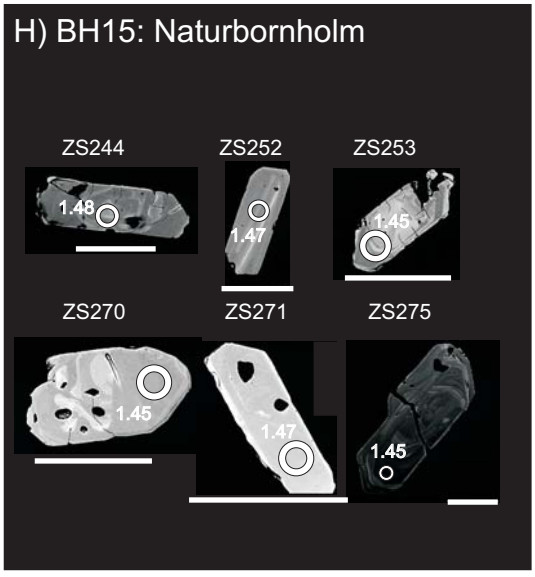
H) BH15: Naturbornholm
ZS244
ZS252
ZS253
1.48
1.47
1.45
ZS270
ZS271
ZS275
1.45
1.47
1.45

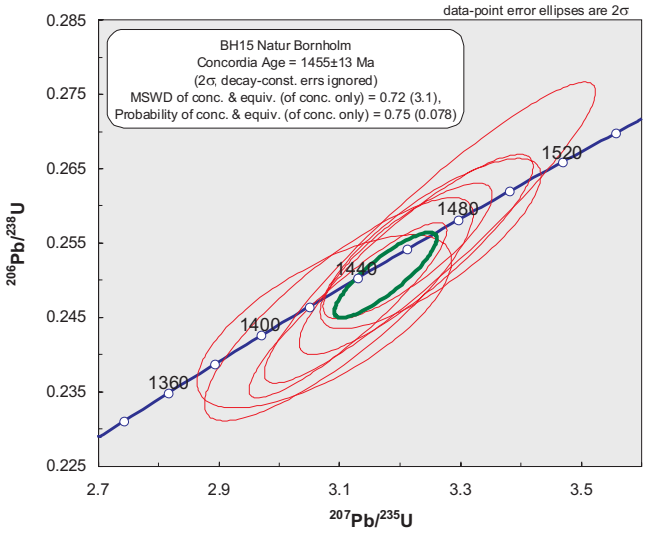
data-point error ellipses are 2σ
BH15 Natur Bornholm
Concordia Age = 1455±13 Ma
(2σ, decay-const. errs ignored)
MSWD of conc. & equiv. (of conc. only) = 0.72 (3.1),
Probability of conc. & equiv. (of conc. only) = 0.75 (0.078)
206Pb/238U
207Pb/235U

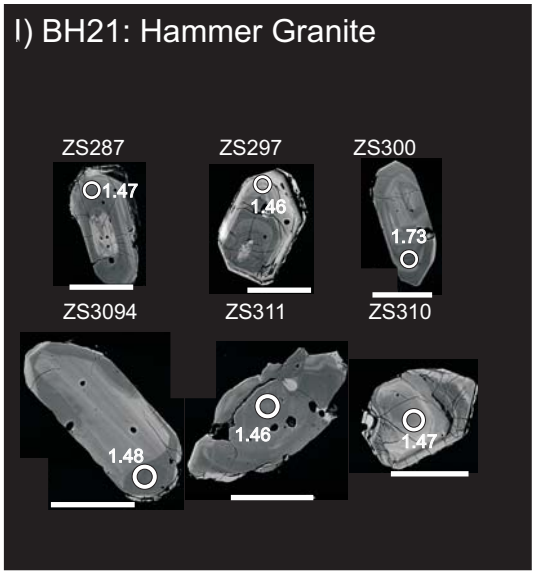
I) BH21: Hammer Granite
ZS287
ZS297
ZS300
1.47
1.46
1.73
ZS3094
ZS311
ZS310
1.48
1.46
1.47

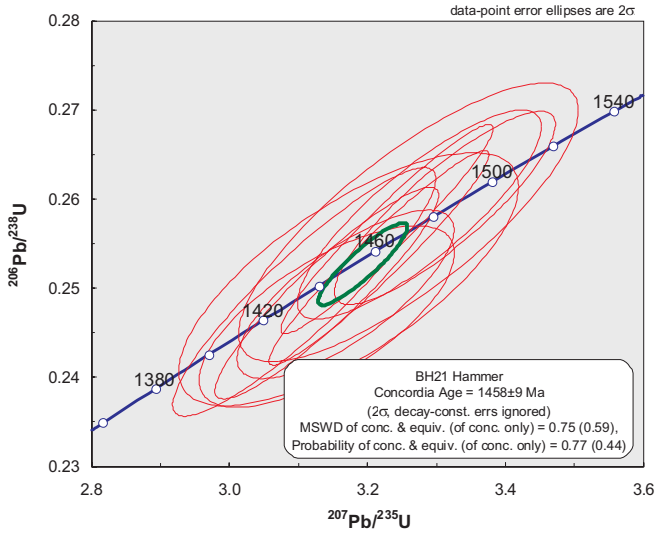
data-point error ellipses are 2σ
BH21 Hammer
Concordia Age = 1458±9 Ma
(2σ, decay-const. errs ignored)
MSWD of conc. & equiv. (of conc. only) = 0.75 (0.59),
Probability of conc. & equiv. (of conc. only) = 0.77 (0.44)
206Pb/238U
207Pb/235U

Fig. 2 G-I.

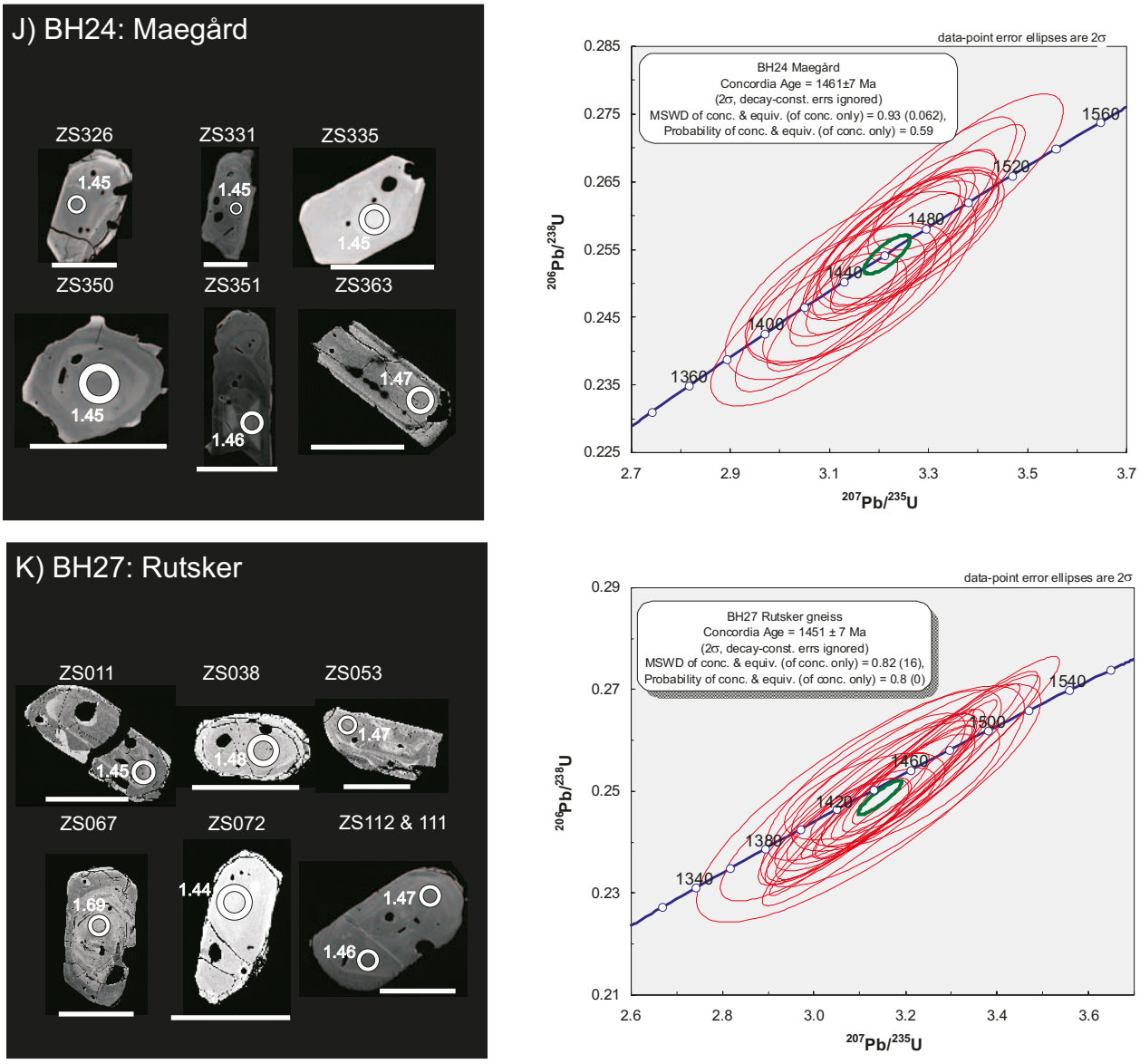

◀▲ Fig 2: Selected BSE images of representative zircons, and concordia ages for all samples investigated in this study. Numbers prefixed 'ZS' above individual zircon images correspond to analyses in Table 2 and the electronic appendix (e.g. for sample BH1, analysis ZS012 refers to Spot-Name 'zircon_sample-012'). Ages on BSE images are $^{207}Pb/^{206}Pb$ ages (in Ga) for individual spot analyses and typically have errors on the order of 0.03–0.05 Ga. Most ages shown are within the range of 97–103% concordant; slightly discordant ages (none less than 93% concordant) are given in brackets. Representative inherited grains are also shown if appropriate. Scale on all zircons = 100 μm, circle represents a spot size of 30 μm. Concordia plots were generated in Isoplot (Ludwig 2003): all ages are calculated using only analyses that are 97-103% concordant, and excluding potentially inherited grains. The small green ellipses represent the calculated age and weighted mean error ellipses.

mm in diameter exhibiting minor undulous extinction, abundant anhedral alkali feldspar crystals up to 0.5 mm across with near-ubiquitous cross-hatch twinning, and plagioclase as generally larger (up to *c.* 2mm) anhedral to subhedral albite-twinned crystals commonly displaying minor sericitisation. Mafic minerals generally occur in clusters and are aligned, defining a relatively strong foliation. They consist of light brown to green pleochroic biotite, occurring as anhedral crystals up to 0.5 mm long, and anhedral light brown to green-to-green-blue pleochroic amphibole crystals up to 0.5 mm in length. Also present are anhedral crystals of titanite up to 0.5 mm in diameter, commonly associated with and surrounding relatively abundant subhedral opaque phases up to 0.5 mm in diameter. Accessory minerals include relatively large (up to 0.5 mm) and abundant apatite and zircon.

Zircons from this sample are typically stubby euhedral crystals 100–200 μm in size and with width to length ratios of *c.* 1:2. Many of the zircons are relatively unzoned particularly in their cores, whereas others show relatively complex growth zoning. Occasional examples with rounded, potentially inherited cores are observed. Representative images are presented in Fig. 2A.

Thirty-two zircons were dated from this sample. Six of these were identified as inherited and have $^{207}Pb/^{206}Pb$ ages that scatter between 1.5 Ga (n=2), 1.6 Ga (n=2) and 1.7 Ga (n=2). The inherited zircons exist either as independent, relatively unzoned anhedral to rounded crystals, or as unzoned cores with thin zoned rims. A number of zircons also show evidence for Pb loss and are discordant; these are typically analyses from the rims of grains. The remaining zircons that are 97–103% concordant define an age of 1462 ± 8 Ma (Fig. 2A); this age is identical to a SIMS age determined on a sample from the same location by Zariņš & Johansson (2009).

BH3b: Gneiss, Saltuna

This sample is a granitic orthogneiss collected on the northern coast *c.* 50 m east of the large doleritic dike at Kelseå. Petrographically, the sample consists of anhedral to subhedral quartz crystals up to 0.25 mm in diameter and displaying weak undulous extinction, patchily zoned and sericitised crystals of anhedral to subhedral plagioclase up to 4 mm in length and containing abundant biotite inclusions, and anhedral crystals of alkali feldspar up to 0.5 mm across characterized by abundant cross hatch twinning. Mafic phases occur in oriented bands and define the foliation in the rock. They comprise yellow to brown pleochroic anhedral crystals of biotite up to *c.* 0.25 mm in length and light green to dark green pleochroic anhedral crystals of amphibole up to 0.25 mm long. Titanite is present as relatively small (*c.* 0.1 mm) anhedral crystals, typically occurring in clusters with, or rimming, anhedral opaque phases. Zircon and apatite occur as accessory phases.

Zircons in this sample are typically stubby, subhedral to euhedral crystals around 100–200 μm in size and with width to length ratios of 1:2. Relatively dark, homogeneous or magmatically zoned cores are common and often display evidence for resorption. Thinner brighter rims with some complex magmatic zoning typically surround these. Some rounded, possibly inherited, cores are also evident. The thin bright rims were generally too small to analyse with a 30 μm spot, although a few partial analyses were possible; these did not yield distinctly different ages from cores. Representative images are presented in Fig. 2B.

About 100 zircons were analysed from this sample, *c.* half of these are more than 3% discordant and are excluded from the final age calculation; they suggest small amounts of Pb loss. Of the entire zircon population analysed, only 11 were considered to be possibly inherited; these have $^{207}Pb/^{206}Pb$ ages clustering at 1.5 (n=8), 1.6 (n=2) and 1.7 Ga (n=1). The remaining zircons (n=30) define a slightly discordant age of 1445 ± 5 Ma (MSWD = 1.5) (Fig. 2B).

BH4: Paradisbakke Migmatite

The Paradisbakke Migmatite displays field evidence for partial melting; however, no physical separation of leucosome from mesosome was attempted in this study. In thin section, the analysed sample is broadly syenogranitic, exhibits only a weak foliation, and includes anhedral crystals of quartz up to 2 mm across and displaying undulous extinction, anhedral to subhedral crystals of plagioclase up to 2mm in length and displaying albite twins and some sericitisation. Abundant alkali feldspar occurs as anhedral, cross-hatch twinned grains typically up to *c.* 1 mm in length, although occasional larger (up to 4 mm) perthitic crystals also occur. Mafic minerals comprise subequal proportions of yellow to brown pleochroic biotite, present as anhedral crystals up to 0.5 mm in diameter, and anhedral light-green to green to blue-green pleochroic crystals of amphibole up to 0.5 mm in length. Opaque phases and titanite are relatively rare and zircon and apatite occur as accessory phases.

The zircons in this sample are typically euhedral to sub-rounded stubby crystals 100–200 μm long, with width to length ratios of 1:2, although longer crystals that are more prismatic are also present. Many show homogeneous or magmatically zoned cores, surrounded by thin rims. There is little evidence in the morphology for partial melting and distinct zircon populations from leucosome and mesosome. The few inherited zircons identified do not show any distinctive morphological features enabling simple discrimination from magmatic zircons. Representative BSE images are presented in Fig. 2C.

About 100 zircons were analysed from BH4; many of these are slightly discordant and have a spread that is indicative of Pb loss. Of the 100 analyses, only eight can be considered inherited and form peaks at *c.* 1.6 and 1.7 Ga, with a single zircon at 1.9 Ga. The remaining 15 zircons define a concordia age of 1449 ± 7 Ma (MSWD = 0.93) (Fig. 2C). This age is somewhat younger than the 1469 ± 6 Ma age presented by Zariņš & Johansson (2009), possibly a consequence of exclusion of a number of zircons with ages around 1500 Ma in this study, which we interpret as being potentially inherited (see electronic appendix).

Table 2. Representative analyses of concordant zircons

SAMPLE & SPOT NAME	U (ppm)	Pb (ppm)	Th/U calc	$^{207}Pb/^{206}Pb$	±2s	$^{207}Pb/^{235}U$	±2s	$^{206}Pb/^{238}U$	±2s	ρ	$^{207}Pb/^{235}U$ age (Ma)	±2s	$^{206}Pb/^{238}U$ age (Ma)	±2s	$^{207}Pb/^{206}Pb$ age (Ma)	±2s	Concordance %
BH1 Knarregård																	
Zircon_sample-012	649	166	0.16	0.092	0.003	3.26	0.30	0.257	0.022	0.95	1472	71	1472	113	1473	55	100
Zircon_sample-015	45	11	0.60	0.092	0.003	3.15	0.13	0.248	0.007	0.67	1445	33	1430	37	1466	60	98
Zircon_sample-016	436	110	0.47	0.091	0.002	3.17	0.10	0.252	0.007	0.79	1451	25	1449	34	1453	39	100
Zircon_sample-026	76	19	0.90	0.092	0.002	3.21	0.22	0.253	0.017	0.95	1460	54	1452	85	1472	41	99
Zircon_sample-027	89	23	0.62	0.092	0.002	3.28	0.10	0.258	0.005	0.63	1477	24	1482	25	1470	45	101
Zircon_sample-033	56	14	0.62	0.092	0.002	3.23	0.12	0.255	0.007	0.71	1465	29	1464	35	1465	50	100
Zircon_sample-036	98	24	0.83	0.092	0.003	3.14	0.26	0.247	0.020	0.94	1442	65	1425	102	1468	53	97
BH3b: Saltuna																	
Zircon_Sample-124	111	27	0.68	0.091	0.002	3.05	0.12	0.243	0.007	0.74	1420	29	1404	35	1444	49	97
Zircon_Sample-138	65	17	0.73	0.093	0.002	3.33	0.17	0.261	0.012	0.89	1489	39	1493	60	1482	44	101
Zircon_Sample-141	92	23	0.55	0.092	0.002	3.14	0.09	0.248	0.005	0.76	1441	22	1426	28	1465	35	97
Zircon_Sample-146	78	19	0.70	0.092	0.003	3.18	0.13	0.250	0.008	0.76	1453	33	1439	42	1475	52	98
Zircon_Sample-156	61	15	0.65	0.091	0.002	3.16	0.14	0.253	0.010	0.88	1448	33	1454	49	1439	39	101
Zircon_Sample-157	114	29	0.68	0.092	0.001	3.16	0.08	0.250	0.005	0.78	1447	19	1438	24	1462	29	98
Zircon_Sample-159	204	52	0.25	0.091	0.003	3.19	0.27	0.254	0.020	0.94	1456	66	1457	104	1454	57	100
BH4 Paridisbakken																	
Zircon_Sample-274	97	24	0.61	0.090	0.003	3.11	0.17	0.250	0.012	0.85	1436	43	1439	61	1431	56	101
Zircon_Sample-277	78	19	0.70	0.091	0.004	3.07	0.20	0.244	0.012	0.74	1424	50	1409	61	1446	85	97
Zircon_Sample-284	328	81	0.74	0.091	0.003	3.08	0.18	0.245	0.012	0.87	1427	44	1415	63	1446	54	98
Zircon_Sample-326	74	18	1.31	0.092	0.002	3.14	0.13	0.248	0.009	0.90	1443	32	1429	48	1463	35	98
Zircon_Sample-341	170	42	0.61	0.092	0.001	3.16	0.09	0.248	0.006	0.83	1447	21	1427	29	1477	29	97
Zircon_Sample-378	79	19	0.55	0.091	0.003	3.07	0.16	0.246	0.010	0.75	1426	41	1416	51	1442	66	98
Zircon_Sample-381	63	16	0.61	0.092	0.002	3.21	0.23	0.252	0.016	0.92	1458	55	1447	84	1475	51	98
BH6: Svaneke																	
Zircon_Sample-059	168	43	0.43	0.092	0.002	3.25	0.20	0.256	0.015	0.93	1469	48	1467	75	1470	42	100
Zircon_Sample-067	137	35	0.39	0.092	0.002	3.24	0.11	0.255	0.007	0.79	1466	27	1466	36	1467	40	100
Zircon_Sample-086	124	31	0.50	0.092	0.002	3.20	0.10	0.251	0.006	0.80	1457	24	1446	33	1472	36	98
Zircon_Sample-090	150	38	0.51	0.092	0.002	3.23	0.11	0.255	0.006	0.66	1464	26	1462	29	1468	47	100
Zircon_Sample-091	89	23	0.65	0.092	0.004	3.28	0.16	0.259	0.007	0.60	1476	37	1485	38	1462	73	102
Zircon_Sample-092	171	42	0.46	0.092	0.002	3.12	0.08	0.247	0.005	0.79	1439	21	1421	27	1464	31	97
Zircon_Sample-093	80	20	1.01	0.092	0.002	3.24	0.10	0.257	0.005	0.63	1467	24	1473	26	1458	46	101
BH8: Almindingen																	
Zircon_Sample-127	516	130	0.64	0.091	0.002	3.18	0.09	0.253	0.005	0.72	1453	23	1452	28	1454	39	100
Zircon_Sample-128	707	177	0.44	0.091	0.001	3.15	0.11	0.251	0.008	0.95	1444	26	1441	42	1448	21	100
Zircon_Sample-131	776	196	0.24	0.091	0.002	3.17	0.11	0.252	0.007	0.83	1451	26	1449	37	1453	36	100
Zircon_Sample-137	1226	303	0.08	0.090	0.002	3.08	0.09	0.247	0.006	0.81	1427	23	1424	31	1432	34	99
Zircon_Sample-141	853	213	0.24	0.090	0.002	3.10	0.17	0.249	0.012	0.88	1433	43	1434	63	1432	50	100
Zircon_Sample-143	558	137	0.76	0.091	0.003	3.08	0.18	0.246	0.012	0.86	1429	45	1417	64	1447	57	98
Zircon_Sample-154	1135	283	0.19	0.090	0.001	3.09	0.11	0.249	0.008	0.88	1430	26	1433	39	1426	31	100
BH11: Vang																	
Zircon_Sample-163	74	18	0.54	0.091	0.005	3.08	0.22	0.244	0.010	0.57	1429	55	1410	52	1457	113	97
Zircon_Sample-164	214	54	0.51	0.092	0.003	3.22	0.18	0.254	0.011	0.75	1461	44	1458	55	1466	72	99
Zircon_Sample-166	110	28	0.55	0.091	0.002	3.19	0.22	0.253	0.016	0.92	1456	53	1456	82	1455	51	100
Zircon_Sample-167	239	59	0.42	0.092	0.002	3.13	0.11	0.248	0.006	0.69	1440	26	1428	30	1459	47	98
Zircon_Sample-169	74	18	0.63	0.092	0.003	3.13	0.11	0.248	0.005	0.54	1439	28	1426	25	1459	58	98
Zircon_Sample-177	110	28	0.76	0.091	0.001	3.17	0.09	0.252	0.006	0.82	1451	21	1447	30	1455	30	99
Zircon_Sample-178	130	33	0.63	0.091	0.002	3.21	0.11	0.254	0.006	0.64	1459	27	1460	29	1457	51	100
BH13: Rønne																	
Zircon_Sample-205	148	38	0.54	0.092	0.004	3.26	0.19	0.256	0.011	0.74	1472	45	1471	56	1472	74	100
Zircon_Sample-214	151	38	0.74	0.092	0.002	3.18	0.07	0.250	0.004	0.69	1452	18	1439	21	1472	32	98
Zircon_Sample-219	74	18	0.54	0.092	0.002	3.17	0.08	0.250	0.004	0.65	1449	19	1438	20	1466	36	98
Zircon_Sample-220	85	22	0.63	0.091	0.001	3.21	0.05	0.255	0.003	0.71	1459	13	1464	15	1450	22	101
Zircon_Sample-221	124	31	0.71	0.092	0.002	3.23	0.14	0.254	0.009	0.81	1464	34	1460	47	1470	49	99
Zircon_Sample-222	164	42	0.78	0.091	0.002	3.20	0.08	0.254	0.003	0.56	1458	18	1460	17	1455	37	100
Zircon_Sample-223	226	58	0.51	0.092	0.002	3.24	0.11	0.255	0.007	0.80	1466	27	1464	36	1468	39	100

SAMPLE & SPOT NAME	U (ppm)	Pb (ppm)	Th/U calc	$^{207}Pb/^{206}Pb$	±2s	$^{207}Pb/^{235}U$	±2s	$^{206}Pb/^{238}U$	±2s	ρ	$^{207}Pb/^{235}U$ age (Ma)	±2s	$^{206}Pb/^{238}U$ age (Ma)	±2s	$^{207}Pb/^{206}Pb$ age (Ma)	±2s	Concordance %
BH15: Naturbornholm																	
Zircon_Sample-244	93	24	0.68	0.092	0.003	3.25	0.15	0.255	0.009	0.80	1469	36	1464	48	1477	52	99
Zircon_Sample-245	132	33	0.63	0.092	0.002	3.21	0.11	0.254	0.007	0.82	1460	28	1459	38	1462	38	100
Zircon_Sample-252	86	22	0.63	0.092	0.002	3.23	0.16	0.253	0.011	0.88	1464	38	1456	57	1474	44	99
Zircon_Sample-253	388	95	0.67	0.091	0.003	3.10	0.18	0.246	0.012	0.85	1432	45	1418	63	1453	59	98
Zircon_Sample-264	99	24	0.55	0.092	0.002	3.11	0.13	0.246	0.010	0.91	1436	33	1418	50	1463	34	97
Zircon_Sample-270	67	16	0.62	0.091	0.004	3.07	0.17	0.244	0.010	0.70	1426	43	1410	49	1451	77	97
Zircon_Sample-271	87	22	0.67	0.092	0.002	3.25	0.22	0.256	0.017	0.94	1469	54	1471	85	1466	46	100
BH21: Hammer																	
Zircon_Sample-284	96	24	0.71	0.092	0.003	3.14	0.15	0.247	0.008	0.70	1443	37	1422	43	1473	65	97
Zircon_Sample-286	144	36	0.56	0.091	0.001	3.14	0.13	0.249	0.010	0.92	1443	32	1436	50	1453	31	99
Zircon_Sample-287	245	63	0.55	0.092	0.002	3.28	0.14	0.258	0.010	0.84	1475	34	1481	49	1467	45	101
Zircon_Sample-292	69	17	0.57	0.092	0.002	3.17	0.13	0.249	0.008	0.77	1449	31	1435	40	1471	49	98
Zircon_Sample-297	568	146	0.56	0.092	0.003	3.26	0.20	0.257	0.013	0.80	1471	48	1477	65	1464	70	101
Zircon_Sample-298	821	205	0.46	0.090	0.002	3.11	0.16	0.250	0.011	0.91	1435	39	1436	59	1432	39	100
Zircon_Sample-303	708	182	0.65	0.091	0.001	3.23	0.13	0.257	0.010	0.96	1464	30	1473	49	1451	21	101
BH24: Mægård																	
Zircon_Sample-326	96	24	0.61	0.091	0.003	3.12	0.16	0.248	0.008	0.67	1439	39	1430	43	1452	71	99
Zircon_Sample-328	86	22	0.70	0.092	0.002	3.23	0.14	0.255	0.008	0.78	1465	33	1463	43	1468	51	100
Zircon_Sample-329	63	15	0.55	0.092	0.002	3.11	0.11	0.246	0.007	0.83	1434	27	1416	37	1461	37	97
Zircon_Sample-331	102	26	0.55	0.091	0.002	3.21	0.13	0.255	0.008	0.82	1459	31	1467	43	1448	44	101
Zircon_Sample-335	103	26	0.51	0.091	0.004	3.14	0.21	0.250	0.011	0.69	1443	51	1437	59	1453	90	99
Zircon_Sample-341	165	43	0.55	0.092	0.002	3.30	0.16	0.259	0.011	0.91	1481	38	1487	59	1472	39	101
Zircon_Sample-342	123	33	0.66	0.092	0.003	3.37	0.16	0.265	0.010	0.81	1499	37	1518	52	1472	54	103
BH27: Rutsker																	
Zircon_sample-008	136	34	0.43	0.090	0.003	3.06	0.22	0.247	0.015	0.86	1424	55	1422	78	1425	70	100
Zircon_sample-011	264	65	0.61	0.091	0.005	3.10	0.29	0.247	0.019	0.81	1433	73	1425	98	1445	105	99
Zircon_sample-012	422	105	0.70	0.091	0.002	3.15	0.19	0.249	0.014	0.92	1444	46	1435	70	1457	44	99
Zircon_sample-020	267	69	0.70	0.092	0.002	3.28	0.17	0.258	0.013	0.94	1475	41	1478	66	1471	34	101
Zircon_Sample-059	90	22	0.51	0.091	0.002	3.13	0.19	0.249	0.013	0.90	1439	46	1432	69	1450	51	99
Zircon_Sample-074	485	121	0.61	0.092	0.001	3.15	0.20	0.249	0.016	0.98	1445	50	1432	81	1465	25	98
Zircon_Sample-087	343	86	0.46	0.091	0.001	3.16	0.15	0.252	0.012	0.97	1448	38	1446	62	1449	22	100

Details on calculation of elemental concentrations, Th/Ucalc, ρ (error correlation) and degree of concordance (concordance %) are given in Frei & Gerdes (2009).

BH6: Svaneke Granite, Listed

This sample is representative of Svaneke Granite (Svaneke Granite type I according to Platou 1970), and was sampled within 10–20 m of a large doleritic dike at Listed. Petrographically, the sample is a relatively coarse-grained granodiorite and displays no apparent foliation in hand specimen although a persistent foliation is evident in outcrop. In thin section, the rock comprises anhedral to subhedral quartz crystals up to 2 mm across and displaying some undulous extinction, anhedral to subhedral plagioclase crystals up to 5 mm in length with albite twinning and some sericitisation and myrmekitic intergrowths along contacts with adjacent quartz. Alkali feldspar occurs as subhedral crystals up to 1 cm in length, displaying cross hatch twinning or perthitic exsolution lamellae. Mafic minerals consist of anhedral crystals of yellow-brown to green-brown pleochroic biotite up to *c.* 4 mm in diameter and showing minor alteration to chlorite, relatively abundant anhedral crystals of titanite up to 1mm in diameter, either present as independent crystals or rimming subhedral opaques. Amphibole occurs as light green to blue green pleochroic anhedral crystals up to 2 mm in diameter. Zircon and apatite are present as accessory phases.

Zircons from this sample are typically subhedral to euhedral prismatic crystals, 100–200 μm long and with width to length ratios of *c.* 1:3. Complex internal magmatic zoning is common, as are darker cores surrounded by thinner brighter rims in BSE images. Representative images are presented in Fig. 2D.

Thirty-one zircons were analysed from this sample. With the exception of a single spot, all analyses are within 10% of being concordant, with the more discordant analyses indicating small amounts of Pb loss. No inherited zircons were identified. Twenty-four zircons fulfilled the requirements of being 97–103% concordant and define a concordia age of 1460 ± 6 Ma (MSWD = 0.57) (Fig. 2D). This age is within error of the three ages presented for Svaneke II (from different localities) by Zariņš & Johansson (2009).

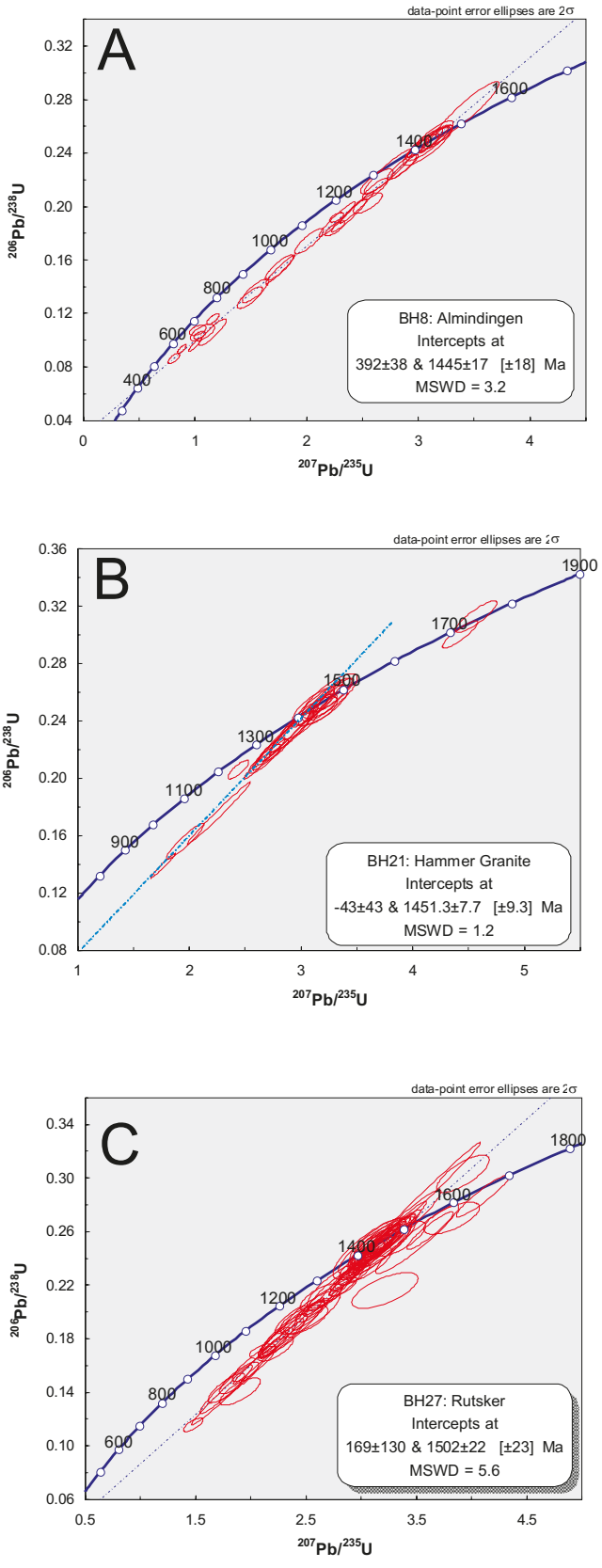

Fig 3. Full concordia plots for three selected samples. These samples show evidence for Palaeozoic to recent Pb loss, as well as rare inherited grains. Intercept ages are calculated using Isoplot (Ludwig 2003) and exclude inherited grains.

BH8: Almindingen Granite

This sample is representative of the Almindingen Granite and is a red, leucocratic, equigranular biotite syenogranite. In thin section, the rock comprises anhedral crystal of quartz up to 4 mm in diameter and displaying undulous extinction, abundant alkali feldspar as anhedral, cross-hatch twinned crystals up to 4 mm in diameter, and subordinate plagioclase as subhedral albite and Carlsbad twinned crystals up to 2 mm in length. Biotite is the dominant mafic phase and is present as anhedral, yellow to brown pleochroic crystals up to 0.5 mm in diameter and often altered to green pleochroic chlorite. Titanite is present as relatively rare anhedral crystals up to 0.5 mm in diameter. Accessory phases include relatively large zircons, possibly allanite, and small subhedral opaque grains up to 0.1 mm in diameter. The rock also displays abundant red iron staining along grain boundaries.

Zircons from this sample are predominantly anhedral to subhedral, stubby crystals *c.* 100–200 μm long and with width to length ratios of *c.* 1:2. Concentric magmatic zoning is common, and many also show patchy zoning; a relatively sharp and thin unzoned rim is developed on many zircons. Sector zoning is evident is a few examples. Representative images of mostly concordant zircons are presented in Fig. 2E.

Thirty-two zircons were analysed from this sample. Many of the zircons have undergone relatively recent Pb loss, possibly associated with the red iron staining observed in thin section, and define an array with an upper intercept age of 1445 ± 7 Ma and a lower intercept of 392 ± 38 Ma (MSWD = 3.2) (Fig. 3A). The discordant zircons do not show any morphological or zoning features to distinguish them from the concordant zircons. The discordant analyses are characterized by relatively high U contents (see appendix) and are therefore likely to be more metamict and more susceptible to Pb loss. The most concordant analyses (better than 97–103% concordant, n = 8) define a concordia age of 1434 ± 8 Ma (MSWD = 1.1) (Fig. 2E). This age is considerably younger than the 1462 ± 5 Ma concordia age presented by Zariņš & Johansson for a sample from the same quarry, although we note that the upper intercept ages for both data sets agree within error. The large degree of Pb loss observed in the sample analysed in this study places the concordia age into question and the upper intercept age of this study or concordia age of Zariņš & Johansson (2009) are preferred here as a crystallization age.

BH11: Vang Granite

This sample is representative of the Vang Granite and was collected from a quarry near the town harbor.

In thin section, the sample is an unfoliated monzogranite and composed of anhedral crystals of quartz up to 1mm in diameter exhibiting undulous extinction and some granophyric intergrowths with alkali feldspar. Plagioclase occurs as subordinate strongly zoned and subhedral crystals up to 5 mm in length, and alkali feldspar is present as abundant relatively fine-grained crystals (*c.* 0.25 mm) with abundant cross hatch twinning. Biotite occurs as yellow-brown to brown pleochroic subhedral crystals up to 0.5 mm in diameter and shows minor alteration to chlorite. Amphibole is present as anhedral yellow-brown to green to blue-green pleochroic crystals up to 2 mm in length. Titanite occurs as a relatively minor phase, typically as generally altered rims on opaque phases, which are present as anhedral crystals up to 1 mm in diameter, commonly forming the cores of clots of mafic minerals (biotite, amphibole, and titanite). Apatite and zircon are present as accessory phases.

Zircons from this sample are subhedral to euhedral stubby to prismatic crystals, typically about 100 μm in length, with width to length ratios of *c.* 1:2. Many are relatively unzoned, although patchy and/or concentric magmatic zoning is also evident. Representative images are presented in Fig. 2F.

Twenty-three zircons were analysed; a few spots are discordant and show evidence for Pb loss, and a single inherited zircon (present as a rounded core with a discordant rim) with an age of 1.9 Ga was identified. The remaining concordant analyses (n = 14) define a concordia age of 1455 ± 8 Ma (MSWD = 0.9) (Fig. 2F). A sample from the same locality investigated in the study of Zariņš & Johansson (2009) yielded a discordant upper intercept age of 1452 ± 22 Ma (MSWD 1.6) and a weighted average $^{207}Pb/^{206}Pb$ age of 1456 ± 8 Ma (MSWD 1.6); nearly all analyses were inversely discordant and therefore a concordia age could not be calculated. The age presented here is in good agreement with, and an improvement on, the previous age determinations.

BH13: Rønne Granite

This is a typical sample of the relatively dark, unfoliated Rønne Granite collected from the Stubbegård quarry. In thin section, this sample is a quartz monzonite comprising anhedral to subhedral crystals of quartz up to 0.5 mm in diameter and displaying minor undulous extinction. Feldspars are present as patchy and strongly zoned, subhedral to anhedral crystals of plagioclase up to 2 mm in length and displaying albite twins and minor sericitisation, and anhedral to subhedral crystals of perthitic or cross-hatch twinned alkali feldspar up to 2 mm in diameter and sometimes occurring as rims on plagioclase crystals (anti-rapakivi texture). Mafic phases include anhedral biotite as yellow-brown to orange-brown to red-brown pleochroic crystals up to 1 mm long and often present as partial clusters of radiating needles. Biotite is subordinate to amphibole, which occurs as abundant anhedral to subhedral green-brown to olive-green pleochroic crystals up to 2 mm in diameter. Many of the amphibole crystals contain a core region consisting of fine-grained complexes of anhedral quartz, opaques and apatite, possibly represented relic cores of clinopyroxene as described by Callisen (1957). Opaque phases occur as subhedral to euhedral crystals up to 0.3 mm in diameter and are commonly surrounded by biotite and hornblende to form the cores of mafic clots. Apatite and zircon are accessory phases.

Zircons from the Rønne Granite sample are generally subhedral to euhedral stubby, prismatic to square crystals displaying generally subtle zoning in the core and relatively bright rims. Crystals are typically 100–150 μm in length with a width to length ratio of 1:2 to 1:3; representative BSE images are presented in Fig. 2G.

Twenty-five zircons were analysed from this sample, and all but four analyses fell within our defined constraints of 97–103% concordance; three analyses show evidence for small amounts of Pb loss, whereas one is slightly older and reversely discordant. Excluding these analyses, the remaining analyses (n = 21) yield a concordia age of 1456 ± 5 Ma (MSWD = 0.9). This age is within error of the 1450 ± 5 Ma age presented by Zariņš & Johansson (2009) on a sample from an adjacent quarry.

BH15: Gneiss, NaturBornholm

This sample comes from the recently excavated 'man-made' exposures at the main car park to NaturBornholm Museum in Aakirkeby, *c.* 400 m north of the fault zone exposed at Klintebakken, and has not been dated in any previous study. Callisen (1934) and Berthelsen (1989) map the region as gneiss, yet in the field the rock bears a strong resemblance to the Svaneke Granite and does not exhibit a well-developed metamorphic fabric. Numerous, metre-wide pegmatite dikes displaying spectacular graphic intergrowths also cut the outcrop. Of all the samples investigated here, this sample is the least fresh. In thin section, the rock is a monzogranite containing quartz as anhedral to subhedral crystals up to 1 mm in diameter and displaying undulous extinction. Plagioclase is present as anhedral to subhedral albite-twinned crystals up to 5 mm in length, is commonly saussiritized, and contains abundant inclusions of fine-grained epidote. Alkali feldspar occurs as sericitised anhedral crystals up top 2 mm in diameter and as perthitic anti-rapakivi rims on plagioclase crystals. Biotite occurs as yellow-brown pleochroic crystals up to 1 mm in length, although

most are altered to green chlorite. Opaques phases occur as subhedral to euhedral crystals up to 0.25 mm in diameter and are commonly rimmed by titanite. Apatite and zircon are accessory phases.

Zircons from this sample are euhedral to subhedral crystals typically 150 μm long, with a width to length ratio of 1:2 to 1:3. Complex zoning is common, but some crystals are relatively homogeneous. Several crystals show metamict cores. Representative BSE images are presented in Fig. 2H.

Nineteen zircons yielded usable analyses from this sample. Several zircons show evidence for Pb loss and were excluded from the data set. A single analysis is inherited with an age of *c.* 1.7 Ga. Only seven remaining zircons fulfil the 97–103% concordance test, possibly a consequence of the alteration observed in thin

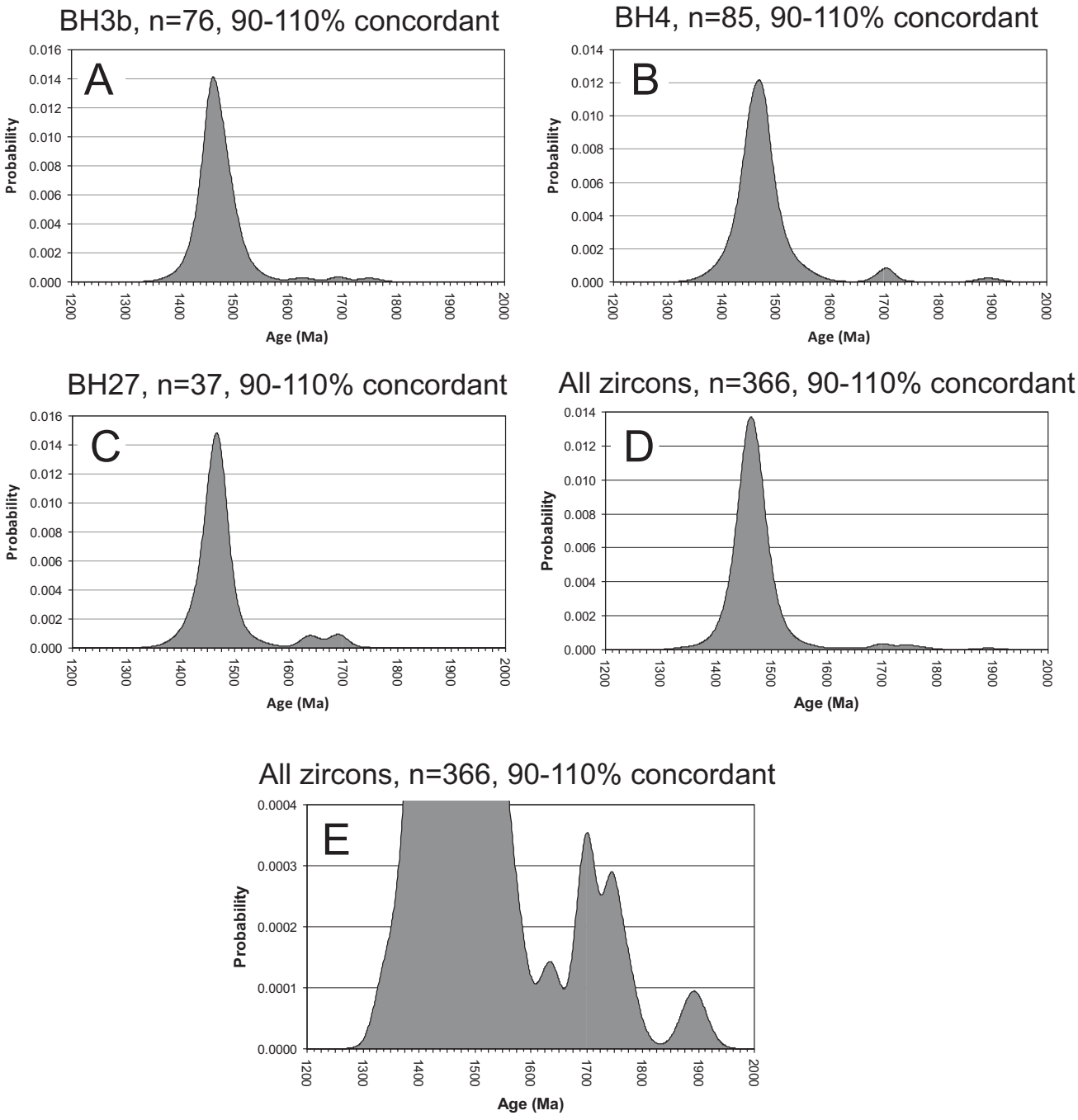

Fig 4: Age probability diagrams for selected samples: A) BH3b (Saltuna gneiss), B) BH4 (Paradisbakke Migmatite), C) BH27 (Rutsker gneiss), D) all zircon analyses from granites and gneisses combined, and E) enlarged view of D illustrating the small peaks in inherited zircons. Diagrams were calculated using AgeDisplay (Sircombe, 2004) and using $^{207}Pb/^{206}Pb$ ages between 90 and 110% concordant, and a bin width of 25 m.y.

section, and combined they yield a concordia age of 1455 ± 13 Ma (MSWD = 0.72) (Fig. 2H).

BH21: Hammer Granite

This sample is a typical example of a weakly foliated variety of the Hammer granite. Petrographically the rock is a syenogranite comprising anhedral crystals of quartz up to 2 mm in diameter and displaying undulous extinction, zoned plagioclase crystals up to 3 mm in length, with both Carlsbad and albite twins and some myrmekitic intergrowths with adjacent quartz, and abundant perthitic alkali feldspar crystals up to 1 cm in length, with some sericitisation. Biotite occurs as subhedral, yellow-green to brown pleochroic crystals up to 0.5 mm in length and sometimes altered to chlorite. Titanite is present as subhedral crystals up to 0.1 mm in diameter in clusters with biotite and relatively rare subhedral opaques up to 0.2 mm in diameter. Amphibole is rare and present as anhedral yellow-brown to green to blue-green pleochroic crystals up to 0.2 mm in diameter. Accessory zircon and apatite are relatively abundant.

Zircons from this sample are typically stubby subhedral to rounded crystals, 100–200 μm long, with width to length ratios of 1:2. Complex magmatic zoning is common. Representative BSE images are given in Fig. 2I.

Twenty-six zircons yielded usable ages from this sample, and of these about half show evidence of Pb loss, trending towards the zero intercept on the concordia diagram (Fig. 3B). Two spots yielded ages indicative of an inherited origin, both at around 1.75 Ga. The remaining analyses define a concordia age of 1458 ± 9 Ma (MSWD = 0.75, n = 9) (Fig. 2I). This age is in excellent agreement with the 1460 ± 7 Ma age presented for a sample from a different location by Zariņš & Johansson (2009).

BH24: Maegård Granite

The Maegård Granite is only exposed in one small, isolated outcrop yet is petrographically and texturally distinct from the other granitoids and gneisses on Bornholm. In hand specimen the rock is relatively fine grained and comprises larger crystals of hornblende and feldspar in a fine-grained matrix. In thin section, the rock is a microgranite and has textures consistent with relatively rapid crystallisation under hypabyssal conditions. It comprises relatively large crystals (phenocrysts) of subhedral, patchily zoned and albite twinned plagioclase up to 5 mm in length and anhedral to subhedral light-green to green pleochroic crystals of amphibole up to 5 mm long in a fine grained microcrystalline mosaical groundmass of anhedral quartz, feldspar, biotite, amphibole and opaques. The amphibole phenocrysts typically contain a core region comprising abundant fine-grained inclusions of quartz and apatite, or weakly green pleochroic clinopyroxene cores. Biotite occurs as rare anhedral red-brown pleochroic phenocrysts up to 2 mm in length. Opaques occur as anhedral to subhedral crystals up to 1 mm in diameter and apatite and zircon are present as accessory phases.

Zircons from this sample are typically anhedral to subhedral crystals around 100–200 μm long and with width to length ratios ranging from 1:2 to 1:3. The crystals are either relatively unzoned or show complex concentric magmatic zoning, with one example of sector zoning observed. Representative images are given in Fig. 2J.

Twenty-nine zircons gave usable results from this sample. Two zircons are highly discordant and preserve evidence for Pb loss. Twenty analyses were 97–103% concordant and combined they yield a concordia age of 1461 ± 7 Ma (Fig. 2J).

BH27: Gneiss, Rutsker

This sample is typical of the more quartz-rich, evolved biotite granitic gneisses that occur throughout Bornholm, and is likely similar to the 'red orthogneisses' described by Zariņš & Johansson (2009). The sample studied here is red, medium grained and equicrystalline and displays a foliation defined by oriented biotite. In thin section, the rock consists of anhedral crystals of quartz up to 0.5 mm in diameter and displaying undulous extinction. Plagioclase is present as relatively rare subhedral, zoned and albite twinned crystals up to 1 mm in length, whereas alkali feldspar is the dominant feldspar and is present as anhedral to subhedral, cross-hatch twinned and perthitic crystals up to 4 mm in length. Biotite defines the foliation and is present as anhedral to subhedral, yellow-brown pleochroic crystals up to 1mm in length, sometimes altered to chlorite. Opaques occur as subhedral to anhedral crystals up to 0.2 mm in diameter and apatite and zircon occur as relatively small accessory phases.

Zircons from this sample are typically subhedral to euhedral prismatic to square 100–150 μm long crystals, with width to length ratios of *c.* 1:2. Complex concentric zoning is common. Representative images are given in Fig. 2K.

Seventy zircons from this sample yielded usable results. Many of these are highly discordant and are indicative of recent Pb loss (see Fig. 3C). Around 10 spots are potentially inherited, normally present as discordant cores to zircons, and yield $^{207}Pb/^{206}Pb$ ages that spread between 1.5 and 1.7 Ga. Twenty-one spots were 97–103% concordant and define a slightly discordant concordia age of 1451 ± 7 Ma (MSWD = 0.16) (Fig. 2K).

Table 3. Results of ^{40}Ar-^{39}Ar step heating experiments on biotite and amphibole from the Rønne Granite

	Laser	Relative Isotopic Abundances										Derived Results					
Lab ID#	Watt	^{40}Ar	±1σ	^{39}Ar	±1σ	^{38}Ar	±1σ	^{37}Ar	±1σ	^{36}Ar	±1σ	$\%^{40}Ar^*$	±1σ	Ca/K	±1σ	Age (Ma)	±1σ
BH13 hornblende																	
1900-01A	2	0.4628	0.0013	0.0054	0.0018	0.0002	0.00001	0.0248	0.0028	0.0006	0.00001	61.29	0.80	9.0853	3.1434	801.6	212.8
1900-01B	3	0.5099	0.0015	0.0114	0.0017	0.0002	0.00001	0.0274	0.0028	0.0003	0.00001	80.34	0.59	4.7260	0.8599	580.6	75.7
1900-01C	4	0.8684	0.0015	0.0229	0.0018	0.0004	0.00001	0.0311	0.0029	0.0003	0.00001	89.60	0.34	2.6634	0.3255	551.6	37.0
1900-01D	5	1.1238	0.0018	0.0467	0.0016	0.0006	0.00001	0.0618	0.0048	0.0003	0.00001	92.34	0.34	2.5941	0.2211	378.3	12.1
1900-01E	6	1.2699	0.0015	0.0873	0.0016	0.0011	0.00001	0.0451	0.0049	0.0003	0.00001	93.14	0.22	1.0141	0.1114	239.9	4.0
1900-01F	7	1.4675	0.0020	0.1015	0.0018	0.0013	0.00002	0.0480	0.0028	0.0003	0.00001	94.22	0.30	0.9272	0.0572	241.0	4.0
1900-01G	10	4.7372	0.0021	0.1275	0.0018	0.0017	0.00002	0.3242	0.0062	0.0009	0.00001	94.90	0.09	4.9850	0.1178	569.4	6.9
1900-01H	13	7.7206	0.0020	0.1186	0.0019	0.0016	0.00001	0.2231	0.0036	0.0008	0.00001	97.24	0.05	3.6888	0.0823	922.0	11.3
1900-01I	16	10.758	0.0021	0.1336	0.0018	0.0017	0.00001	0.0697	0.0032	0.0005	0.00001	98.71	0.04	1.0228	0.0482	1097.6	11.0
1900-01J	19	13.337	0.0023	0.1334	0.0016	0.0018	0.00002	0.1263	0.0051	0.0004	0.00001	99.13	0.03	1.8563	0.0783	1290.8	11.1
1900-01K	22	22.540	0.0027	0.2005	0.0018	0.0029	0.00002	0.4601	0.0039	0.0005	0.00001	99.47	0.02	4.4973	0.0550	1406.7	8.8
1900-01L	25	25.442	0.0026	0.2241	0.0018	0.0033	0.00002	0.5935	0.0042	0.0006	0.00001	99.53	0.02	5.1901	0.0553	1417.1	7.9
1900-01M	27	20.111	0.0026	0.1792	0.0018	0.0025	0.00002	0.4378	0.0038	0.0005	0.00001	99.50	0.02	4.7872	0.0635	1405.2	9.8
1900-01N	29	26.065	0.0026	0.2202	0.0018	0.0033	0.00002	0.7057	0.0065	0.0005	0.00001	99.59	0.02	6.2811	0.0771	1459.8	8.2
1900-01O	31	28.737	0.0028	0.2486	0.0016	0.0037	0.00002	0.8461	0.0080	0.0006	0.00001	99.64	0.02	6.6706	0.0772	1436.6	6.6
1900-01P	33	27.872	0.0026	0.2383	0.0017	0.0036	0.00002	0.8286	0.0044	0.0005	0.00001	99.66	0.02	6.8146	0.0607	1448.6	7.2
1900-01Q	35	24.974	0.0025	0.2177	0.0017	0.0032	0.00002	0.7394	0.0048	0.0005	0.00001	99.66	0.02	6.6565	0.0680	1429.3	7.8
1900-01R	36	11.763	0.0022	0.0999	0.0016	0.0015	0.00001	0.3151	0.0040	0.0002	0.00001	99.65	0.03	6.1796	0.1282	1454.7	16.5
1900-01S-fuse	n.a.	244.11	0.0150	2.0967	0.0019	0.0313	0.00007	7.8954	0.0204	0.0038	0.00002	99.80	0.01	7.3807	0.0202	1445.7	1.0
BH13-biotite																	
1901-01A	2	6.7114	0.0036	0.1801	0.0021	0.0027	0.00002	0.0103	0.0029	0.0021	0.00002	90.81	0.11	0.1121	0.0316	548.6	5.5
1901-01B	3	16.021	0.0042	0.3971	0.0021	0.0055	0.00003	0.0129	0.0031	0.0024	0.00001	95.46	0.04	0.0637	0.0152	612.9	2.7
1901-01C	4	33.713	0.0053	0.6275	0.0022	0.0085	0.00003	0.0184	0.0032	0.0029	0.00002	97.45	0.03	0.0575	0.0099	791.1	2.2
1901-01D	5	62.928	0.0066	0.9152	0.0022	0.0122	0.00004	0.0375	0.0028	0.0035	0.00002	98.34	0.02	0.0802	0.0059	969.4	1.9
1901-01E	6	98.510	0.0079	1.1832	0.0021	0.0154	0.00005	0.0550	0.0033	0.0032	0.00002	99.05	0.01	0.0911	0.0054	1127.6	1.5
1901-01F	7	116.36	0.0093	1.2215	0.0022	0.0157	0.00005	0.0461	0.0032	0.0021	0.00001	99.46	0.01	0.0740	0.0050	1248.8	1.7
1901-01G	8	146.30	0.0101	1.4144	0.0021	0.0179	0.00006	0.0472	0.0032	0.0017	0.00001	99.66	0.01	0.0654	0.0044	1326.8	1.5
1901-01H	9	151.72	0.0101	1.4091	0.0020	0.0178	0.00005	0.0305	0.0033	0.0011	0.00001	99.78	0.01	0.0425	0.0045	1366.2	1.5
1901-01I	10	149.58	0.0121	1.3687	0.0021	0.0173	0.00005	0.0374	0.0034	0.0009	0.00001	99.82	0.01	0.0536	0.0048	1381.0	1.6
1901-01J	11	153.18	0.0111	1.3940	0.0022	0.0174	0.00006	0.0257	0.0035	0.0008	0.00001	99.85	0.01	0.0362	0.0049	1386.6	1.6
1901-01K	14	296.41	0.0151	2.6668	0.0023	0.0332	0.00009	0.0380	0.0034	0.0012	0.00001	99.88	0.01	0.0279	0.0025	1398.0	1.0
1901-01L	16	284.15	0.0180	2.5528	0.0023	0.0318	0.00009	0.0560	0.0034	0.0009	0.00001	99.91	0.01	0.0430	0.0026	1399.7	1.0
1901-01M	18	262.79	0.0150	2.3483	0.0021	0.0293	0.00008	0.1116	0.0034	0.0007	0.00001	99.93	0.01	0.0931	0.0028	1405.1	1.0
1901-01N	20	262.68	0.0160	2.3374	0.0024	0.0290	0.00008	0.0681	0.0031	0.0006	0.00001	99.93	0.01	0.0571	0.0026	1409.3	1.1
1901-01O	22	262.81	0.0160	2.3398	0.0021	0.0291	0.00008	0.0726	0.0027	0.0006	0.00001	99.94	0.01	0.0608	0.0023	1408.9	1.0
1901-01P	24	256.18	0.0170	2.2896	0.0020	0.0283	0.00007	0.0975	0.0032	0.0006	0.00001	99.94	0.01	0.0834	0.0027	1405.1	1.0
1901-01Q	26	242.22	0.0150	2.1652	0.0021	0.0269	0.00008	0.1041	0.0030	0.0005	0.00001	99.94	0.01	0.0943	0.0027	1405.0	1.1
1901-01R	28	227.85	0.0161	2.0368	0.0022	0.0253	0.00007	0.1475	0.0033	0.0005	0.00001	99.94	0.01	0.1420	0.0032	1405.0	1.1
1901-01S	30	211.14	0.0120	1.8840	0.0022	0.0234	0.00006	0.1741	0.0036	0.0005	0.00001	99.94	0.01	0.1811	0.0037	1406.7	1.3
1901-01T	32	185.79	0.0140	1.6577	0.0021	0.0206	0.00006	0.1177	0.0029	0.0004	0.00001	99.94	0.01	0.1392	0.0034	1406.8	1.3
1901-01U	34	157.55	0.0111	1.4081	0.0022	0.0175	0.00005	0.0788	0.0033	0.0003	0.00001	99.94	0.01	0.1096	0.0046	1405.1	1.6
1901-01V	36	128.19	0.0090	1.1489	0.0022	0.0142	0.00004	0.0547	0.0033	0.0002	0.00001	99.95	0.01	0.0933	0.0056	1402.4	2.2

Final step (fusion) sample gas was lost through instrumental error

Separates were irradiated for 40 h in the CLICIT facility of the Oregon State University TRIGA reactor. Sanidine from the Fish Canyon Tuff was used as the neutron fluence monitor with a reference age of 28.172 Ma (Rivera et al., 2011). Nucleogenic production ratios: $(^{36}Ar/^{37}Ar)_{Ca} = 2.646 \pm 0.008 \times 10^{-4}$, $(^{39}Ar/^{37}Ar)_{Ca} = 6.95 \pm 0.09 \times 10^{-4}$, $(^{38}Ar/^{37}Ar)_{Ca} = 0.196 \pm 0.00816 \times 10^{-4}$, $(^{40}Ar/^{39}Ar)_{K} = 7.3 \pm 0.92 \times 10^{-4}$, $(^{38}Ar/^{39}Ar)_{K} = 1.22 \pm 0.0027 \times 10^{-2}$, $(^{36}Ar/^{38}Ar)_{Cl} = 3.2 \times 10^{2}$, $^{37}Ar/^{39}Ar$ to Ca/K = 1.96. Isotopic constants and decay rates: $\lambda(^{40}K_e)$ /yr = 5.8 ± 0.07 x 10^{-11}, $\lambda(^{40}K_{b-})$ /yr = 4.884 ± 0.0495 x 10^{-10}, $\lambda(^{37}Ar)$/d = 1.975 x 10^{-2}, $\lambda(^{39}Ar)$/d = 7.068 x 10^{-6}, $\lambda(^{36}Cl)$/d = 6.308 x 10^{-9}, $(^{40}Ar/^{36}Ar)_{Atm} = 298.56 \pm 0.31$, $(^{40}Ar/^{38}Ar)_{Atm} = 1583.9 \pm 2$, $^{40}K/K_{Total} = 0.01167$.

Inherited zircons and age probability diagrams

Age probability diagrams for three gneiss samples are presented in Fig. 4 A–C. They illustrate that most zircons plot close to the inferred crystallisation age of *c.* 1.45 Ga. Combining all 97–103% concordant zircon analyses from the 11 samples investigated in this study (n = 180) yields a concordia age of 1453 ± 2 Ma (not shown). The age probability diagrams also show that the proportion of inherited zircons is relatively low (generally < 5%). In Fig. 4D, the zircon data (90–110% concordant; n = 366) from all samples are compiled. There is a clear peak at 1460 Ma, representing primary igneous zircon. Additional peaks are identified at 1.63, 1.70, 1.75, and 1.90 Ga (Fig. 4E). Out of the 366 zircons represented in this diagram, only 14 (4%) fall between the age of 1.6 and 1.8 Ga, and 2 fall between the age of 1.8 and 1.9 Ga.

^{40}Ar-^{39}Ar ages

^{40}Ar-^{39}Ar step heating age spectra for amphibole (BH13-hb) and biotite (BH13-bio) separated from Rønne granite sample BH13 are presented in Table 3 and Fig. 5. The amphibole separate yielded a well-defined plateau age of 1446 ± 2 Ma (MSWD = 1.92). The final fusion step for the biotite separate was not measurable due to instrumental issues, and the biotite does not yield a true age plateau in the sense of Fleck *et al.* (1977), i.e. 3 or more contiguous heating steps comprising 50% or more of the ^{39}Ar released and overlapping at the 2 sigma confidence level. Our calculated age for the BH13 biotite is 1405.4 ± 1.3 Ma (MSWD = 0.84) and is based on 7 contiguous steps that overlap at the 2 sigma level and represent just under 40% of the released gas; therefore we are confident that this represents an accurate age. Both these ages are significantly younger than the U-Pb zircon age for the same sample of 1456 ± 5 Ma.

Rb-Sr age

The amphibole, biotite and feldspar separates from Rønne Granite sample BH13 yield a poorly-defined 3-point errorchron, giving an age of 1378 ± 110 Ma with a high MSWD; addition of the whole rock sample improves the error on the age (1372 ± 33 Ma), yet the MSWD remains high suggesting disequilibrium or alteration of some mineral phases (Table 4). The Rb-Sr age in this study is primarily defined by the highly radiogenic biotite separate (^{87}Sr/^{86}Sr = 3.94) and various 2-point isochrons can be calculated using different minerals or by assuming an initial ^{87}Sr/^{86}Sr within geologically reasonable limits. These calculations all result in ages of around 1370 ± 14 Ma.

Discussion

Zircon ages

The U-Pb zircon ages presented here confirm the results of Zariņš & Johansson (2009) and indicate that all granitic magmatism on Bornholm took place over a relatively restricted period at 1.45 Ga. This event includes the previously undated Maegård Granite that, despite its textural contrasts with other Bornholm felsic basement lithologies, was emplaced during the same event. There is no evidence for an older and younger suite of granitoids as proposed by Micheelsen

Table 4: Rb-Sr isotope data for mineral separates and whole rock powder for sample BH13 from the Rønne Granite

Sample	^{87}Rb/^{86}Sr	2SE%	^{87}Sr/^{86}Sr	2SE%	
BH13 Biotite	164.3	0.012	3.9432	0.0006	
BH13 Amphibole	2.995	0.476	0.77779	0.0011	
BH13 Feldspar	2.18	0.032	0.74913	0.0011	
BH13 Whole rock	2.356	0.023	0.75695	0.0014	
Age calculations	**Age (Ma)**	**error (Ma)**	**^{87}Sr/^{86}Sr$_{(i)}$**	**error**	**MSWD**
Bio+Amp+Fsp+whole rock	1372	33	0.712	0.016	516
Bio+Amp+Fsp	1372	110	0.713	0.082	1032
Bio+whole rock	1372	14	0.71059	0.00065	na
Bio+Amp	1369	14	0.719	0.00083	na
Bio+Fsp	1374	14	0.70618	0.0006	na
Bio model	1375	13	0.703		na
Bio model	1364	13	0.73		na

Bio = biotite, Amp = amphibole, Fsp = feldspar. na = not applicable. Ages were calculated in Isoplot (Ludwig 2003) assuming reproducibilities of 1% for ^{87}Rb/^{86}Sr and 0.003% for ^{87}Sr/^{86}Sr (Waight *et al.* 2002a,b). The model ages are calculated assuming initial ^{87}Sr/^{86}Sr ratios of 0.703 and 0.730. Errors on measured Rb/Sr and ^{87}Sr/^{86}Sr are based on in-run statistics.

(1961) and Berthelsen (1989). Furthermore, our zircon dating of additional gneissic lithologies to those studied by Zariņš & Johansson (2009) has failed to identify any older 1.8 Ga basement lithologies on Bornholm, as observed to the north in southern Sweden in the Blekinge Province (e.g. Johansson & Larsen, 1989; Johansson *et al.* 2006). The relatively low abundance of inherited zircons in the Bornholm granitoids suggests that basement of this age was not significantly involved as a source region or contaminant during granitic magmatism. Callisen (1956), Platou (1970) and Friis (1996) described occurrences of high-grade metasedimentary inclusions (muscovite-bearing quartz-rich gneisses, quartzite, garnet-epidote and wollastonite skarns) between Gudhjem and Svaneke along the north coast of Bornholm, in Rønne Granite, Vang Granite, and near Paradisbakkerne, that potentially represent older sediments. However, without more detailed chronological investigations their provenance and relationship to older basement lithologies elsewhere in Scandinavia remains unknown.

A geological history on Bornholm where the gneissic rocks represent older metamorphic basement and the less deformed to undeformed granitoids represent younger intrusions is not confirmed by the available modern geochronological data. Instead, there is no statistical difference in age between essentially undeformed granitoids (e.g. Rønne and Maegård),

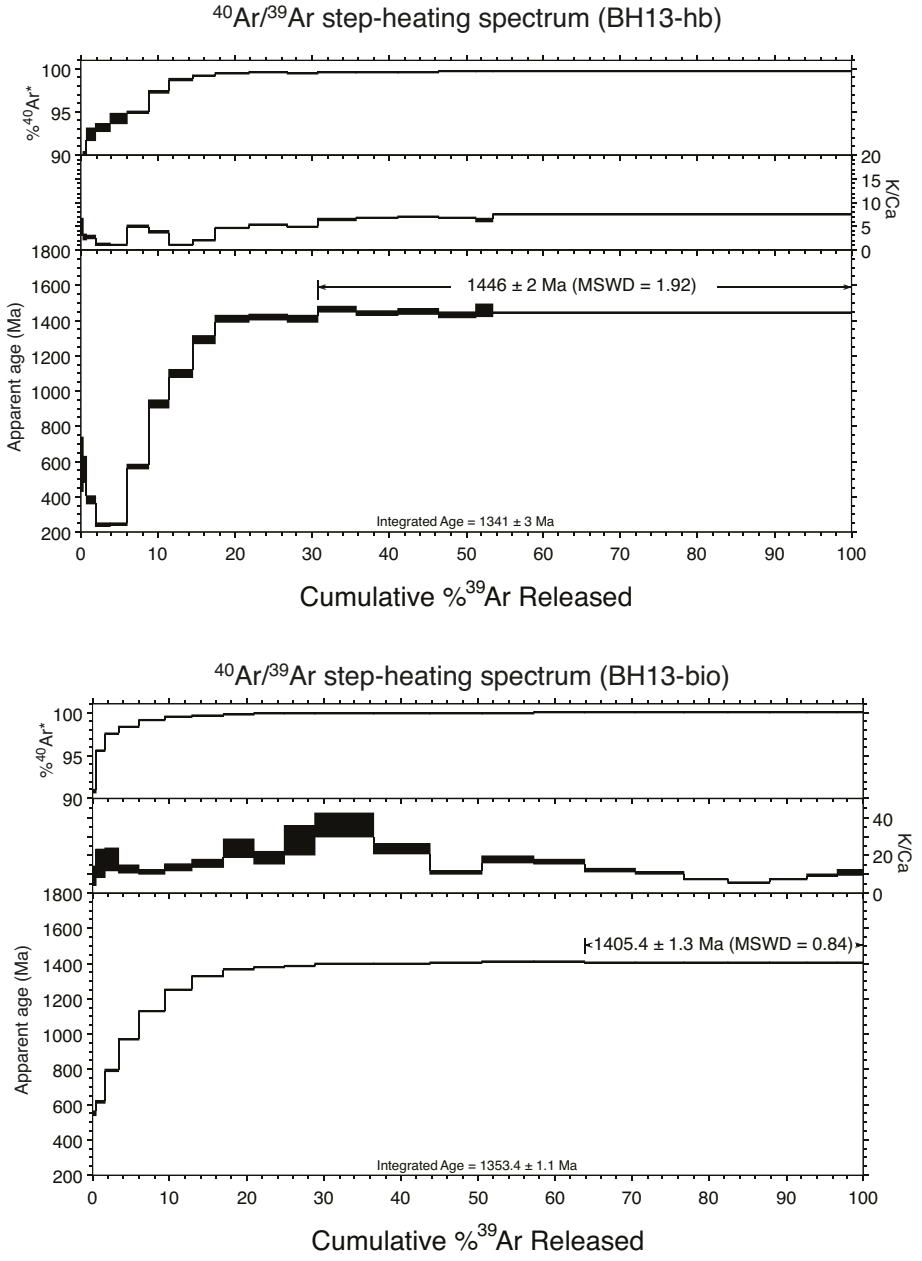

Fig 5. ^{40}Ar-^{39}Ar laser step heating age spectra for amphibole (BH13-hb) and biotite (BH13-bio) from the Rønne Granite. Boxes represent individual steps and two sigma errors.

more deformed granitoids such as Svaneke, and gneisses with clear metamorphic fabrics such as BH1 from Knarregård. Therefore, magmatism, deformation, and metamorphism must have occurred largely 'simultaneously' at *c.* 1.45 Ga. We note however that these deformational and magmatic events may have occurred over a period of up to 20 Ma given the errors of the geochronological techniques used here. Petrographically and geochemically the gneisses and granitoids resemble each other and can be broadly grouped into either relatively felsic biotite granitoids/gneisses (e.g. Hammer Granite, Almindingen Granite, Rutsker gneiss) or more intermediate amphibole-bearing lithologies (e.g. Rønne Granite, Vang Granite, Knarregård gneiss) (e.g. Berthelsen 1989; Waight & Bogdanova unpublished data). It is therefore likely that the basement lithologies on Bornholm represent a multiphase magmatic event that occurred in part contemporaneously with deformation. The distinction between the gneiss and granitoid on Bornholm is therefore primarily a consequence of varying degrees of fabric development and does not represent different intrusive events. In fact, many of the basement lithologies defined as granitoid also show signs of fabric development, likely a consequence of deformation at mid-lower crustal conditions during the later stages of crystallization and/or immediately post-solidus. Fabric development likely represents deformation of slightly older intrusions (either at close to solidus or subsolidus conditions) during emplacement of slightly younger plutons. Similar arguments have been presented based on detailed structural, textural, and magnetic susceptibility studies of the contemporaneous Karlshamn pluton in southern Sweden (Čečys & Benn 2007).

Pb loss

A number of samples show evidence for substantial Palaeozoic to recent Pb loss. The sample most affected by Pb loss is BH8 from the Almindingen Granite. This sample was collected from a large loose block located near to a crosscutting, NW-trending mugearite (kullaite) dike (Jensen 1988; Obst 2000). Holm *et al.* (2010) have suggested that the NW-trending dikes on Bornholm are relatively young (*c.* 300 Ma). This age is close to the age of Pb loss at Almindingen as defined by the lower intercept age of 392 ± 38 Ma (Fig. 3A) and we suggest that Pb loss in this sample was a result of thermal disturbance during dike emplacement. However, it is also interesting to note that in contrast sample BH3b collected *c.* 50 m from the Kelseå dike (1326 Ma; Holm *et al.* 2010) and BH6 collected within 10-20 m of the Listed Dike (950 Ma; Holm *et al.* 2010) show limited evidence for Pb loss, despite the relatively large size of the nearby dikes. Furthermore, the sample of Almindingen Granite analysed by Zariņš & Johansson (2009) was collected from the same quarry as BH8 yet exhibits little evidence for Pb loss.

Cooling and uplift

The wide range in ages (1.46–1.37 Ga) recorded using different isotope systems and mineral phases within a single sample (BH13) from the Rønne Granite is consistent with the wide scatter of ages that have been presented using different isotopic systems on Bornholm and elsewhere in southern Scandinavia (see Obst *et al.* 2004 for a summary). For example, the various two-point biotite ages calculated in this study (Table 4) of *c.* 1370 Ma are in good agreement with unpublished Rb-Sr mineral-whole rock ages for the Rønne Granite (1372 ± 9 Ma) and Vang Granite (1347 ± 12 Ma) (Tschernoster 2000 in Obst *et al.* 2004). These ages are also in broad agreement with mineral - whole rock ages for various intrusions on Bornholm and elsewhere that range between 1240 and 1380 Ma and are clearly younger than U-Pb zircon ages on the same lithologies (see Obst 2004). As the ages from different isotope systems presented in this study are based on a single sample, we can assume that this range in temperatures reflects variations in the closure temperatures for different minerals and different isotopic systems and therefore use this information to place constraints on the cooling and uplift history of Bornholm in the Proterozoic.

Sources for closure temperature estimates used here are taken in part from the compilations made by Villa (1998) and Willigers *et al.* (2001). Assumed closure temperatures used are: U-Pb in zircon = 900+°C (Lee *et al.* 1997); K-Ar in amphibole = 600°C (Kamber *et al.* 1995; Villa 1998); K-Ar in biotite = 450°C (Villa 1998); and Rb-Sr in biotite = 300°C (Dodson 1973), although we note that even lower closure temperatures for Rb-Sr in biotite (<200°C) have been suggested (e.g. Brabander & Giletti 1995). We use the biotite-whole rock 2-point isochron as a best estimate of the age at which biotite closed to Sr isotopic diffusion with the whole rock composition. Use of any of the other 2-point isochron ages has little consequence for the results, and we discuss the possible origins of the failure of the combined mineral and whole rock data to form an isochron below. Combined, the closure temperatures and ages presented above define a potential cooling curve for the Rønne Granite, and by inference, for the entire basement block of Bornholm (Fig. 6). Combining the geochronological data with assumed closure temperatures presented above (solid symbols in Fig. 6) suggests a period of relatively rapid cooling of at least 30°C per million years immediately following

emplacement of the granitoid and crystallisation of zircon and down to the closure of the K-Ar system in amphibole at *c.* 600°C. This initial period of rapid cooling was followed by cooling from *c.* 600°C at a rate that was around an order of magnitude slower (4°C per million years) until closure of the Sr system in biotite at around 300°C.

We note that potential errors in the decay constant of ^{40}K have not been taken into account in our age calculations. Recent studies have highlighted potential problems caused by uncertainties in decay constants when comparing ages determined using different decay schemes. In particular, these uncertainties result in a potential bias such that $^{206}Pb/^{238}U$ ages can be up to 0.5% older than ^{40}Ar-^{39}Ar ages in the same sample for rocks of approximately the same age as those on Bornholm (Renne *et al*. 2010). Taking this into account, it is thus possible that the U-Pb zircon and ^{40}Ar-^{39}Ar amphibole age on the Rønne Granite are effectively the same within analytical error, as illustrated in Fig. 6. However, it is important to note that the differences between the biotite and amphibole ^{40}Ar-^{39}Ar age determinations are unaffected by decay constant complications and therefore this age difference is real and must be a consequent of different closure temperatures.

Zariņš & Johansson (2009) report U-Pb ages for titanite from a number of Bornholm basement samples, although not specifically from the Rønne Granite where titanite is absent to sparse. Concordia ages for titanite range from 1452 ± 11 Ma (red orthogneiss at Gudhjem) to 1437 ± 18 Ma (Vang) (average = 1445 Ma, n=5) and are generally within error of, or slightly younger than, the U-Pb zircon age from the same samples. Closure temperatures for U-Pb in titanite are somewhat lower than for zircon and estimated at 670°C by Dahl (1997). As shown in Fig. 6, this lower closure temperature is consistent with the U-Pb ages and Ar age in amphibole representing isotopic closure during relatively rapid cooling following emplacement and crystallisation of the granitoids.

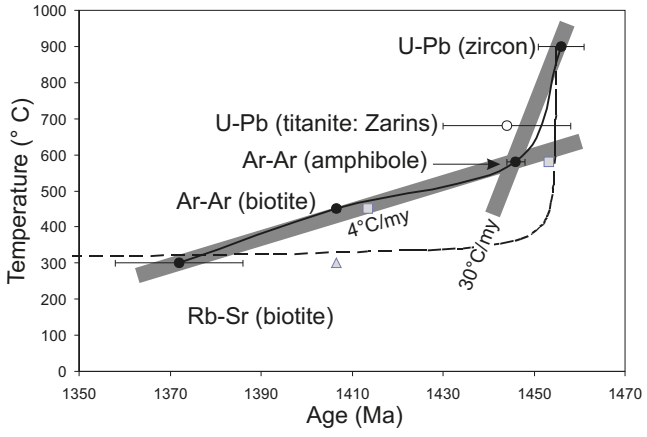

Fig. 6. Cooling history for the Rønne Granite (see text for discussion). Solid line represents a cooling curve predicted using recent literature values for closure temperatures (solid symbols). The open circle represents U-Pb ages on titanite from Zariņš & Johansson (2009). The dashed line represents a cooling curve modelled using the one dimensional heat conduction equation (e.g. Stuŵe 2007) assuming a temperature drop from 900°C to 300°C at emplacement depths of 10 km and assuming a thermal conductivity constant of $10^{-6}m^2s^{-1}$. The grey squares represent the effect of increasing the Ar age for amphibole and biotite by 0.5% to account for potential discrepancies between the decay constants for U-Pb and K-Ar. The grey triangle represents the Ar biotite age assuming a lower closure temperature of 300°C.

Emplacement conditions of the Rønne Granite are estimated at *c.* 750°C and 3.1 kb (around 10 km) using Al-in-amphibole contents and calculated using the spreadsheet of Anderson *et al.* (2008), and using the plagioclase-hornblende geothermobarometers of Blundy & Holland (1990) and Andersen & Smith (1995) (Waight, unpublished data). These data suggest that the initial period of cooling was associated with the initial emplacement and crystallisation of the granitoids. All deformation of the granitoids and gneisses must also have occurred during this period and at these pressure-temperature conditions, based on the overlap within error of the U-Pb zircon ages of deformed and undeformed lithologies.

Using the relatively recent closure temperatures from the literature discussed previously, the initial period of rapid cooling subsequent to emplacement was followed by cooling from *c.* 600–750°C (closure temperature for Ar in amphibole and crystallisation temperature of the granitoids). This occurred at a rate that was around an order of magnitude slower (4°C per million years) until closure of the Sr system in biotite at around 300°C. Assuming a geothermal gradient of 30°C/km, this is equivalent to an uplift rate of *c.* 0.1 mm/yr. Such relatively slow cooling rates are typical for regions of post-orogenic exhumation by erosion in the Precambrian and contrast markedly with rapid tectonic uplift of mid-deep crustal lithologies seen in Phanerozoic orogens (see Willigers *et al.* 2002 for a review and discussion). However, as discussed below, this apparent cooling curve should be viewed with caution.

Heat loss following emplacement of plutons will be dominated by conduction to the surface, and this can be modelled using the one dimensional diffusion or heat conduction equation (e.g. Stuŵe 2007). Such a curve illustrating cooling from 900°C to 300°C at emplacement depths of 10 km is shown as a dashed line in Fig. 6. This model predicts an initially relatively rapid drop in temperature over a period of < 20 Ma to around 350°C followed by near isothermal conditions

and is significantly different from the apparent cooling rate as defined primarily by the Ar age for biotite. The exact closure temperature for the Ar system in biotite is unresolved (e.g. Reno *et al.* 2012) and may be as low as *c.* 300°C in slowly cooled, fluid-bearing systems (Harrison *et al.* 1985). Allaz *et al.* (2011) have shown that minor chloritisation of biotite during uplift, retrograde metamorphism, or deuteric alteration can have important consequences for resetting Ar isotope systematic in biotite, and alteration of biotite to chlorite is common in the Bornholm granitoids. Use of this lower closure temperature places the ^{40}Ar-^{39}Ar biotite age on the cooling curve predicted by one-dimensional heat conduction. Furthermore, a potential 0.5% increase in the ^{40}Ar-^{39}Ar amphibole age to account for potential calibration issues between decay constants of the U-Pb and K-Ar systems moves the amphibole age onto the theoretical cooling curve. A similar 0.5% increase in the biotite ^{40}Ar-^{39}Ar age will just shift the age along the cooling curve. As the slope of the cooling curves are primarily defined by the Ar age on biotite, the 'true' cooling history of the Rønne Granite may lie anywhere between the two extremes presented in Fig. 6. However, as most Rb-Sr biotite ages from Bornholm are significantly younger than U-Pb zircon ages (see summary in Obst *et al.* 2004), a relatively slow cooling rate is implied. These results illustrate the complications involved in constructing cooling curves; however the clear differences between U-Pb systematics in zircon (Zariņš & Johansson 2009; this study) and Rb-Sr ages based on mica (Obst *et al.* 2004; this study) indicate that the latter cannot be used to define intrusion ages for the Bornholm granitoids. Furthermore, the Rb-Sr ages based on biotite in the granitoids also suggest that the approximate ambient temperature of the crust at the time of onset of the oldest mafic dike activity on Bornholm at *c.* 1330 Ma (Holm *et al.* 2010) was around 300°C.

Apatite fission track data from the Hammer Granite indicate that the basement on Bornholm was last uplifted through 100°C (*c.* 3 km depth assuming 30°C/km) at around 260 Ma (Hansen 1995) although the basement granites were likely exposed prior to this to provide sources for sediments such as the Cambrian Nexø sandstone. It is therefore clear from the geochronological data presented here that the crust in Bornholm has remained relatively stable for a prolonged period from *c.* 1350 Ma through to the modern day, and has not been affected significantly by subsequent tectonic events elsewhere in the region such as the Sveconorwegian or Caledonian orogenies.

The differing closure temperatures of mineral systems can also potentially explain the high MSWD for the combined mineral and whole rock Rb-Sr data for sample BH13, which clearly indicate that the sample is disturbed or that some other geological or analytical factor is involved in causing disequilibrium between coexisting phases. Brabander & Giletti (1995) have shown that the estimated closure temperatures for Sr isotopes in hornblende (*c.* 625–700° C) are higher than for Na-rich feldspar (*c.* 500° C) which are in turn higher than those estimated for biotite (300° C or lower). Variations in closure temperature, as well as the potential effects of radiogenic ingrowth during cooling, will result in variations in ages and initial isotope compositions, and therefore statistically perfect isochrons will be unlikely to be preserved.

Correlation

As stated above, the felsic basement lithologies of Bornholm were emplaced during a relatively restricted, multi-phase event at 1.45 Ga. Correlations of these rocks with intrusions of similar ages throughout southern Scandinavia as well as Eastern Europe and southwards towards Poland (drill hole G-14) have been summarised by Obst *et al.* (2004) and Zariņš & Johansson (2009), and readers are referred to those works for a more comprehensive summary of previous geochronological studies. A magmatic event at 1.45 Ga is evident throughout the western Eastern European craton and has been referred to as the Danolopolian orogeny by Bogdanova *et al.* (2008). The magmatism is linked to deformation and shearing along large-scale E–W and NW–SE trending shear zones, which commonly accommodate syntectonic granitoids. It is likely that the basement rocks of Bornholm were also emplaced into such a shear zone. Bogdanova (2001) suggested that the Danolopolian event was the result of collision between Baltica and another continental block, potentially Amazonia or another South American crustal block.

The granitoids of Bornholm and southern Sweden (e.g. Stenshuvud and Tåghusa) share chemical characteristics that suggest classification as A-type or 'within-plate granites' according to the tectonic discrimination diagrams of Pearce *et al.* (1984) (e.g. Čečys *et al.* 2002; Obst *et al.* 2004; Waight & Bogdanova, unpublished data). Within-plate granitoids are typically considered to be anorogenic, in the sense that they are not associated with crustal collision or subduction processes. Within-plate granitoids form in extensional, rift-type environments such as observed in the East African Rift and in the Oslo Rift; in post-collisional settings; or are associated with plume activity (Pearce *et al.* 1984; Eby 1990). Use of the term anorogenic can be misleading, however, as these tectonic settings may also be structurally active, as suggested by Čečys & Benn (2007), and as also indicated by the apparently contemporaneous nature of deformation and magma-

tism on Bornholm as indicated by our U-Pb geochronological results from Bornholm. If deformation is not purely extensional, but also includes a component of transtensional or transpressional shearing, then synmagmatic deformation is likely. Moreover, this may also provide a mechanism for creating space in the crust for the upwards migration and emplacement of granitoid magmas (e.g. Hutton *et al.* 1990; Hutton & Reavy 1992). More detailed structural studies are needed to further clarify the intrusive/deformational environment on Bornholm, and these may well be hampered by the limited exposure available.

Comparison between SIMS and LA-ICPMS

As a final note, the duplication of age determinations on samples from the same lithologies and, in some cases, from similar locations, in this study using LA-ICPMS and in the study of Zariņš & Johansson (2009) using ion microprobe, offers a perfect opportunity to compare the two techniques. In most cases, ages obtained on the same lithologies and/or localities in the two studies agree closely or within error, and the errors obtained on the ages (*c.* 0.5% absolute) are similar for both techniques. In those cases where the ages do not agree, the discrepancies can generally be explained by close examination of the data and as in, for example, the Almindingen Granite can be explained using well-established complications in the U-Pb zircon system such as Pb loss. The example of the Almindingen granite also illustrates the role that sample selection plays, with two samples from effectively the same locality displaying significant differences in the degree of disturbance of the zircons. A clear advantage of the LA-ICPMS method is the rapid throughput of samples and production of data with each analysis taking only a few minutes at most, compared with around 20 minutes for a typical SIMS analysis. All U-Pb data in this study were produced over an analytical session of two days, and all analyses (including standards) were run automatically following pre-programming of the points to be analysed. The main time factor involved in LA-ICPMS analysis (and SIMS for that matter) is thus sample preparation and characterisation. This rapid throughput is especially useful for provenance studies and large-scale geochronological campaigns. Advantages of the SIMS method are potentially smaller spot-sizes (down to 10 μm) although both methods typically use similar spot-sizes, and that it is much less destructive. SIMS typically evacuates pits of around 5 μm, thus making it the preferred method for valuable and unique samples such as meteorites, and leaving zircon mounts more amenable to subsequent investigations such as for Hf isotopic composition. A disadvantage to both techniques is the error on obtained ages, which are limited to around 1–1.5% absolute, in this case equating to *c.* ± 10 Ma on a 1450 Ma sample. In both this study and that of Zariņš & Johansson (2009), we were unable to make age distinctions between different intrusions. Determining the relative ages of the intrusives must therefore rely on observations of cross-cutting relationships in the field (e.g. Callisen 1934; Micheelsen 1961; Berthelsen 1989 and references therein), potentially coupled with more precise absolute age determinations through application of more time-consuming and arduous geochronological techniques, such as single-zircon and chemical abrasion TIMS methods (e.g. Mattinson 2005).

Conclusions

New LA-ICPMS U-Pb zircon ages for 11 samples of granitoid and gneiss from the Danish island of Bornholm indicate that the felsic basement was formed at 1455 ± 10 Ma. At the levels of error available using this technique no age distinction can be made between deformed gneissic samples and less deformed or undeformed granitoids, indicating that magmatism and deformation on Bornholm occurred within this relatively restricted timeframe. Analyses of several gneissic samples, combined with the previous analyses of Zariņš & Johansson (2009), have failed to identify any outcrops of 1.8 Ga basement on Bornholm. No evidence for resetting during later large-scale tectonic events has been found.

More detailed studies of a number of samples, involving analyses of up to 100 zircons from each, indicate that the degree of zircon inheritance in the Bornholm granitoids and gneisses is low (<4%), with broad peaks identified at *c.* 1.6–1.8 Ga and 1.8–1.9 Ga. These results indicate that older basement components did not play a large role as sources or contaminants during magma genesis.

Chronological studies of a single sample of the Rønne Granite using U-Pb in zircon, ^{40}Ar-^{39}Ar in amphibole and biotite, and Rb-Sr in biotite, suggest a cooling history for Bornholm that was initially relatively fast (*c.* 30° C per million years), likely indicative of the period of magma emplacement, crystallization and post-emplacement cooling. This was followed by a longer period of slower cooling or isothermic conditions, and the region appears to have first cooled through the closure temperature of Sr isotopes in biotite (*c.* 300°C) 70–90 Ma after pluton emplacement. More detailed constraints on the post-emplacement cooling history are complicated by precise definition of the closure temperature of the Ar system in biotite.

Acknowledgments

We would like to thank Peter Venslev for assistance with crushing and for excellent mineral separation work, without which this work would probably have never happened. Barry Reno is thanked for discussions on closure temperatures and cooling curves, and for providing a spreadsheet for calculating thermal conductive cooling. Anne and Clara-Marie Dyreborg are thanked for their assistance during fieldwork. The manuscript benefitted from the constructive and clarifying comments of Henrik Friis and Svetlana Bogdanova. This study was funded by a grant from the Carlsberg Foundation. QUADLAB is supported by the Villum Foundation.

References

Åberg, G. 1988: Middle Proterozoic anorogenic magmatism in Sweden and worldwide. Lithos 21, 279–289.

Allaz , J., Engi, M., Berger, A. & Villa, I.M. 2011: The effects of retrograde reactions and of diffusion on ^{40}Ar-^{39}Ar ages of micas. Journal of Petrology 52, 691–716.

Anderson, J.L. & Smith, D.R. 1995: The effect of temperature and oxygen fugacity on Al-in-hornblende barometry. American Mineralogist 80, 549–559.

Anderson, J.L., Barth, A.P., Wooden, J.L. & Mazdab, F. 2008: Thermometers and thermobarometers in granitic systems. Reviews in Mineralogy and Geochemistry 69, 121–142.

Blundy, J. D. & Holland, T. J. B. 1990: Calcic amphibole equilibria and a new amphibole-plagioclase geothermometer. Contributions to Mineralogy and Petrology 104, 208–224.

Berthelsen, A. 1989: Bornholms geologi III: Grundfjeldet. Varv 1989(1), 1–40.

Bogdanova, S. 2001: Tectonic settings of 1.65–1.4 Ga AMCG Magmatism in the Western East European Craton (Western Baltica). Journal of Conference Abstracts, EUG XI, 6, 769 only.

Bogdanova, S.V., Bingen, B., Gorbatschev, R., Kheraskova, T.N., Kozlov, V.I., Puchkov, V.N. & Volozh, Y.A. 2008: The East European Craton (Baltica) before and during the assembly of Rodinia. Precambrian Research 160, 23–45.

Brabander, D.J. & Giletti, B.J. 1995: Strontium diffusion kinetics in amphiboles and significance to thermal history determinations. Geochimica et Cosmochimica Acta 59, 2223–2238.

Brumm, A., Jensen, G.M., van der Bergh, G.D., Morwood, M.J., Kurniawan, I., Aziz, F. & Storey, M. 2010: Hominins on Flores, Indonesia, by one million years ago. Nature 464, 748–752.

Callisen, K. 1934: Das Grundgebirge von Bornholm. Danmarks Geologiske Undersøgelse II Række 50, 266 pp.

Callisen, K. 1956: Fragmenter og spor efter bjergarter ældre end graniten på Bornholm. Meddelelser fra Dansk Geologisk Forening 13, 158–173.

Callisen, K. 1957: Hornblende with pyroxene core in the Rønne granite. Meddelelser fra Dansk Geologisk Forening 13, 236–237.

Čečys, A. & Benn, K. 2007: Emplacement and deformation of the c. 1.45 Ga Karlshamn granitoid pluton, southeastern Sweden, during ENE–WSW Danopolonian shortening. International Journal of Earth Sciences 96, 397–414.

Čečys, A., Bogdanova, S., Jansson, C., Bibikova, E. & Kornfält, K.-A., 2002: The Stenshuvud and Tåghusa granitoids: new representatives of Mesoproterozoic magmatism in southern Sweden. Geologiska Föreningens i Stockholm Förhandlingar 124, 149–162.

Dahl, P.S. 1997: A crystal-chemical basis for Pb retention and fission tracks annealing systematics in U-bearing minerals, with implications for geochronology. Earth and Planetary Science Letters 150, 277–290.

Dodson, M.H. 1973: Closure temperatures in cooling geochronological and petrological systems. Contributions to Mineralogy and Petrology 40, 259–274.

Eby, G.N. 1990: The A-type granitoids: A review of their occurrence and chemical characteristics and speculations on their petrogenesis. Lithos 26, 115–134.

Fleck, R.J., Sutter, J.F. & Elliot, D.H. 1977: Interpretation of discordant ^{40}Ar-^{39}Ar age-spectra of Mesozoic tholeiites from Antarctica. Geochimica et Cosmochimica Acta 41, 15–32.

Frei, D. & Gerdes, A. 2009: Precise and accurate in situ U–Pb dating of zircon with high sample throughput by automated LA-SF-ICPMS. Chemical Geology 261, 261–270.

Friis, H. 1996: A quartzite inclusion in the Rønne Granite - the first Danish sediment. Bulletin of the Geological Society of Denmark 43, 4–8.

Gerdes, A. & Zeh, A. 2006: Combined U-Pb and Hf isotopes LA-(MC)-ICP-MS analyses of detrital zircons: comparison with SHRIMP and new constraints for the provenance and age of an Armorican metasediment in Central Germany. Earth and Planetary Science Letters 249, 47–61.

Gorbatschev, R. & Bogdanova, S. 1993: Frontiers in the Baltic Shield. Precambrian Research 64, 3–21.

Graversen, O. 2009: Structural analysis of superposed fault systems of the Bornholm horst block, Tornquist Zone, Denmark. Bulletin of the Geological Society of Denmark 57, 25–49.

Gravesen, P. 1996: Geologisk set – Bornholm. Geografforlaget: Brenderup, 208 pp.

Hansen, K. 1995: Fennoscandian Border zone: thermal and tectonic history of a tuffaceous sandstone and granite from fission track analysis, Bornholm, Denmark. Tectonophysics 244, 153–160.

Harrison, T.M., Duncan, I., & McDougall, I. 1985: Diffusion of ^{40}Ar in biotite: Temperature, pressure and compositional effects. Geochimica et Cosmochimica Acta 49, 2461–2468.

Holm, P.M., Pedersen, L.E. & Højsteen, B. 2010: Geochemistry and petrology of mafic Proterozoic and Permian dykes on Bornholm, Denmark: Four episodes of magmatism on the margin of the Baltic Shield. Bulletin of the Geological Society of Denmark 58, 35–65.

Hutton, D.H.W. & Reavy, R.J. 1992: Strike-slip tectonics and granite petrogenesis. Tectonics 11, 960–967.

Hutton, D.H.W., Dempster, T.J., Brown, P.E. & Becker, S.D. 1990: A new mechanism of granite emplacement – intrusion in active extensional shear zones. Nature 343, 452–455.

Jensen, A. 1988: The Bjergebakke dyke - a kullaite from Bornholm. Bulletin of the Geological Society of Denmark 37, 123–140.

Johansson, Å. & Larsen, O. 1989: Radiometric age determinations and Precambrian chronology of Blekinge, southern Sweden. Geologiska Föreningens i Stockholm Förhandlingar 111, 35–50.

Johansson, Å., Bogdanova, S. & Čecys, A., 2006: A revised geochronology for the Blekinge Province, southern Sweden. GFF 128, 287–302.

Kamber, B.S., Kramers, J.D., Napier, R., Cliff, R.A. & Rollinson, H.R. 1995: The triangle shear zone, Zimbabwe, revisited: new data document and important event at 2.0 Ga in the Limpopo Belt. Precambrian Research 70, 191–213.

Kornfält, K-A. 1993: U-Pb zircon ages of three granite samples from Blekinge County, south-eastern Sweden. Sveriges Geologiske Undersøgelse Serie C 823, 17–23.

Kornfält, K-A. 1996: U-Pb zircon ages of six granite samples from Blekinge County, southeastern Sweden. Sveriges Geologiske Undersøgelse Serie C 828, 15–31.

Larsen, O. 1971: K/Ar Age determinations from the Precambrian of Denmark. Danmarks Geologiske Undersøgelse II Række 97, 1–37.

Lee, J.K.W., Williams, I.S. & Ellis, D.J. 1997: Pb, U and Th diffusion in natural zircon. Nature 390, 159–162.

Ludwig, K.R., 2003: Isoplot/Ex 3.00. A geochronological toolkit for Microsoft Excel. Special Publication, vol. 4. Berkeley Geochronological Center, Berkeley, CA.

Mattinson, J.M. 2005: Zircon U–Pb chemical abrasion ("CA-TIMS") method: Combined annealing and multi-step partial dissolution analysis for improved precision and accuracy of zircon ages. Chemical Geology 220, 47– 66.

Micheelsen, H.I. 1961: Bornholms grundfjæld. Meddelelser fra Dansk Geologisk Forening 14, 308–347.

Nasdala, L., Hofmeister, W., Norberg, N., Mattinson, J.M., Corfu, F., Dörr, W., Kamo, S.L., Kennedy, A.K., Kronz, A., Reiners, P.W., Frei, D., Košler, J., Wan, Y., Götze, J,, Häger, T., Kröner, A. & Valley, J.W. 2008: Zircon M257 – a homogeneous natural reference material for the ion microprobe U-Pb analysis of zircon. Geostandards and Geoanalytical Research 32, 247–265.

Obst, K. 2000: Permo-Carboniferous dyke magmatism on the Danish island Bornholm. Neues Jahrbuch für Geologie und Paläontologie Abhandlungen 218, 243–266.

Obst, K., Hammer, J., Katzung, J. & Korich, D. 2004: The Mesoproterozoic basement in the southern Baltic Sea: insights from the G 14-1 off-shore borehole. International Journal of Earth Sciences 93, 1–12.

Pearce, J.A., Harris, N.B.W., Tindle, A.G. 1984: Trace element discrimination diagrams for the tectonic interpretation of granitic rocks. Journal of Petrology 25, 956–983.

Platou, S.W. 1970: The Svaneke Granite Complex and the gneisses on East Bornholm. Bulletin of the Geological Society of Denmark 20, 93–133.

Renne, P.R., Mundil, R., Balco, G., Min, K. & Ludwig, K.R. 2010: Joint determination of ^{40}K decay constants and $^{40}Ar^*/^{40}K$ for the Fish Canyon sanidine standard, and improved accuracy for $^{40}Ar/^{39}Ar$ geochronology. Geochimica et Cosmochimica Acta 74, 5349–5367.

Reno, B.L., Piccoli, P.M., Brown, M. & Trouw, R.A.J. 2012: In situ monazite (U–Th)–Pb ages from the Southern Brasília Belt, Brazil: constraints on the high-temperature retrograde evolution of HP granulites. Journal of Metamorphic Geology 30, 81–112.

Rivera, T.A., Storey, M., Zeeden, C., Hilgen, F. & Kuiper, K. 2011: A refined astronomically calibrated $^{40}Ar/^{39}Ar$ age for Fish Canyon sanidine. Earth and Planetary Science Letters 311, 420–426.

Simon, E., Jackson, S.E., Pearson, N.J., Griffin, W.L. & Belousova, E.A. 2004: The application of laser ablation-inductively coupled plasma-mass spectrometry to in situ U–Pb zircon geochronology. Chemical Geology 211, 47–69.

Sircombe, K.N. 2004: AgeDisplay: an EXCEL workbook to evaluate and display univariate geochronological data using binned frequency histograms and probability density distributions. Computers and Geosciences 30, 21–31.

Sláma, J., Košler, J., Condon, D.J., Crowley, J.L., Gerdes, A., Hanchar, J.M., Horstwood, M.S.A., Morris, G.A., Nasdala, L., Norberg, N., Schaltegger, U., Schoene, B., Tubrett, M.N. & Whitehouse, M.J. 2008: Plešovice zircon – a new natural reference material for U-Pb and Hf isotopic microanalysis. Chemical Geology 249, 1–35.

Stuŵe, K. 2007: Geodynamics of the Lithosphere. Springer: Berlin, Heidelberg, 504 pp.

Tschernoster, R. 2000: Isotopengeochemishe untersuchungen am detritus der Dänisch-Norddeutsch-Polnischen Kaledoniden und deren Vorland. Unpublished Ph.D. thesis, Rheinisch-Westfälischen Technischen Hochschule, Aachen, 128 pp.

Villa, I.M. 1998: Isotopic closure. Terra Nova 10, 42–47.

Waight, T.E., Baker, J.A. & Peate, D.W. 2002a: Sr isotope ratio measurements by double focusing MC-ICPMS: techniques, observations and pitfalls. International Journal of Mass Spectrometry 221, 229–244.

Waight, T.E., Baker, J.A. & Willigers, B.J.A. 2002b: Rb isotope dilution analyses by MC-ICPMS using Zr to correct for mass fractionation: towards improved Rb-Sr geochronology? Chemical Geology 186, 99–116.

Willigers, B.J.A., Krogstad, E.J. & Wijbrans, J.R. 2001: Comparison of thermochronometers in a slowly-cooled granulite terrain: Nagssugtoqidian Orogen, West Greenland. Journal of Petrology 42, 1729–1749.

Willigers, B.J.A., van Gool, J.A.M., Wijbrans, J.R., Krogstad, E.J. & Mezger, K. 2002: Posttectonic cooling of the Nagssugtoqidian Orogen and a comparison of contrasting cooling histories in Precambrian and Phanerozoic Orogens. Journal of Geology 110, 503–517.

Zariņš, K. & Johansson, Å. 2009: U–Pb geochronology of gneisses and granitoids from the Danish island of Bornholm: new evidence for 1.47–1.45 Ga magmatism at the southwestern margin of the East European Craton. International Journal of Earth Science 98, 1561–1580.

The middle Danian Faxe Formation – new lithostratigraphic unit and a rare taphonomic window into the Danian of Denmark

BODIL WESENBERG LAURIDSEN, MORTEN BJERAGER & FINN SURLYK

Lauridsen, B.W., Bjerager, M. & Surlyk, F. 2012. The middle Danian Faxe Formation – new lithostratigraphic unit and a rare taphonomic window into the Danian of Denmark. © 2012 by Bulletin of the Geological Society of Denmark, Vol. 60, pp. 47–60. ISSN 0011–6297 (www.2dgf.dk/publikationer/bulletin).

The new middle Danian Faxe Formation is defined on the basis of the succession exposed in the large Faxe quarry in eastern Denmark. The formation is defined as a distinct mappable lithostratigraphic unit of interfingering coral and bryozoan limestone passing laterally into bryozoan limestones of the Stevns Klint Formation. The Baunekule facies is recognized in the upper part of the coral mound complex of the Faxe Formation, where it forms isolated lensoidal bodies in the flanks of some of the coral mounds. It is characterised by a high diversity invertebrate fauna with both calcite and originally aragonite-shelled benthic invertebrates set in weakly consolidated coral-dominated floatstone to rudstone. The diagenesis of the Baunekule facies is of special significance because a high proportion of the originally aragonite-shelled fauna is preserved by recrystallization to calcite during early burial diagenesis. More than 80% of the species from the Baunekule facies are unknown from other parts of the Faxe Formation. The carbonate mud matrix is only slightly consolidated and the invertebrate fossils are accordingly easy to prepare in contrast to the fossils from the lithified parts of the Faxe Formation, which are commonly only preserved as moulds or casts. The facies therefore presents an exceptional taphonomic window into a cold-water coral mound fauna, giving an unusually complete picture of the diversity and density of the shelly invertebrate fauna.

Keywords: Faxe Formation, Baunekule facies, Danian, Denmark, coral limestone, fossil invertebrates, taphonomy.

Received 7 February 2012
Accepted in revised form
10 September 2012
Published online
2 October 2012

Bodil Wesenberg Lauridsen [Bodill@geo.ku.dk; bwl@geus.dk], Finn Surlyk [Finns@geo.ku.dk], Department of Geography and Geology, University of Copenhagen, Øster Voldgade 10, DK-1350 Copenhagen K, Denmark. Morten Bjerager [mbj@geus.dk], Geological Survey of Denmark and Greenland, Øster Voldgade 10, DK-1350 Copenhagen K, Denmark.

A new kind of bryozoan biogenic mounds developed in the Danish Basin in the early Danian shortly after the mass extinction at the Cretaceous/Paleogene (K/T or K/PG) boundary (Thomsen 1995; Surlyk 1997; Surlyk *et al.* 2006; Bjerager & Surlyk 2007a, b; Nielsen *et al.* 2008). In the middle Danian a low diversity azooxanthellate scleractinian coral fauna started to form extensive cold-water coral mound complexes intercalated with bryozoan mounds (Cheetham 1971; Floris 1980; Bernecker and Weidlich 1990, 2005; Willumsen 1995; Bjerager *et al.* 2010). The coral mounds started to grow in relatively deep water below the photic zone over the easternmost part of the Ringkøbing-Fyn High only 2 myr after the mass extinction at the K/T boundary (Fig. 1).

The basal Danian Fiskeler Member and the overlying Cerithium Limestone Member of the Rødvig Formation are followed by bryozoan limestone of the Stevns Klint Formation, the København Limestone Formation, and the Selandian Lellinge Greensand Formation and its correlatives (Fig. 2; Surlyk *et al.* 2006). The cold-water coral mound complex exposed in the Faxe quarry in eastern Denmark is a distinct rock unit which is not included in the Stevns Klint Formation and is covered by the new Faxe Formation defined here (Fig. 2).

Other middle Danian cold-water coral mounds occur at Limhamn in southern Sweden (Brotzen 1959; Cheetham 1971; Holland and Gabrielson 1979). Danian coral limestones are known from boreholes in southern Sjælland and Sweden and are recognized in seismic sections and in cores in the Øresund region (Ødum 1928; Rosenkrantz 1937; Jakobsen *et al.* 1997; Bjerager *et al.* 2010). Framebuilding corals from West

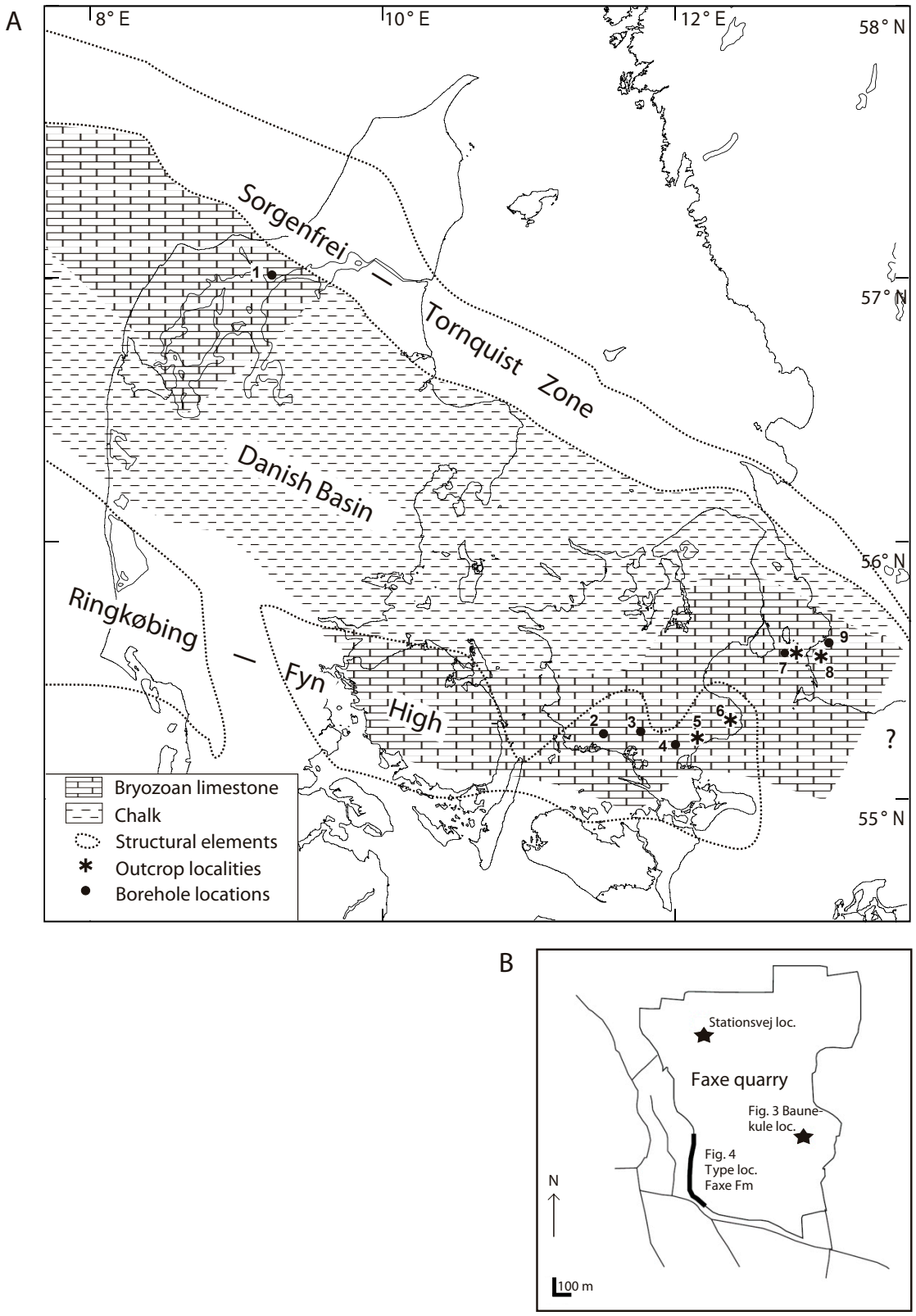

Fig. 1. **A**, Map of the Danish Basin with the main structural elements and distribution of middle Danian bryozoan limestone and chalk (coccolith zone 5 of Thomsen 1995). Locations of selected outcrops and boreholes where middle Danian coral limestone has been encountered: 1, Aggersborggaard; 2, Spjellerup; 3, Herlufsholm; 4, Everdrup; 5, Faxe quarry; 6, Stevns Klint; 7, Flinterenden-Trindelrenden, Øresund (both outcrop and boring); 8, Limhamn quarry; 9, Malmø. **B**, Map of Faxe quarry with the type section of the Faxe Formation and the position of the Baunekule facies indicated. Modified from Bjerager *et al.* (2010).

Greenland are of Danian age, but the dating is uncertain and based on bivalves (Floris 1972). They mainly occur in low monospecific thickets in tuff with only a very limited distribution, and without evidence of calcareous algae. The by far most extensive Danian mound complex is thus the one found in Faxe.

The lithological characteristics are key factors when defining a formation and according to articles 24e and 30f of the North American Stratigraphic Code (ACSN, 2005) a series of organic reefs and carbonate mounds can be distinguished formally as lithostratigraphic units if they are distinct from their surroundings and have a clear stratigraphic position. In that case the fossil content is a diagnostic lithologic property. This approach is followed here. The new Faxe Formation represents a mound complex with a faunal composition of mainly framebuilding corals markedly different from the Stevns Klint Formation which is predominantly composed of mound-forming bryozoans. The Baunekule facies defined here differs from the rest of the Faxe Formation with respect to its palaeontological composition and special diagenesis.

The aim of this study is to define the Faxe Formation as a new lithostratigraphic unit which passes laterally into the bryozoan limestone of the Stevns Klint Formation, to describe a special Baunekule facies, and to highlight the important taphonomic characteristics of this facies.

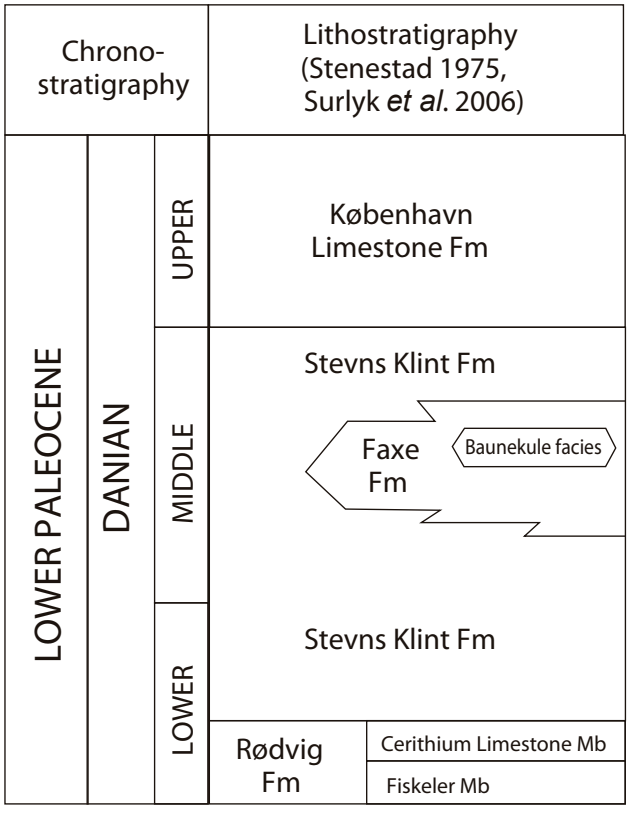

Fig. 2. Stratigraphic scheme of the Danian in the Danish Basin showing the position of the new Faxe Formation and Baunekule facies.

Faxe quarry

The middle Danian limestone exposed in the Faxe quarry represents an extraordinary preservation of a 63 Ma old cold-water coral mound complex (Fig. 1). Coral mounds occur intercalated with smaller bryozoan mounds and are exposed in mainly N–S and E–W oriented profiles. Bryozoan mounds dominate the stratigraphically lower parts and are overlain by interfingering coral and bryozoan mounds. The coral limestone is topped by an extensive hardground with pronounced topographic relief. Coarse-grained bryozoan grainstone rests locally directly on the hardground and fills fissures in the coral limestone (Willumsen 1995). The youngest preserved Danian deposits exposed in the northern end of the quarry are large-scale cross-bedded, flint-free and moderately sorted bryozoan skeletal packstone and grainstone.

The corals from Faxe are termed cold-water corals because they belong to the group of azooxanthellate corals which in modern settings live in cold and commonly deep waters. Their optimal environmental conditions in modern settings are sites with upwelling of cold waters, constant or periodic flow of water, hard substrate, and high zoo- and phytoplankton production in the surface waters. Cold-water corals are therefore commonly concentrated on ridges or rocky outcrops where currents are accelerated (Roberts *et al*. 2006). Modern cold-water coral mounds are long-lived structures where growth is balanced by (bio)erosion to form local topographic highs that alter the hydrodynamic and sedimentary regimes, trap sediment, and provide structural habitats for many other species (Roberts *et al*. 2009). Accordingly, cold-water coral mounds are topographic seafloor structures that have formed over long geological time spans through successive periods of individual mound development, deposition and (bio)erosion. The mound complexes typically contain stratified successions of mound deposits separated by non-mound deposits and erosion surfaces (Roberts *et al*. 2009).

The Faxe quarry exposes a large mound complex that includes individual coral mound bodies. The cold-water corals of the formation lived in a carbonate sedimentary regime devoid of hermatypic corals and algae, and non-skeletal chlorozoan grains are absent. The mound complex is dominated by the framebuilding scleractinian coral species *Dendrophyllia candelabrum* (Hennig 1899) with common *Faksephyllia faxoensis* (Lyell 1837) and a minor content of *Oculina becki* (Nielsen

1922). Modern *Dendrophyllia* and *Oculina* live in cold to cool and commonly deep oceanic waters (Freiwald *et al*. 2004). The modern cold-water corals are generally found in water depths of 50–1000 m at high latitudes and at depths down to 4000 m beneath warm water masses at low latitudes (Roberts *et al*. 2006). Species of *Dendrophyllia* are known to form mounds in the Mediterranean today (Zibrowius 1980) and modern *Oculina* mounds occur offshore Florida where they are believed to form the only extant deepwater *Oculina* mounds (Reed 2002). *Faksephyllia* is only known from the middle Danian of northern Europe (Floris 1980; Bernecker & Weidlich 1990, 2005) and the Danian of West Greenland (Floris 1972). The genus *Dendrophyllia* has been reported from the Upper Cretaceous (Baron-Szabo 2008). However, *D. candelabrum* was not mound-forming before the middle Danian. Other Late Cretaceous scleractinian framebuilding corals are rare and the Danian cold-water coral mound complex at Faxe is possibly the oldest and best developed mound complex of its kind.

A high diversity invertebrate fauna is associated with the coral mound complex of the Faxe Formation. The degree of preservation is extremely variable. In rare cases the aragonite-shelled fossils were, however, recrystallized to calcite during very early burial. Early in the 19th century J.P.J. Ravn found a specific facies which was later informally referred to as 'næsekalk' (nose limestone) because the main outcrop looked like Ravn's nose (Fig. 3). It is here termed the Baunekule facies and contains abundant solitary scleractinian corals and octocorals of the genus *Moltkia*. Framebuilding corals are rare with *Oculina becki* being the most prominent. In addition, the facies contains a high diversity and extremely well preserved fauna.

Most of the older studies are taxonomic descriptions of the rich fauna (Table 1), whereas only a few studies have dealt with the stratigraphy, sedimentology and palaeoecology of the coral mound complex in Faxe (Rosenkrantz 1937; Asgaard 1968; Floris 1972, 1980; Jørgensen 1988; Bernecker and Weidlich 1990, 2005; Willumsen 1995).

Table 1. List of publications dealing with the Faxe fauna; 10 out of the 55 publications are based solely on the fossils from the Baunekule facies. The full references are given in the reference list.

Class	Baunekule facies	Other facies in the Faxe Formation
Porifera		Ravn 1899; Nielsen 1929; Rasmussen 1973; Clausen 1982
Coelenterata	Nielsen 1919	Steenstrup 1847; Nielsen 1913b, 1917, 1922, 1925a; Voigt 1958; Bernecker & Weidlich 2006
Annwelida	Nielsen 1931	
Arthropoda		Darwin 1851; Nielsen 1912; Jakobsen 2003; Jakobsen & Feldmann 2004; Collins & Jakobsen 1994; Jakobsen & Collins 1997
Mollusca, Bivalvia	Ravn 1902a, 1933	Lundgren 1867
Mollusca, Gastropoda	Ravn 1902b, 1933; Schilder, 1928; Schnetler *et al.* 2001; Schnetler & Petit 2006	Lundgren 1867
Mollusca, Polyplacophora	Sigwart *et al.* 2007	
Bryozoa		Pergens & Meunier 1886; Levinsen 1925; Voigt 1923; Berthelsen 1962; Cheetham 1971
Brachiopoda	Nielsen 1911	Lundgren 1867; Posselt 1894; Nielsen 1909, 1914, 1921, 1928; Asgård; 1968, 1970
Echinodermata, Crinoidea and Asteroidea		Hennig 1899; Ravn 1904; Nielsen 1913a, 1943; Rasmussen 1950, 1961, 1972, 1973; Donovan & Jakobsen 2004; Wisshak *et al.* 2009
Echinodermata, Echinoidea		Nielsen 1925b; Ravn 1927, 1928; Brotzen 1959; Gravesen 1993

Fig. 3. View from the SE of the Faxe quarry showing the earliest recorded outcrop of the Baunekule facies, in the literature termed 'Ravns Næse'. The position of the outcrop is marked with an arrow. A horse is encircled for scale. The original picture is from Milthers (1908, his plate 31). Reproduced with permission from GEUS.

Lithostratigraphy

Faxe Formation

New formation

Name. After the type locality, the Faxe quarry, eastern Denmark.

History. The coral limestone of the Faxe Formation has been known for centuries due to the extensive quarrying. In old literature the limestone is referred to as "Faxe Kalk" (Faxe limestone) by Forchhammer (1825), Desor (1847), Johnstrup (1864), Fischer-Benzon (1866), Lundgren (1867) and Milthers (1908). The coral limestone complex is here formally described as a new formation with a prominent occurrence in the Faxe area. Lower to middle Danian bryozoan limestone exposed in the Limhamn quarry in southern Sweden was named the Limhamn Member of the Höllviken Formation in a geological map description (Sivhed *et al*. 1999). The member contains small coral mounds which are here referred to the Faxe Formation together with the interfingering bryozoan limestone. The type locality of the Faxe Formation is a Danish GeoSite and is publicly accessible. More information can be found at www.geosites.dk.

Faxe is the name of the adjacent town and the word Faxe (earlier also spelled Fakse or Faxae) means the mane of a horse. Quarrying has been ongoing since mediaeval times but there are no historical accounts on when the quarry started working. However, in many of the mediaeval churches and other buildings and constructions in the Faxe area, the hard coral limestone has been used as a building stone for the last 600 to 700 years (Gravesen 2001).

Type section. The type section is the protected N–S oriented quarry wall below Geomuseum Faxe in the SW part of the quarry. It is easily accessible and shows the main part of the formation (Figs 1 and 4).

Reference sections. The E–W oriented profile in the southern quarry wall shows the lower boundary of the formation and the initial stages of individual coral mound development. Additional reference sections are exposed in the NW part of the quarry (Fig. 1).

Thickness. Boreholes from the central part of the quarry demonstrate a total thickness of up to 45 m (Floris 1980), but only 25 m are exposed below the Quaternary erosion surface at the type section. Laterally the thickness decreases to a few metres over 3–5 km and the formation passes into the bryozoan limestone of the Stevns Klint Formation of Surlyk *et al*. (2006).

Lithology and palaeontology. The Faxe Formation consists of a number of different coral limestone facies and intercalated bryozoan limestone. The dominant biogenic mound-building facies with essentially in-place fossils include mainly coral rudstone to floatstone and bafflestone (Fig. 5). Associated facies comprise a wide range of fine to coarse grainstone, packstone, and wackestone. A distinct facies in the upper part of the formation composed of a slightly consolidated coral limestone with an unusually well preserved high-diversity invertebrate fauna is termed the Baunekule facies. The intercalated bryozoan limestone facies consists of rudstone, floatstone, packstone, and wackestone.

The degree of diagenesis varies throughout the formation from extensively diagenetically altered to almost unaffected coral limestone. Early diagenesis

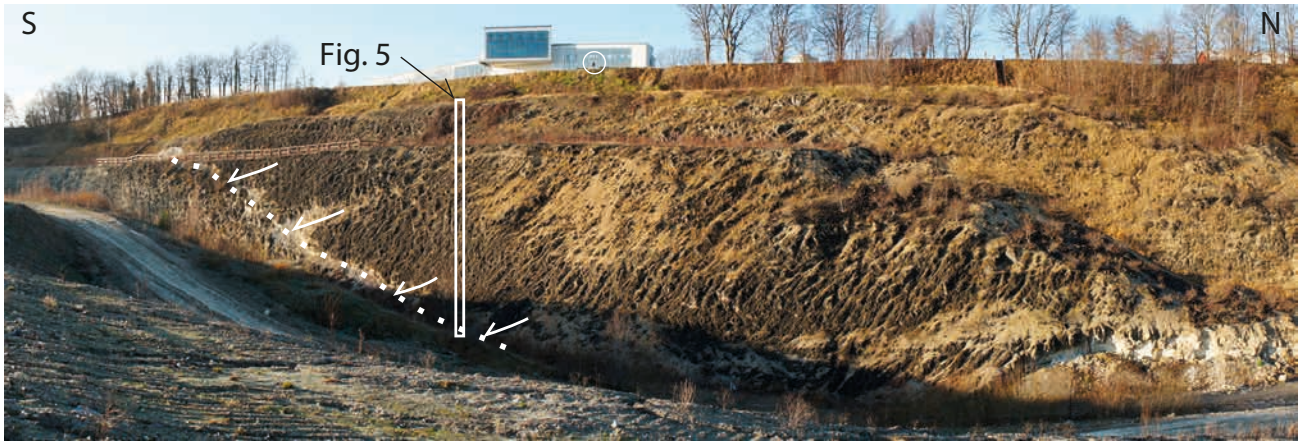

Fig. 4. Type section of the Faxe Formation in the western part of the Faxe quarry. The diachronous boundary (dotted line) between the bryozoan limestone to the left and the overlying coral limestone of the Faxe Formation is indicated. Arrows show the progressive downlap surfaces towards the south. Person is encircled for scale.

was characterised by dissolution of aragonite skeletons and associated calcite deposition and precipitation of matrix cement, cement rims, and interparticle and intraparticle replacement cements (Bernecker & Weidlich 1990; Willumsen 1995; Bjerager *et al.* 2010). Later diagenesis involved recrystallization of shells and hardening of the limestones. Diagenetically precipitated layers of flint nodules are common in the bryozoan limestones but absent from the coral limestone. In a few places meteoric quartz cement occurs in voids in the coral limestone.

The fauna of the coral limestone is dominated by the mound-forming corals *Dendrophyllia candelabrum*, *Faksephyllia faxoensis* and less common occurrences of *Oculina becki*. In addition, a rich benthic invertebrate fauna is associated with the mounds (Fig. 6). The preservation varies markedly due to large variations in diagenesis, resulting in dissolution or only rarely in recrystallization to calcite of aragonitic skeletons of corals, gastropods, bivalves, nautiloid cephalopods and annelids. These fossil groups are therefore mainly preserved either as moulds or casts. *D. candelabrum* and *F. faxoensis* are occasionally preserved in life position, whereas *O. becki* is only found as colony fragments. All corals had a bushy growth form and provided excellent habitats and feeding grounds for a large and diverse benthic invertebrate fauna. Attached brachiopods, bivalves, serpulids and moulds of decapods and gastropods are common.

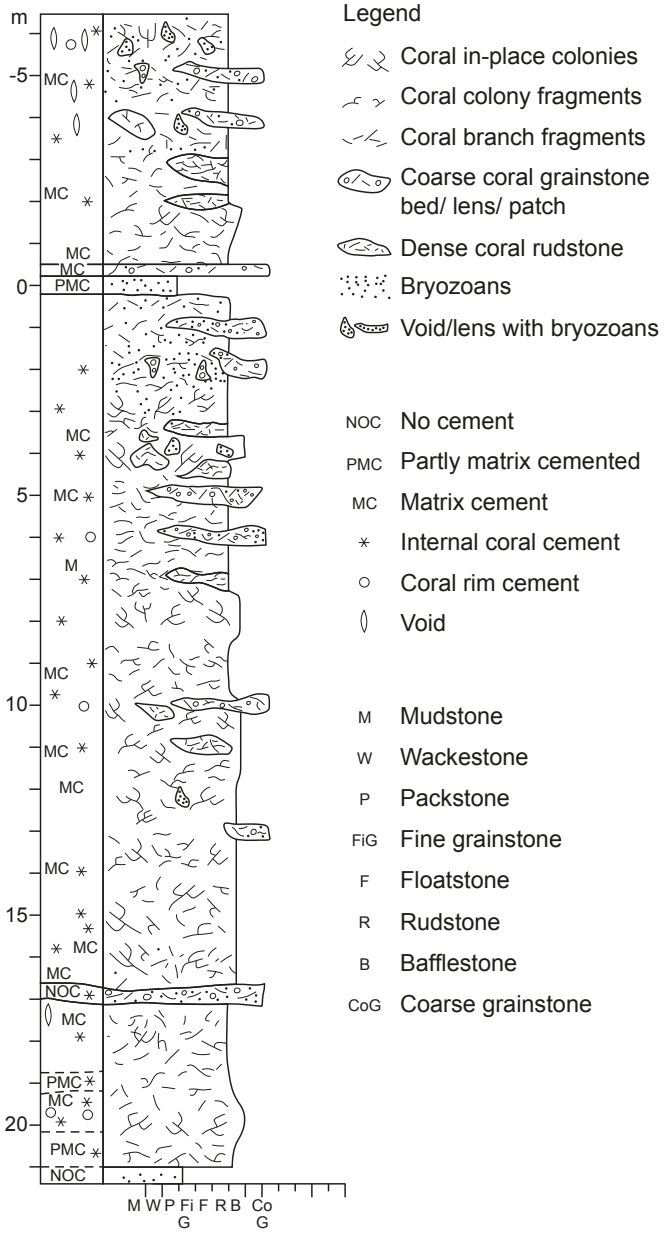

Fig. 5. Sedimentological log through the Faxe Formation at the type locality (Fig. 4). Left column shows diagenetic features and right column shows carbonate facies. The material collected at the type locality for this sedimentological log was difficult to access due to the steepness of the outcrop. At level 0 was a narrow path and material was collected below and above that plateau by rock climbing.

Boundaries. The lower boundary of the formation is situated at about 25 m above present day sea level in the western part of the quarry. However, elsewhere in the quarry the altitude ranges from -10 to +30 m above present day sea level. At the type section it is marked by the boundary between the bryozoan and coral limestone (Figures 4 and 5). In some areas the lower boundary shows a gradual transition from bryozoan-dominated to coral-dominated limestone. The upper boundary is placed at an erosional hardground overlain by bryozoan packstone and grainstone. This boundary is at present poorly exposed in the quarry, but is known from a profiles excavated in the northern part of the quarry present in the early 1990s and 2000s (Fig. 7).

Distribution. The formation is exposed in the Faxe area of Denmark and at Limhamn near Malmø in southern Sweden both in the eastern part of the Danish Basin (Fig. 1). It is recorded in boreholes and seismic profiles in Øresund offshore Malmø and along the northern margin of the Ringkøbing–Fyn High. The formation is contemporaneous with the middle Danian part of the Stevns Klint Formation and passes laterally into this formation in the Faxe area.

Chronostratigraphy. Middle Danian coccolith zones NP3 of Martini (1971), D5–6 of Perch-Nielsen (1979), 5 and lower part of 6 of Thomsen (1995) and NNTp3–NNTp4a of Varol (1998) (E. Sheldon and N. Thibault, personal communications 2011).

Baunekule facies

The Baunekule facies is known from the east central part of the Faxe quarry from four closely located sections at the old Baunekule quarry (Ravn 1903; Milthers 1908; Nielsen 1919; A. Rosenkrantz unpublished notes from the 1930s) and from the north-western part of the quarry (Fig. 7). It is considered to represent a stratigraphic level of isolated, unconsolidated units with unusually abundant and well preserved fossils.

Fig. 6. Fossils from the Faxe Formation in different modes of preservation. **A**, The scleractinian coral *Dendrophyllia candelabrum* in life position, covered with calcite crystals. Note the budding angle of 90º. There is no associated fauna between the branches. **B**, Moulds of *D. candelabrum* in life position. The moulds of the septae are easily recognised. Two small *Moltkia* (*Mo*) octocorals and external moulds of the bivalve *Barbatia* sp. (*Ba*) and the crab *Dromiopsis* sp. (*Dr*) are encircled. **C**, Only the casts of *D. candelabrum* are left and the associated fauna is dissolved or difficult to recognize. **D**, The scleractinian coral *Faksephyllia faxensis* partly recrystallized to calcite. Note the septae and the budding angle of 20° – 30° of the branches. **E**, The scleractinian coral *Oculina becki* showing a regular budding of branches with a constant spacing in two opposite rows. **F**, Mould of the decapod species *Dromiopsis rugosa (Dr)*. **G**, Moulds of the bivalve *Protocardia vogeli*. **H**, The calcitic bivalve *Chlamys hennigi* (*Ch*) is well hidden between the branches of *D. candelabrum*. **I**, Casts of the boring *Entobia* formed by clionid sponges. Picture I is from Damholt and Rasmussen (2005) and is reproduced with permission from Østsjællands Museum.

The variations in the faunal content of the individual occurrences are minor. The facies is named after the position of the first outcrop of the facies close to an old small quarry, Baunekule, which today is part of the large Faxe quarry.

The facies and the well preserved fossils were first described by Ravn (1903 p. 86), and the locality and the name 'næsekalk' were discussed by Nielsen (1919, p. 5). The photograph of the section (Fig. 3) was also published by Nielsen (1919, fig. 1). The old profile described by Ravn has now disappeared due to quarrying, probably sometime during the 1930s or 1940s (Fig. 7). Stratigraphic logs of the old sections are not known. However, the Baunekule facies has later been recorded in Faxe in the 1970s from a locality in the east-central part of the quarry just below that part of the road Stationsvej which is now quarried away. The Stationsvej section was recorded by Sten Lennart Jakobsen and Søren Bo Andersen and later exposed again at more or less the same location in the early 1990s. Material from this outcrop was sampled by Mads Willumsen and Alice Rasmussen (Figures 7, 8) close to profile M of Bernecker and Weidlich (1990). The thickness of the facies has not been recorded, but at the Stationsvej locality the lens was about 1 m thick and 7 m long (Fig. 8).

The facies consists of isolated lensoidal bodies in the flanks of the coral mounds, of weakly consolidated coral rudstone to floatstone, with a well preserved, high diversity calcitic and recrystallized, formerly aragonitic fauna. The facies was relatively matrix-poor in the lower part with upward increasing matrix

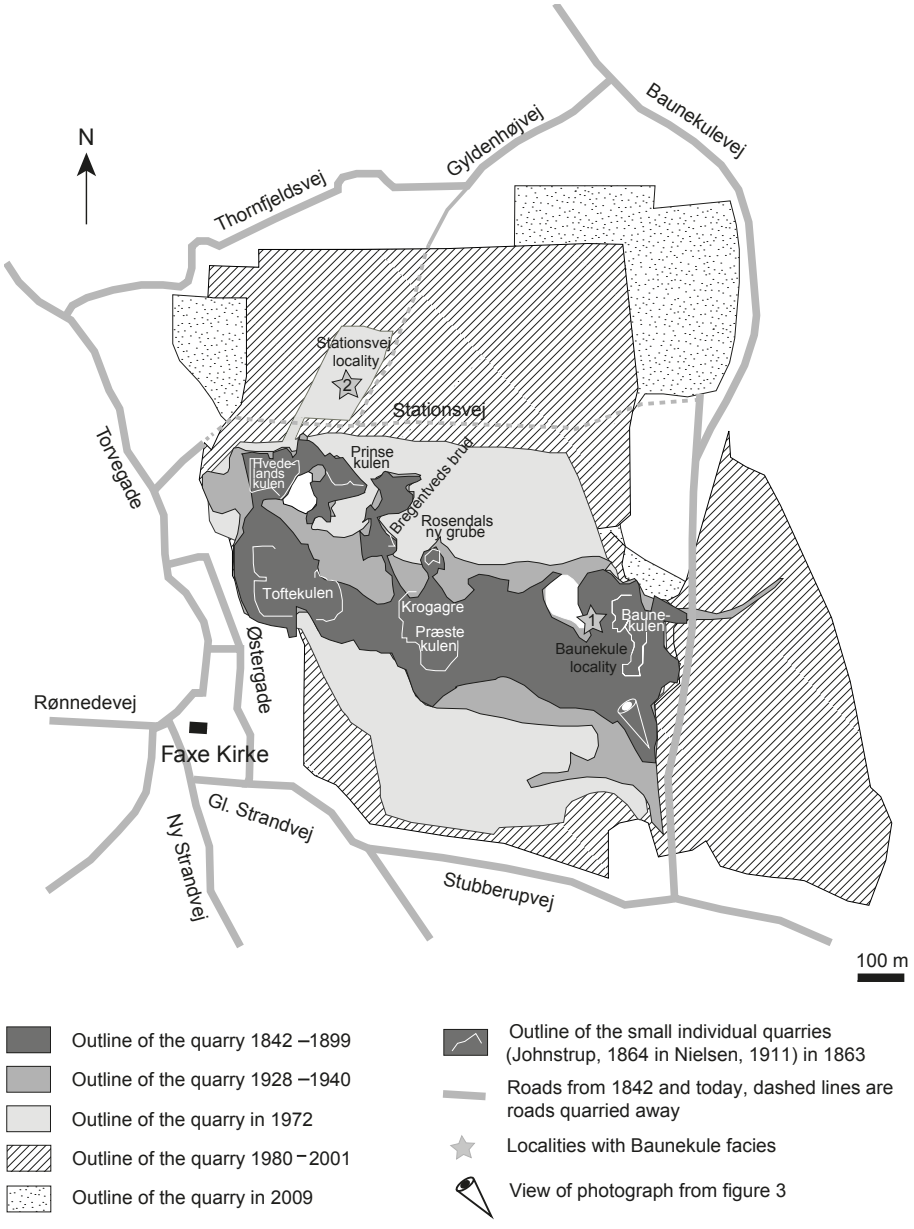

Fig. 7. Map showing the historical development of the quarry and positions of the Baunekule locality (asterisk 1) and the Stationsvej locality (asterisk 2) where the Baunekule facies previously cropped out. The quarry has been active since mediaeval times. In the first many hundred years quarrying took place in small individual pits with different owners and names and the outlines of the pits are marked with white lines. Their positions are from Nielsen (1911).

content. In addition it showed an upwards gradually increasing cementation of the limestone with increasing dissolution of aragonite-shelled fossils. Flint nodules are absent.

The diagenesis of the facies is of special importance as early burial diagenesis resulted in preservation of many of the aragonitic faunal elements by recrystallization to calcite prior to the precipitation of high Mg-calcite cement (Fig. 9). The carbonate mud matrix is only slightly consolidated and the macro- and microfossils are accordingly easy to prepare out in contrast to the fossils from the lithified part of the Faxe Formation. More than 25 000 invertebrate fossils have been collected at the Stationsvej locality, representing at least 300 species. The 12 most common species are shown in Fig. 10. Approximately 60% of the identified species were originally aragonite-shelled, 18% were originally calcitic, 15% were originally a mixture of aragonite and calcite, and the remaining 7% had either phosphatic or unknown shell material. At present no systematic information is available on the dominance of aragonite- versus calcite-shelled species living on modern cold-water coral mounds (André Freiwald, personal communication 2011).

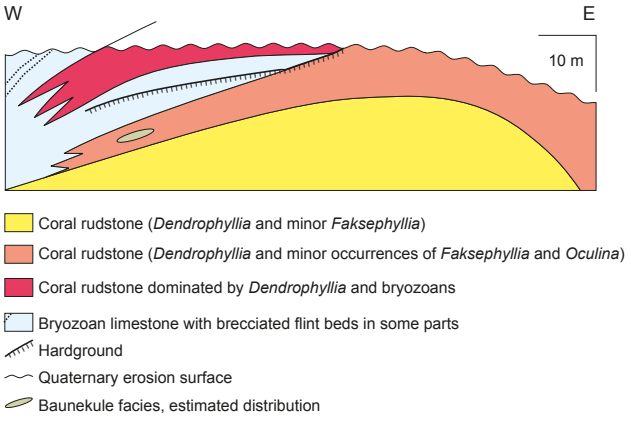

Fig. 8. Sketch of the 1970–1990 Stationsvej locality with the occurrence of the Baunekule facies and section M of Bernecker and Weidlich (1990) and Willumsen (1995). The section was approximately 20 m high, subvertical with an almost E–W orientation. Toward the west it is terminated by a fairly wide, glacially faulted crush zone, containing bryozoan limestone and deformed flint bands. The eastern boundary is placed in a more or less homogeneous coral limestone with no internal structures (modified from Willumsen 1995). Glacial tectonics has exaggerated the flank dips of the mounded structure.

The fossils found in the facies represent a wide range of modes of life and trophic levels. The corals are dominated by species of the octocoral *Moltkia* and by scleractinian solitary coral species of *Parasmilia*. Originally aragonitic stylasterine hydrocorals are also rather common in spite of their very low fossilisation potential. Framebuilding corals are rare and at the Baunekule locality the most common species is *Oculina becki*. Most of the colonial corals are fragmented and no corals have been found in life positions. The originally aragonitic corals have many delicate structures preserved and the associated originally aragonite-shelled fauna provides a rare taphonomic window into the past ecosystem. This is exemplified by the high abundance of millimetre-sized gastropods representing up to about 200 different species. In other parts of the Faxe Formation the small gastropods are only found as rare moulds or casts that are almost impossible to identify to species or even to genus level.

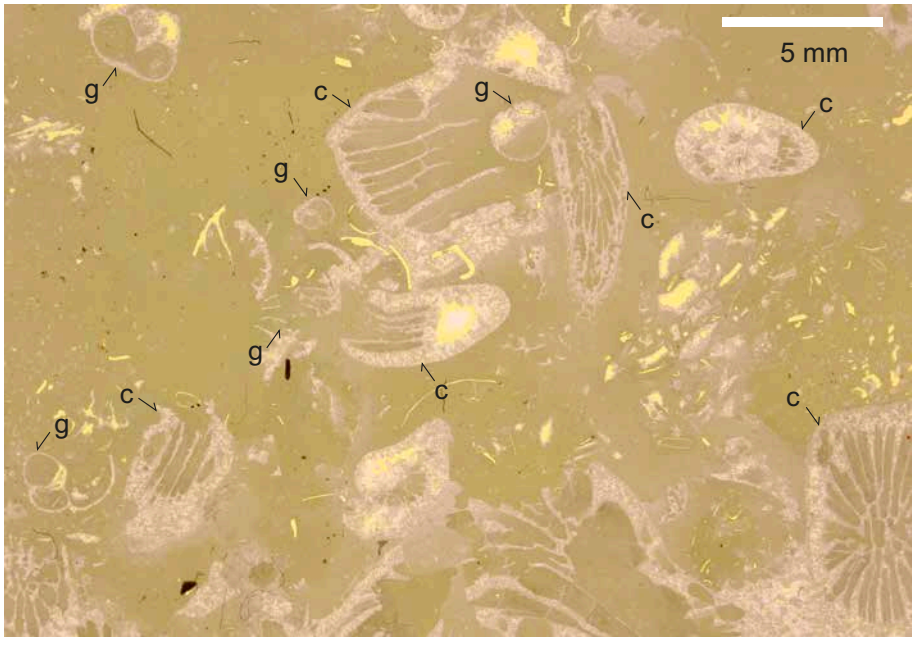

Fig. 9. Thin section of Baunekule facies from the Stationsvej locality. The original aragonite shells of corals (c) and gastropods (g) are recrystallized into calcite.

Infaunal bivalves are also common. Fragile specimens of Aristotle's lantern from regular echinoids and jaw pieces from nereid polychaetes show that the fauna is autochthonous.

The Baunekule facies at the Stationsvej locality and the adjacent hard coral limestone show similar nannofossil ages. The diversity of nannofossils is very low; *Sullivania danica* is very common and *Coccolithus pelagicus* and a few poorly preserved *Praeprinsius tenuiculus* are present, suggesting that the facies belongs to the middle Danian (N. Thibault, personal communication 2011).

Conclusion

The Baunekule facies is important as it preserves an exceptional and high-diversity, originally aragonite-shelled fauna of the middle Danian cold-water coral mound complex of the new Faxe Formation. More than 80% of the species from the mound complex are only known from these relatively thin and isolated lensoidal units that flank the individual mounds in the upper part of the complex. The well preserved invertebrate fauna recorded from the facies shows a very high diversity of more than 300 species in a lim-

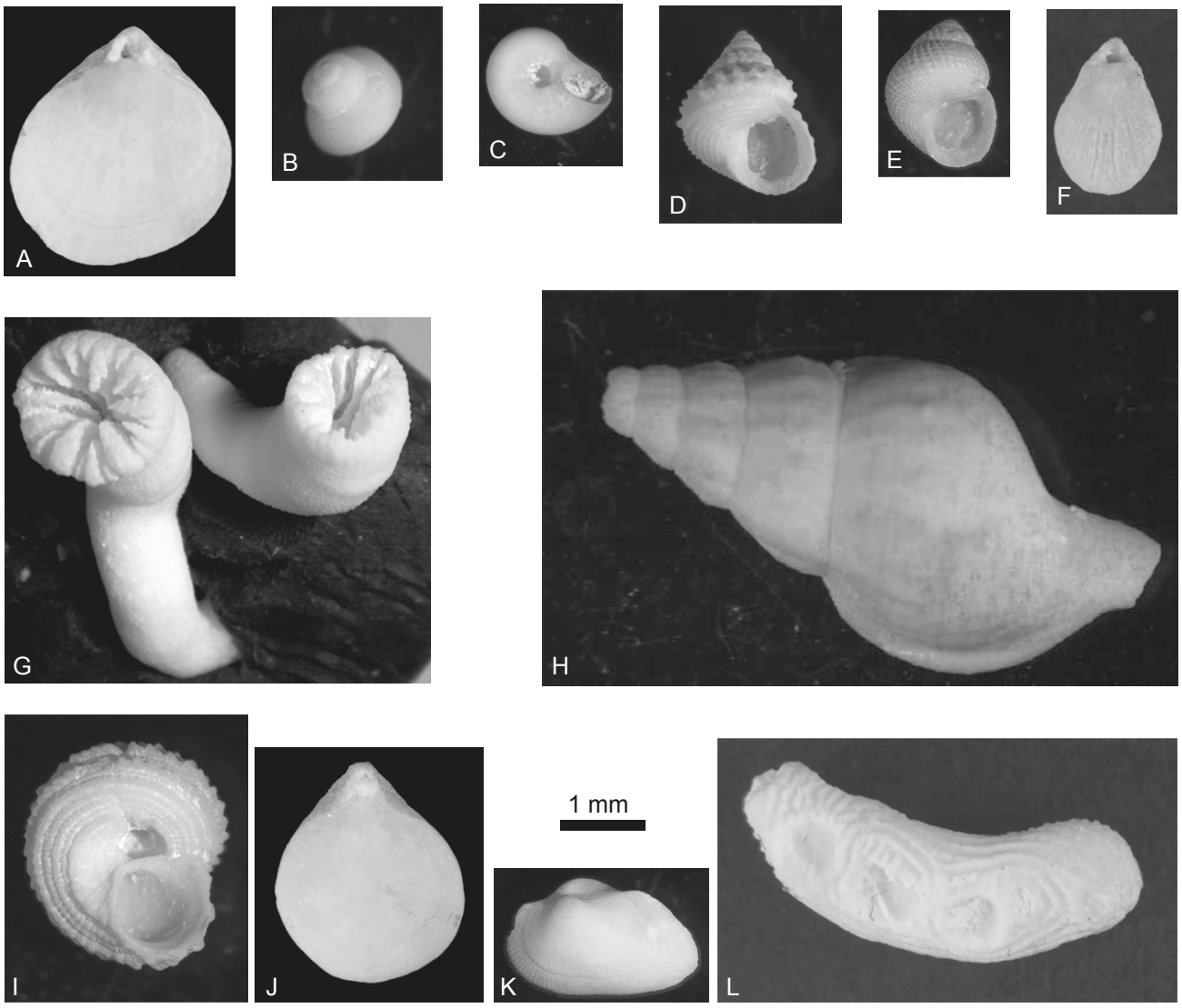

Fig. 10. The 12 most common species from the Baunekule facies. The species highlighted in bold below were originally aragonitic. Note the excellent preservation of the gastropods and corals. **A**, The brachiopod "*Rhynchonella*" *flustracea*. **B**, the gastropod ***Monodonta carinata***. **C**, the gastropod ***Collonia pusilla***. **D**, the gastropod ***Monodonta faxensis***. **E**, the gastropod ***Monodonta fenestra***. **F**, the brachiopod *Terebratulina chrysalis*. **G**, the coral ***Parasmilia elongata***. **H**, the gastropod ***Buccinofusus parvus***. **I**, the gastropod ***Delphinula depressa***. **J**, the brachiopod "*Rhynchonella*" *faxensis*. **K**, the bivalve ***Meiocardia faxensis***. **L**, the coral *Moltkia isis*.

ited stratigraphic interval. This is attributed to special diagenetic conditions which resulted in preservation by recrystallization of the originally aragonite-shelled fauna without cementation of the surrounding matrix. In contrast, other parts of the coral mound complex of the Faxe Formation show a relatively low diversity of the associated fauna.

Dansk sammendrag

En ny mellem Danien litostratigrafisk enhed, Faxe Formationen, er opstillet, og en særlig facies, Baunekule facies, i formationen er beskrevet. Den nye Faxe Formation er en markant enhed, der er nem at kortlægge og repræsenterer et velbevaret kompleks af fossile koldtvandskoralbanker og -bryozobanker. Formationen går lateralt over i mellem Danien bryozokalk tilhørende Stevns Klint Formationen. Faxe Formationen består hovedsaglig af hærdnet koralkalksten af primært scleractine rammebyggende koraller med matriks af karbonatmuddersten samt af mindre dominerende forekomster af ukonsolideret koralkalk primært bestående af oktokoraller. Baunekule facies er i den ældre litteratur benævnt 'næsekalk'. Den findes i den øvre del af Faxe Formationen, hvor den forekommer som isolerede linseformede legemer i koralbankernes flanker. Baunekule facies består af svagt konsolideret koraldomineret floatstone til rudstone og er kendetegnet af en artsrig fauna med velbevarede kalcitskallede og oprindelig aragonitskallede bentiske invertebrater. Denne facies har gennemgået en markant anderledes diagenetisk historie end de øvrige dele af Faxe Formationen. Mere end 80% af faunaen i Baunekule facies er ikke kendt fra andre dele af Faxe Formationen. Denne facies repræsenter derfor et enestående tafonomisk vindue til en stor gruppe af aragonitskallede invertebrater, der levede på det fossile bankekompleks.

Acknowledgements

This study forms part of a Geocenter Denmark project. Support from the Carlsberg Foundation is gratefully acknowledged. BWL thanks the Science International Stipends from the University of Copenhagen for financing a six month visit as a guest researcher studying modern cold-water corals at Senckenberg am Meer, Wilhelmshaven. André Freiwald is thanked for sharing his great knowledge of the modern cold-water coral mounds. Alice, Henning and Leif Rasmussen are thanked for access to their large collection of fossils from the Baunekule facies and for numerous discussions on the fossils from Faxe. Sample material and information from the Stationsvej locality has kindly been provided by Sten L. Jakobsen, Søren B. Andersen and Mads Willumsen. Nicolas Thibault and Emma Sheldon are thanked for nannofossil dating. Faxe Kalk A/S is thanked for access to the quarry. We are grateful to journal reviewers Jon Ineson and Peter Scholle for their constructive comments.

References

ACSN (American Commission on Stratigraphic Nomenclature) 2005: North American stratigraphic code. AAPG Bulletin 89, 1547–1591.

Asgaard, U. 1968: Brachiopod palaeoecology in middle Danian limestones at Fakse, Denmark. Lethaia 1, 103–121.

Asgaard, U. 1970: The syntypes of *Carneithyris incisa* (Buch, 1835). Bulletin of the Geological Society of Denmark 19, 361–367.

Baron-Szabo, R.C. 2008: Corals of the K/T-boundary: Scleractinian corals of the suborders Dendrophylliina, Carophylliina, Fungiina, Microsolenina, and stylinina. Zootaxa 1952, 244 pp.

Bernecker, M. & Weidlich, O. 1990: The Danian (Paleocene) coral limestone of Fakse, Denmark; a model for ancient aphotic, azooxanthellate coral mounds. Facies 22, 103–138.

Bernecker, M. & Weidlich, O. 2005: Azooxanthellate corals in the Late Maastrichtian – Early Paleocene of the Danish basin: bryozoan and coral mounds in a boreal shelf setting. In: Freiwald, A. & Roberts, J.M. (eds): Cold-Water Corals and Ecosystems. Springer-Verlag, Berlin and Heidelberg, 3–25.

Bernecker, M. & Weidlich, O. 2006: Paleocene bryozoan and coral mounds of Fakse, Denmark: Habitat preferences of isidid octocorals. Courier Forschungsinstitut Senckenberg 257, 7–20.

Berthelsen, O. 1962: Cheilostome Bryozoa in the Danian deposits of East Denmark. Danmarks Geologiske Undersøgelse II. Række 82, 290 pp.

Bjerager, M. & Surlyk, F. 2007a: Benthic palaeoecology of Danian deep-shelf bryozoan mounds in the Danish Basin. Palaeogeography, Palaeoclimatology, Palaeoecology 250, 184–215.

Bjerager, M. & Surlyk, F. 2007b: Danian cool-water bryozoan mounds at Stevns Klint, Denmark – a new class of non-cemented skeletal mounds. Journal of Sedimentary Research 77, 634–660.

Bjerager, M., Surlyk, F., Lykke-Andersen, H., Thibault, N. & Stemmerik, L. 2010: Danian cool-water coral reefs in southern Scandinavia localised over seafloor highs. Marine and Petroleum Geology 27, 455–466.

Brotzen, F. 1959: On *Tylocidaris* species (Echinoidea) and the stratigraphy of the Danian of Sweden. Sveriges Geologiska Undersökning Serie C 571, Årsbok 54, 1–81.

Cheetham, A.H. 1971: Functional morphology and biofacies distribution of cheilostome Bryozoa in the Danian Stage (Paleocene) of southern Scandinavia. Smithsonian Contributions to Paleobiology 6, 52 pp.

Clausen, C.K. 1982: *Wienbergia*, new genus for *Barroisia faxensis* (Porifera: Demospongea) from the Middle Danien of Denmark. Bulletin of the Geological Society of Denmark 30, 111–115.

Collins, J.S.H. & Jakobsen, S.L. 1994: A synopsis of the biostratigraphic distribution of the crab genera (Crustacea, Decapoda) of the Danian (Palaeocene) of Denmark and Sweden. Bulletin of the Mizunami Fossil Museum 21, 35–46.

Damholt, T. & Rasmussen, A. 2005: Fossiler fra Faxe Kalkbrud. Østsjællands Museum, 44 pp.

Darwin, C. 1851: A Monograph on the Fossil Lepadidae, or, Pedunculated Cirripedes of Great Britain. London. The Palaeontographical Society, 88 pp.

Desor, E. 1847: Sur le terrain Danien, nouvel étage de la craie. Bulletin de la Societé geologique de la France, Série 2, 4, 179–182.

Donovan, S.K. & Jakobsen, S.L. 2004: An unusual crinoid–barnacle association in the type area of the Danian (Paleocene, Denmark). Lethaia 37, 407–415.

Fischer-Benzon, R. von 1866: Ueber das relative Alter des Faxekalkes und über die in demselben vorkommenden Anomuren und Brachyuren. Kiel Schwers'sche Buchhandlung, 30 pp.

Floris, S. 1972: Scleractinian corals from the Upper Cretaceous and Lower Tertiary of Nûgssuaq, West Greenland. Bulletin Grønlands Geologiske Undersøgelse 100, 1–132.

Floris, S. 1980: The coral banks of the Danian of Denmark. Acta Palaeontologica Polonica 25, 531–540.

Forchhammer, J.G. 1825: Om de geognostiske Forhold i en Deel af Sielland og Naboeöerne. Det Kongelige Danske Videnskabernes Selskab, Physiske og Mathematiske Skrifter II. Deel, 248–280.

Freiwald, A., Fosså, J.H., Grehan, A., Koslow, T. & Roberts, J.M. 2004: Cold-water Coral Reefs. UNEP-World Conservation Monitoring Centre, Cambridge, UK, 86 pp.

Gravesen, P. 1993: Early Danian species of the echinoid genus *Tylocidaris* (Cidaridae, Psychocidarinae) from eastern Denmark. Contributions to Tertiary and Quaternary Geology 30, 41–73.

Gravesen, P. 2001: Den geologiske udforskning af Fakse Kalkbrud fra midten af 1700-tallet til nu. Geologisk Tidsskrift 2001, 2, 1–40.

Hennig, A. 1899: Studier öfver den baltiska Yngre kritans bildningshistoria. Geologiska Föreningens i Stockholm Förhandlingar 21, 19–82 and 133–188.

Holland, B. & Gabrielson, J. 1979: Guide to Limhamn quarry. In: Birkelund, T. & Bromley, R.G. (eds): Cretaceous–Tertiary Boundary Events, Symposium. 1. The Maastrichtian and Danian of Denmark, 142–151. University of Copenhagen.

Jakobsen, P.R., Wilken, U.G. & Lund, N.S. 1997: Feltrapport over dykkergeologisk undersøgelse af udgravninger i Øresund. Danmarks og Grønlands Geologiske Undersøgelse Rapport 150, 1–55.

Jakobsen, S.L. 2003: A new preparatory approach of decapods and thoracian crustaceans from the middle Danian at Fakse, Denmark. Contributions to Zoology 70, 141–145.

Jakobsen, S.L. & Collins, J.S.H. 1997: New middle Danian species of anomuran and brachyuran crabs from Fakse, Denmark. Bulletin of the Geological Society of Denmark 44, 89–100.

Jakobsen, S.L. & Feldmann, R.M. 2004: Epibionts on *Dromiopsis rugosa* (Decapoda: Brachyura) from the late middle Danian limestones at Fakse Quarry Denmark: Novel preparation techniques yield amazing results. Journal of Paleontology 78, 953–960.

Johnstrup, F. 1864: Faxekalkens Dannelse og senere undergaaede Forandringer. Det Kongelige Danske Videnskabernes Selskabs Skrifter 5. Række, Naturvidenskabelig og Mathematisk Afdeling 7, 1–46.

Jørgensen, N.O. 1988: Dolomite and dedolomitization in Danian bryozoan limestone from Fakse, Denmark. Bulletin of the Geological Society of Denmark 37, 63–74.

Levinsen, G.M.R. 1925: Undersøgelser over Bryozoerne i den danske Kridtformation. Det Kongelige Danske Videnskabernes Selskabs Skrifter 8. Række, Naturvidenskabelig og Mathematisk Afdeling 7, 3, 281–445.

Lundgren, B. 1867: Palaeontologiska iakttagelser öfver Faxekalken på Limhamn. Lunds Universitets Årsskrift 1867, 1–31.

Lyell, C. 1837: On the Cretaceous and Tertiary Strata of the Danish Islands of Seeland and Moen. Transactions of the Geological Society of London 6, 243–257.

Martini, E. 1971: Standard Tertiary and Quaternary calcareous nannoplankton zonation. In: Farinacci, A. (ed.): Proceedings 2nd International Conference Planktonic Microfossils, Roma, 739–785.

Milthers, V. 1908: Kortbladene Faxe og Stevns Klint. Beskrivelse til geologiske Kort over Danmark. Danmarks Geologiske Undersøgelse 1. Række 11, 1–291.

Nielsen, K.B. 1909: Brachiopoderne i Danmarks Kridtaflejringer. Det Kongelige Danske Videnskabernes Selskabs Skrifter 6. Række, Naturvidenskabelig og Mathematisk Afdeling 4, 127–178.

Nielsen, K.B. 1911: Brachiopoderne i Faxe. Meddelelser fra Dansk Geologisk Forening 3, 599–618.

Nielsen, K.B. 1912: Cirripederne i Danmarks Danien aflejringer. Meddelelser fra Dansk Geologisk Forening 4, 19–42.

Nielsen, K.B. 1913a: Crinoiderne i Danmarks Kridtaflejringer. Reitzel, København. 113 pp.

Nielsen, K.B. 1913b: *Moltkia isis*, Steenstrup, og andre Octocorallia fra Danmarks Kridttidsaflejringer. Særtryk af Kap. XVIII i Mindeskrift for Iapetus Steenstrup, 1–19.

Nielsen, K.B. 1914: Some remarks on the brachiopods of the chalk in Denmark. Meddelelser fra Dansk Geologisk Forening 4, 287–296.

Nielsen, K.B. 1917: *Heliopora incrustans* nov. sp. with a survey of the Octocorallia in the deposits of the Danian in Denmark. Meddelelser fra Dansk Geologisk Forening 5, 8, 1–13.

Nielsen, K.B. 1919: En Hydrocoralfauna fra Faxe. Meddelelser fra Dansk Geologisk Forening 5, 16, 5–63.

Nielsen, K.B. 1921: Nogle Bemærkninger om de store Terebratler i Danmarks Kridt- og Danienaflejringer. Meddelelser fra Dansk Geologisk Forening 6, 3, 1–18.

Nielsen, K.B. 1922: Zoantharia from Senone and Paleocene Deposits in Denmark and Skaane. Det Kongelige Danske Videnskabernes Selskabs Skrifter 8. Række, Naturvidenskabelig og Mathematisk Afdeling 3, 199–233.

Nielsen, K.B. 1925a: Nogle nye Octocoraller fra Danienet. Meddelelser fra Dansk Geologisk Forening 6, 28, 1–6.

Nielsen, K.B. 1925b: Nogle Echinidrester fra Danmarks Senon og Danien. Meddelelser fra Dansk Geologisk Forening 6, 29, 1–10.

Nielsen, K.B. 1928: *Argiope*-Arterne i Danmarks senone, daniske og paleocæne Aflejringer. Meddelelser fra Dansk Geologisk Forening 7, 215–226.

Nielsen, K.B. 1929: Kalksvampe i Danmarks Senonium og Danium. Meddelelser fra Dansk Geologisk Forening 7, 323–342.

Nielsen, K.B. 1931: Serpulidae from the Senonian and Danian deposits of Denmark. Meddelelser fra Dansk Geologisk Forening 8, 71–113.

Nielsen, K.B. 1943: The Asteroids of the Senonian and Danian deposits of Denmark. Det Kongelige Danske Videnskabernes Selskab, Biologiske Skrifter 2, 68 pp.

Nielsen, L., Brockdorff, A.S. von, Bjerager, M. & Surlyk, F. 2008: Reconstructing three dimensional architecture and development of Danian bryozoan mounds at Limhamn, southwest Sweden, using ground penetrating radar. Sedimentology 56, 695–708.

Perch-Nielsen, K. 1979: Calcareous nannofossil zonation at the Cretaceous–Tertiary boundary in Denmark. In: Birkelund, T. & Bromley, R.G. (eds): Cretaceous–Tertiary Boundary Events. Symposium. 1. The Maastrichtian and Danian of Denmark, 115–135. University of Copenhagen.

Pergens, É. & Meunier, A. 1886: La Faune des Bryozoaires Garumniens de Faxe. Annales de la Société Royale Malacologique de Belgique, 187–242.

Posselt, H.J. 1894: Brachiopoderne i den danske Kridtformation. Danmarks Geologiske Undersøgelse II Række 4, 59 pp.

Rasmussen, H.W. 1950: Cretaceous Asteroidea and Ophiuroidea with special reference to the species found in Denmark. Danmarks Geologiske Undersøgelse II. Række 77, 134 pp.

Rasmussen, H.W. 1961: A monograph on the Cretaceous Crinoidea. Det Kongelige Danske Videnskabernes Selskab, Biologiske Skrifter 12, 1, 428 pp.

Rasmussen, H.W. 1972: Lower Tertiary Crinoidea, Asteroidea and Ophiuroidea from Northern Europe and Greenland. Det Kongelige Danske Videnskabernes Selskab, Biologiske Skrifter 19, 7, 83 pp.

Rasmussen, H.W. 1973: En lyssky hulefauna fra Fakse som vidnesbyrd om koralkalkens dannelse i lyszonen. Dansk Geologisk Forening Årsskrift 1972, 87–91.

Ravn, J.P.J. 1899: Et par danske Kridtspongier. Meddelelser fra Dansk Geologisk Forening 1, 23–30.

Ravn, J.P.J. 1902a: Molluskerne i Danmarks Kridtaflejringer. I Lamellibranchiater. Det Kongelige Danske Videnskabernes Selskabs Skrifter 6. Række, Naturvidenskabelig og Mathematisk Afdeling 11, 2 , 1–70.

Ravn, J.P.J. 1902b: Molluskerne i Danmarks Kridtaflejringer. II Scaphopoder, Gastropoder og Cephalopoder. Det Kongelige Danske Videnskabernes Selskabs Skrifter 6. Række, Naturvidenskabelig og Mathematisk Afdeling 11, 4 , 5–66.

Ravn, J.P.J. 1903: Molluskerne i Danmarks Kridtaflejringer. III Stratigrafiske Undersøgelser. Det Kongelige danske Videnskabernes Selskabs Skrifter 6. Række, Naturvidenskabelig og Mathematisk Afdeling 11, 6, 335–446.

Ravn, J.P.J. 1904: Bemærkninger om lagserien i Stevns Klint samt om *Cyathidium holopus* STEENSTRUP. Geologiska Föreningens i Stockholm Förhandlingar 26, 347–354.

Ravn, J.P.J. 1927: De Irregulære Echinider i Danmarks Kridtaflejringer. Det Kongelige Danske Videnskabernes Selskabs Skrifter 8. Række, Naturvidenskabelig og Mathematisk Afdeling 11, 4, 307–355.

Ravn, J.P.J. 1928: De Regulære Echinider i Danmarks Kridtaflejringer. Det Kongelige Danske Videnskabernes Selskabs Skrifter 9. Række, Naturvidenskabelig og Mathematisk Afdeling 9, 1, 1–63.

Ravn, J.P.J. 1933: Études sur les Pélécypodes et Gastropodes du Calcaire de Faxe. Det Kongelige Danske Videnskabernes Selskabs Skrifter 9. Række, Naturvidenskabelig og Mathematisk Afdeling 9, 2, 1–74.

Reed, J.K. 2002: Deep-water *Oculina* coral reefs of Florida: biology, impacts and management. Hydrobiologica 471, 43–55.

Roberts, J.M., Wheeler, A.J. & Freiwald, A. 2006: Reefs of the deep: the biology and geology of cold-water coral ecosystems. Science 312, 543–547.

Roberts, J.M., Wheeler, A., Freiwald, A. & Cairns, S.D. 2009: Cold-water Corals: The Biology and Geology of Deep-sea Coral Habitats. Cambridge University Press, 334 pp.

Rosenkrantz, A. 1937: Bemærkninger om det østsjællandske Daniens stratigrafi og tektonik. Meddelelser fra Dansk Geologisk Forening 9, 199–212.

Schilder, F.A. 1928: Die Cypraeacea des Daniums von Dänemark und Schonen. Danmarks Geologiske Undersøgelse IV. Række, 2, 1–29.

Schnetler, K.I. & Petit, R.E. 2006: Revision of the gastropod family Cancellariidae from the Danian (Early Paleocene) of Fakse, Denmark. Cainozoic Research 4, 97–108.

Schnetler, K.I., Lozouet, P. & Pacaud, J.-M. 2001: Revision of the gastropod family Scissurellidae from the Middle Danian (Paleocene) of Denmark. Bulletin of the Geological Society of Denmark 48, 79–90.

Sigwart, J. D., Andersen, S.B. & Schnetler, K.I. 2007: First record of a chiton from the Palaeocene of Denmark (Polyplacophora: Leptochitonidae) and its phylogenetic affinities. Journal of Systematic Palaeontology 5, 123–132.

Sivhed, U., Wikman, H. & Erlström, M. 1999: Beskrivning til berggrundskarta 1C Trelleborg NV och SO samt 2C Malmö SV, SO, NV och NO. Sveriges Geologiska Undersökning Serie Af 191, 192, 193, 194, 196, 198, 143.

Steenstrup, J. 1847: Über Korallen in der Faxöer Kreide, Moltkia und Cyathidium. Amtlicher Bericht über die 24. Versammlung deutscher Naturforscher und Ärzte in Kiel im September 1846. Akademische Buchhandlung, Kiel, pp. 148–150.

Surlyk, F. 1997: A cool-water carbonate ramp with bryozoan mounds; Late Cretaceous – Danian of the Danish Basin. In: James, N. P., Clarke, J. A. D. (eds): Cool-water Carbonates. Special Publication – SEPM (Society for Sedimentary Geology) 56, 293–307. Tulsa, OK, USA.

Surlyk, F., Damholt, T. & Bjerager, M. 2006: Stevns Klint, Denmark: Uppermost Maastrichtian chalk, Cretaceous–Tertiary boundary, and lower Danian bryozoan mound complex. Bulletin of the Geological Society of Denmark 54, 1–48.

Thomsen, E. 1995: Kalk og kridt i den danske undergrund. In: Nielsen, O.B. (ed.): Århus Geokompendier 1, 31–67.

Varol, O. 1998: Palaeogene. In: Bown, P.R. (ed.): Calcareous Nannofossil Biostratigraphy. British Micropalaeontological Society Series. Chapman & Hall/Kluwer Academic, Cambridge, 200–224.

Voigt, E. 1923: Über einige neue und wenig bekannte Bryozoen der Gattung *Floridina* aus dem Danien von Faxe. Meddelelser fra Dansk Geologisk Forening 6, 20, 1–9.

Voigt, E. 1958: Untersuchungen an Oktokorallen aus der oberen Kreide. Mitteilungen aus dem Geologischen Staatsinstitut in Hamburg 27, 5–49.

Willumsen, M. 1995: Early lithification in Danian azooxanthellate scleractinian lithoherms, Faxe Quarry, Denmark. Beiträge zur Paläontologie 20, 123–131.

Wisshak, M., Neumann, C., Jakobsen, J. & Freiwald, A. 2009: The 'living-fossil community' of the cyrtocrinoid *Cyathidium foresti* and the deep-sea oyster *Neopycnodonte zibrowii* (Azores Archipelago). Palaeontology, Palaeoclimatology, Palaeoecology 271, 77–83.

Zibrowius, H. 1980: Les scleractiniaires de la Mediterranee et de l'Atlantique nord-oriental. Mémoires de l'Institut Océanographique, Monaco 11, 284 pp.

Ødum, H. 1928: Vort sydligste Danium. Meddelelser fra Dansk Geologisk Forening 7, 201–214.

Genesis of the glaciotectonic thrust-fault complex at Halk Hoved, southern Denmark

TILLIE M. MADSEN & JAN A. PIOTROWSKI

Madsen, T. M. & Piotrowski, J. A. 2012. Genesis of the glaciotectonic thrust-fault complex at Halk Hoved, southern Denmark. © 2012 by Bulletin of the Geological Society of Denmark, Vol. 60, pp. 61–80. ISSN 0011–6297 (www.2dgf.dk/publikationer/bulletin).

The coastal cliff of Halk Hoved, southern Jutland, Denmark, is a major glaciotectonic complex formed by proglacial deformation of the North-East (NE) advance from the Scandinavian Ice Sheet in Late Weichselian. We describe and interpret the pre-, syn- and post-tectonic sedimentary successions and macro-scale architecture of this complex. Initially, the Lillebælt Till Formation (unit 1) and the overlying glaciofluvial sediments (unit 2) were deposited during the Warthe glaciation in Late Saalian. During the NE advance towards the Main Stationary Line (MSL) in Late Weichselian, these sediments were pushed along a décollement surface whereby a thrust-fault complex was formed. In a cross section the complex extends for more than 900 m and consists of eighteen c. 15–20 m thick thrust sheets stacked by piggyback thrusting. Accumulated displacement amounts to at least 235 m along thrust faults dipping at 30–40° towards N-NE, resulting in at least 24% glaciotectonic shortening of the complex. Deformation was presumably facilitated by elevated pore-water pressure in the Lillebælt Till Formation. As the compressive stress exceeded the shear strength of the weakened till, failure occurred, and a décollement horizon formed along the lithological boundary between the Lillebælt Till Formation and the underlying aquifer. During deformation, piggyback basins formed wherein sediments of hyperconcentrated flow (unit 3) and glaciolacustrine diamicton (unit 4) were deposited. The whole thrust-fault complex and the intervening sediments were truncated subglacially as the NE advance finally overrode the complex. Following the retreat of the NE advance, a succession of glaciofluvial sediments (unit 5) and finally the East Jylland Till Formation (unit 6) were deposited during the advance of the Young Baltic Ice Sheet. The Halk Hoved thrust-fault complex is a prominent example of glaciotectonism at the southern fringe of the Scandinavian Ice Sheet.

Keywords: Glaciotectoctonic, thrust-fault complex, pore-water pressure, lithostratigraphy.

Tillie M. Madsen [tlm@ramboll.dk], Rambøll Danmark A/S, Olof Palmes Allé 22, DK-8200 Aarhus N, Denmark. Jan A. Piotrowski [jan.piotrowski@geo.au.dk], Department of Geoscience, Aarhus University, Høegh-Guldbergs Gade 2, DK-8000 Aarhus C, Denmark.

Received 24 November 2011
Accepted in revised form
26 September 2012
Published online
5 December 2012

Glaciotectonic deformation is a common phenomenon in Denmark (Jakobsen 1996, 2003). During the Pleistocene multiple ice sheet advances over Denmark generated large glaciotectonic complexes in which sediments were deformed by folding and/or displaced along thrust faults. These ancient glaciotectonic complexes, as well as modern complexes found along ice margins of present-day glaciers, provide information about the glaciodynamics and environmental conditions at the ice sheet margins. The purpose of this paper is to present the spatial and sedimentological characteristics and a model of formation of the prominent Late Pleistocene glaciotectonic complex exposed along the coastal cliff of Halk Hoved in the southern part of Denmark. The study comprises an examination of pre-, syn- and post-tectonic sedimentary successions and large-scale architecture of the glaciotectonic structures, and a genetic interpretation of the entire complex. Furthermore, by comparing with other well known glaciotectonic features we discuss the factors that played a key role in the formation of the Halk Hoved complex.

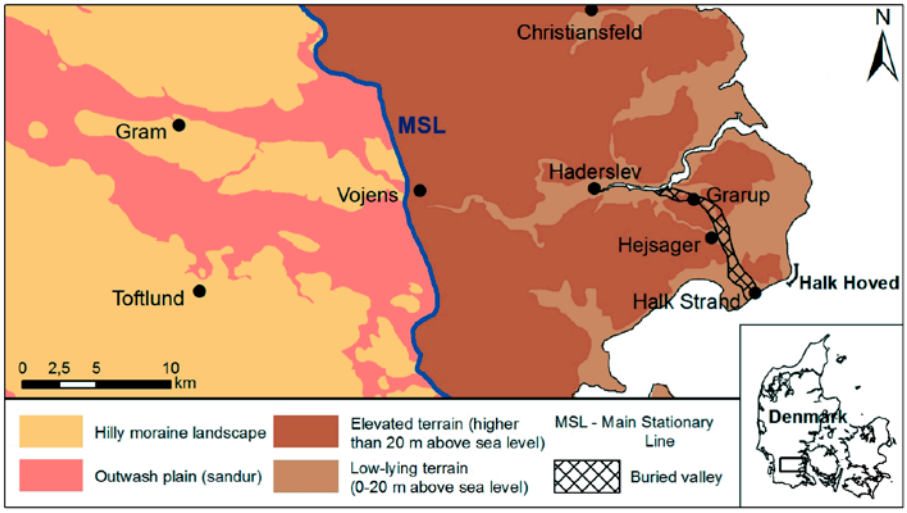

Fig. 1. Map showing the location of Halk Hoved and the surrounding landscape. The Main Stationary Line is drawn on the basis of Smed (1981).

Study area and geological setting

The coastal cliff Halk Hoved is located along the eastern coast of the southern part of Jutland approximately 12 km southeast of Haderslev (Fig. 1). The cliff face is approximately 900 m long and 10–20 m high and is generally well exposed due to high sea erosion rates and mass movement. The large-scale architecture of the cliff and its sediments has previously been investigated by Jessen (1930, 1935), Frederiksen (1975, 1976) and Houmark-Nielsen (1987). At Halk Hoved there is evidence of two glaciations: the Saalian and the Weichselian glaciation. During Late Saalian and Weichselian the area was overridden by several ice advances of the Scandinavian Ice Sheet. In Late Saalian, the ice sheet advanced through the Baltic depression and deposited the Lillebælt Till Formation (Warthe glaciation; *c.* 150–130 kyr ago) (ICS 2010). After the Eemian Interglacial the area underwent a long period of periglacial conditions that was briefly interrupted in Middle Weichselian by ice sheets advancing through the Baltic depression (Ristinge glaciation; *c.* 55–50 kyr ago) during which the Ristinge Klint Till Formation was deposited (Houmark-Nielsen 2007). In Late Weichselian (*c.* 25 kyr ago) during the Last Glacial Maximum (LGM) the area was covered by an ice sheet from Sweden referred to as the North-East (NE) advance that deposited the Mid Danish Till Formation (Houmark-Nielsen 2007). The NE advance had an extended period of ice-marginal standstill at the Main Stationary Line (MSL), approximately 20 km west of Halk Hoved (Fig. 1), where the landscape changes abruptly from a hilly terrain to a flat sandur plain that encloses older moraine hills (Kjær *et al.* 2003, Houmark-Nielsen 2007). During the subsequent Young Baltic advance (*c.* 19 kyr ago) the ice sheet passed through the Baltic depression and deposited the East Jylland Till Formation (Houmark-Nielsen 2007) which is the youngest glacial deposit in the study area. The Weichselian glaciers shaped the landscape surrounding Halk Hoved into hilly moraine plateaus that are traversed by E–W and SSE–NNW oriented valleys.

Methods

During field work, serial sketches were drawn of the cliff faces at a scale of 1:100, recording the large-scale geometry of the lithofacies and glaciotectonic structures. The general architecture of the macro-scale glaciotectonic structures was described and recorded by measuring the orientation (strike and dip) of folds, faults and bedding planes. The lithofacies were described and classified according to the scheme by Krüger & Kjær (1999). Each lithofacies was described in terms of lithology, grain size, sedimentary structures, and main characteristics, and assigned a lithofacies code.

Additional descriptive information was provided for diamicton and glaciofluvial facies by analysing the granulometric and petrographical composition. Samples were collected at different intervals along the cliff face. The granulometric composition was determined by sieve and pipette methods and is graphically presented by the weight percentage for each size class. The grain-size distribution was defined within the range of 0.001 mm to 4 mm, limited by the sample volume.

The petrographical composition was determined for the fine-gravel fraction (2–4 mm) after Kronborg (1986) and Kronborg *et al.* (1990). The fine-gravel fraction was divided into two main groups according

to their stability against chemical weathering, viz. a stable and an unstable group (Kjær *et al*. 2003). The stable group with at least three hundred identified grains per sample was classified into crystalline rocks, quartz, flint and sedimentary rocks, while the unstable group was classified into Cretaceous–Danian limestone and Palaeozoic limestone. In accordance with Ehlers (1979) each stable subgroup (crystalline, quartz, flint and sedimentary rocks) is calculated as a percentage of the sum of stable grains, so that the stable group is depicted as 100% in diagrams. The unstable subgroups (Cretaceous–Danian limestone and Palaeozoic limestone) are calculated separately as a percentage of the sum of stable grains and are in diagrams expressed as a percentage of the stable group. Both the granulometric and petrographical composition were used to define and distinguish lithostratigraphical units.

Lithostratigraphy

In the Halk Hoved cliff section six lithostratigraphical units were recognised. The two lowermost units (unit 1 and 2) were subjected to macro-scale deformation. Unit 2 is overlain by an erosional unconformity upon which lithostratigraphical units 3 and 4 were deposited. The whole assemblage of units 1–4 is truncated by a glaciotectonic unconformity, whereupon lithostratigraphical unit 5 is deposited. This is in turn overlain by an erosional unconformity and the laterally extensive unit 6. Fig. 2 shows the large-scale architecture and the lithofacies geometry of the Halk Hoved cliff section. A simplified log of the lithostratigraphical units is presented in Fig. 3.

Unit 1

Unit 1 is a grey, fine-grained (clayey-silty), matrix-supported diamicton with a moderate content of clasts. In general, the diamicton is characterised by a firm, massive, homogeneous structure (DmF(m_2)3). Only few structural elements have been observed, such as a 2–3 cm thick, heavily tectonized, silty string of sand, a small lens of gravel, and a relatively large displaced gravel lens (between points 117 m and 225 m on Fig. 2). The diamicton has a minimum thickness of 4 m and is traversed by subvertical and subhorizontal fissures. On average, the matrix of the diamicton contains 36% sand (σ 2.3%; σ is the standard deviation), 43% silt (σ 2.5%), and 21% clay (σ 2.1%) (Fig. 3). The matrix is characterised by a bimodal grain-size distribution with a primary mode in fine sand and a secondary mode in fine silt (Fig. 4). The petrographical composition is on average 67% crystalline rocks (σ 3.0%), 7% quartz (σ 1.2%), 20% flint (σ 2.7%), and 6% sedimentary rocks (σ 2.0%) (Fig. 3). The unit is also characterised by a relatively high content of both Cretaceous–Danian limestone (32%; σ 5.5%) and Palaeozoic limestone (38%; σ 6.1%).

Unit 1 is interpreted as a subglacial till. The interpretation is consistent with the granulometric composition, since subglacial tills commonly show bi- and polymodal grain-size distributions as a result of comminution during which particle sizes are reduced through crushing and abrasion (Dreimanis & Vagners 1971; Boulton 1978; Haldorsen 1981, 1983; Piotrowski 1992; Larsen *et al.* 2004; Piotrowski *et al.* 2006). Depositional processes may have included lodgement, deformation, clast ploughing and the development of a liquefied till layer, and the unit is therefore classified as a subglacial traction till *sensu* Evans *et al.* (2006).

Unit 2

Unit 2 overlies unit 1 with a sharp, erosive contact. It forms a fining-upward succession of glaciofluvial sediments consisting of five facies (unit 2a–2e) with a total thickness of 6–12 m. The first facies (unit 2a) consists of localised clusters of open-work to matrix-supported, massive, angular to rounded boulders and gravelly pebbles (B) with a general thickness of 0.3–1.5 m. It is overlain by a facies (unit 2b) comprising discontinuous, thin sheets (*c.* 1 m thick) of coarse- to medium-grained sand that are massive (Sm), horizontally bedded (Sh), and cross-bedded (Sp). Unit 2b is overlain by unit 2c which consists of laterally extensive, stacked sheets of massive (Gm) and horizontally bedded (Gh), clast- to sand-supported, imbricated gravel. The thickness of unit 2c is 1–4 m. It is succeeded by a sandy facies (unit 2d), the thickness of which varies greatly from 2 to 10 m. This facies consists of coarse- to medium-grained sand that is massive (Sm), horizontally bedded (Sh) and trough cross-bedded (St), with intercalations of massive gravel (Gm). Upward, the sand becomes medium- to fine-grained and exhibits trough cross-bedding (St) and horizontal bedding (Sh) with intercalations of silt flasers (Fm). As unit 2d gradually turns into unit 2e the silt flasers become more pronounced, so that unit 2e consists of massive (Fm) and laminated silty clay (Fl) with intercalations of laminated (Sh) and cross-laminated (Sr) fine-grained sand. Unit 2e is heavily contorted by open and overturned folds due to ductile deformation. The thickness of unit 2e varies greatly in relation to the degree of deformation. When the sediment is heavily deformed the thickness can be up to 8 m due to tectonic repetition and superimposition, while a more or less undisturbed sediment has a thickness around 2 m.

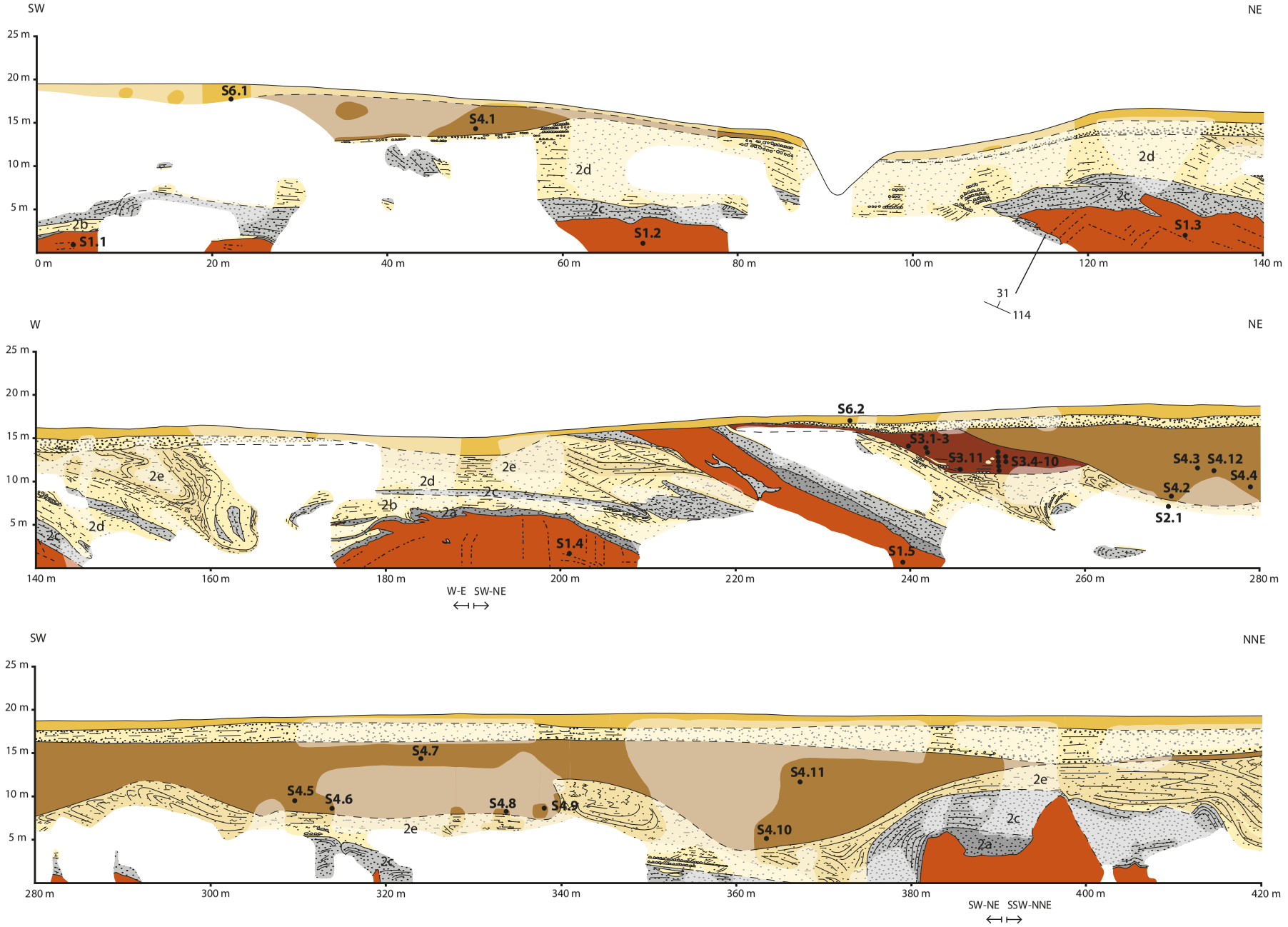
SW
NE
25 m
20 m
15 m
10 m
5 m
S6.1
S4.1
2d
2c
2b
S1.1
S1.2
S1.3
0 m
20 m
40 m
60 m
80 m
100 m
120 m
140 m
31
114
W
NE
S6.2
S3.1-3
S3.11
S3.4-10
S4.3
S4.12
S4.4
S4.2
S2.1
2e
2d
2c
2b
2a
S1.4
S1.5
140 m
160 m
180 m
200 m
220 m
240 m
260 m
280 m
W-E
SW-NE
SW
NNE
S4.7
S4.5
S4.6
S4.8
S4.9
S4.11
S4.10
2e
2c
2a
280 m
300 m
320 m
340 m
360 m
380 m
400 m
420 m
SW-NE
SSW-NNE

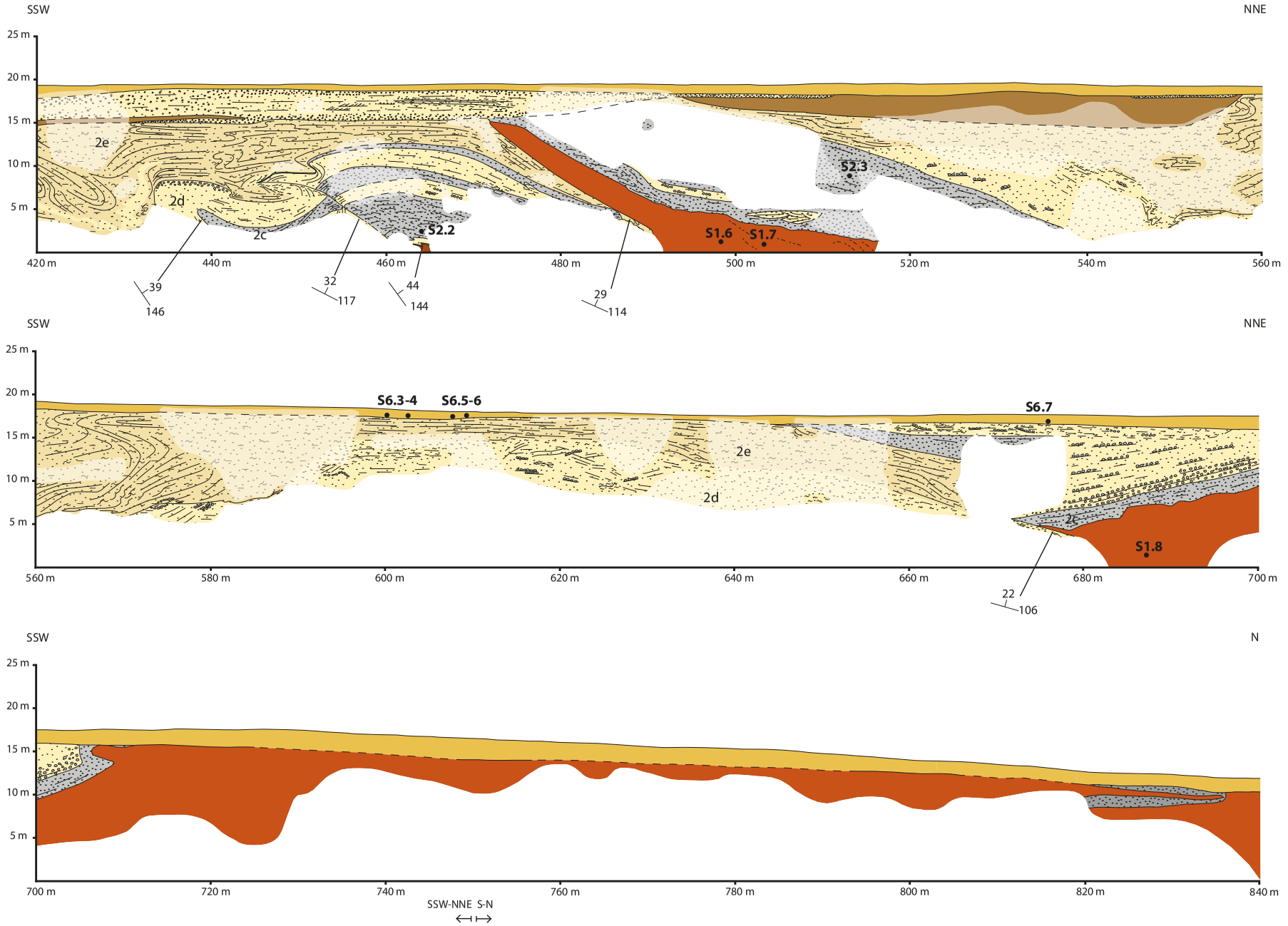
SSW
NNE
25 m
20 m
15 m
10 m
5 m
2e
2d
2c
S2.2
S2.3
S1.6
S1.7
420 m
440 m
460 m
480 m
500 m
520 m
540 m
560 m
39
146
32
117
44
144
29
114
SSW
NNE
S6.3-4
S6.5-6
S6.7
2e
2d
2c
S1.8
560 m
580 m
600 m
620 m
640 m
660 m
680 m
700 m
22
106
SSW
N
700 m
720 m
740 m
760 m
780 m
800 m
820 m
840 m
SSW-NNE S-N

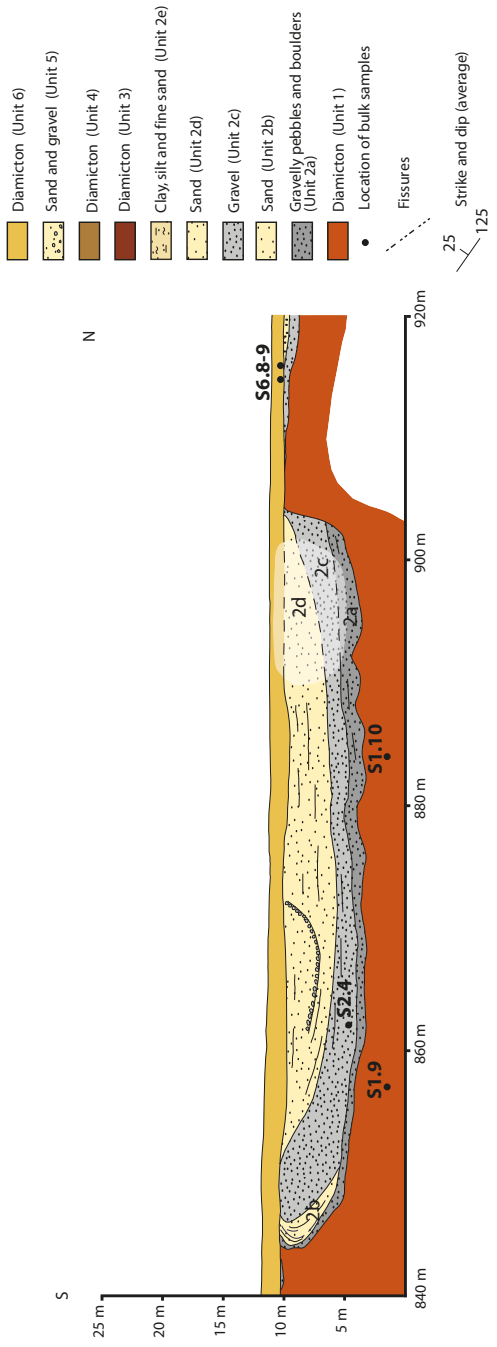

◀▲ Fig. 2. Halk Hoved cliff section as mapped in 2005 and 2006. The 'faded' colours represent interpreted areas. The different subunits of unit 2 (2a-2e) are shown on the cross section. Bulk samples at different intervals along the cliff face were taken for granulometric and petrographical analyses of the lithostratigraphic units 1, 3, 4 and 6. Additional samples were taken from unit 2c and 2d for petrographical analysis. The location of samples is shown in the profile. A sample named S1.3 means sample 3 from unit 1.

The petrographical composition of the glaciofluvial sediment shows an average fine-gravel content of 54% crystalline rocks (σ 7.1%), 19% quartz (σ 4.9%), 21% flint (σ 7.6%) and 6% sedimentary rocks (σ 1.5%), and in the unstable group of 12% Cretaceous–Danian limestone (σ 5.8%) and 9% Palaeozoic limestone (σ 3.8%) (Fig. 3). This fining-upward succession of glaciofluvial sediments reflects the change from a proximal to a distal glaciofluvial environment likely due to a receding ice margin.

Unit 3

Unit 3 is a brown, massive, compact, medium-grained (silty–sandy) diamicton. The matrix consists of 61% sand (σ 1.8%), 30% silt (σ 1.7%) and 9% clay (σ 1.7%) and is characterised by a unimodal grain-size distribution with a mode in medium-grained sand (Fig. 4). The gravel content is moderate (DmM(m_2)3) but seems to diminish upward (DmM(m_1)3), primarily within the lowermost 1.5 m. The diamicton contains a few structural elements such as sand lenses, a string of laminated fine-grained sand and silt, and a layer of massive gravel (Fig. 5a and b). Furthermore, the lower part of the sediment is stratified, with small, no more than 1 cm thick, grey, clayey laminae. These interbedded layers of sorted sediment are parallel to the basal contact of the unit. Unit 3 is only observed in the cliff section at 220-260 m, where it lies discordantly over the deformed assemblage of unit 1 and 2 (Fig. 2). The thickness of unit 3 increases towards north from *c.* 0.5 m to a maximum of 5 m, after which it thins into a wedge. The lower boundary of the sediment is very sharp and along its base small overturned folds (drag folds) are observed in the underlying glaciofluvial clay and silt (unit 2e).

Unit 3 has a petrographical composition with 56% crystalline rocks (σ 3.0%), 16% quartz (σ 2.6%), 24% flint (σ 2.9%), 4% sedimentary rocks (σ 1.7%); 22% Cretaceous–Danian limestone (σ 5.4%) and 11% Palaeozoic limestone (σ 1.8%) (Fig. 3).

Unit 3 is interpreted as deposited from a hyperconcentrated flow. A hyperconcentrated flow was originally defined by Beverage & Culbertson (1964) as a subaerial turbulent flow that in the rheological terms of flow behaviour is transitional between normal stream flow and debris flow. It is characterised by a suspended sediment concentration that exceeds 25% by volume (Mulder & Alexander 2001). The suspended material is a mixture of two populations; one in the sand fraction and the other in the silt-clay fraction (Beverage & Culbertson 1964), which is consistent with the granulometric composition of unit 3. The clay content is generally very low because a hyperconcentrated flow is a friction-dominated non-cohesive flow (Mulder & Alexander 2001).

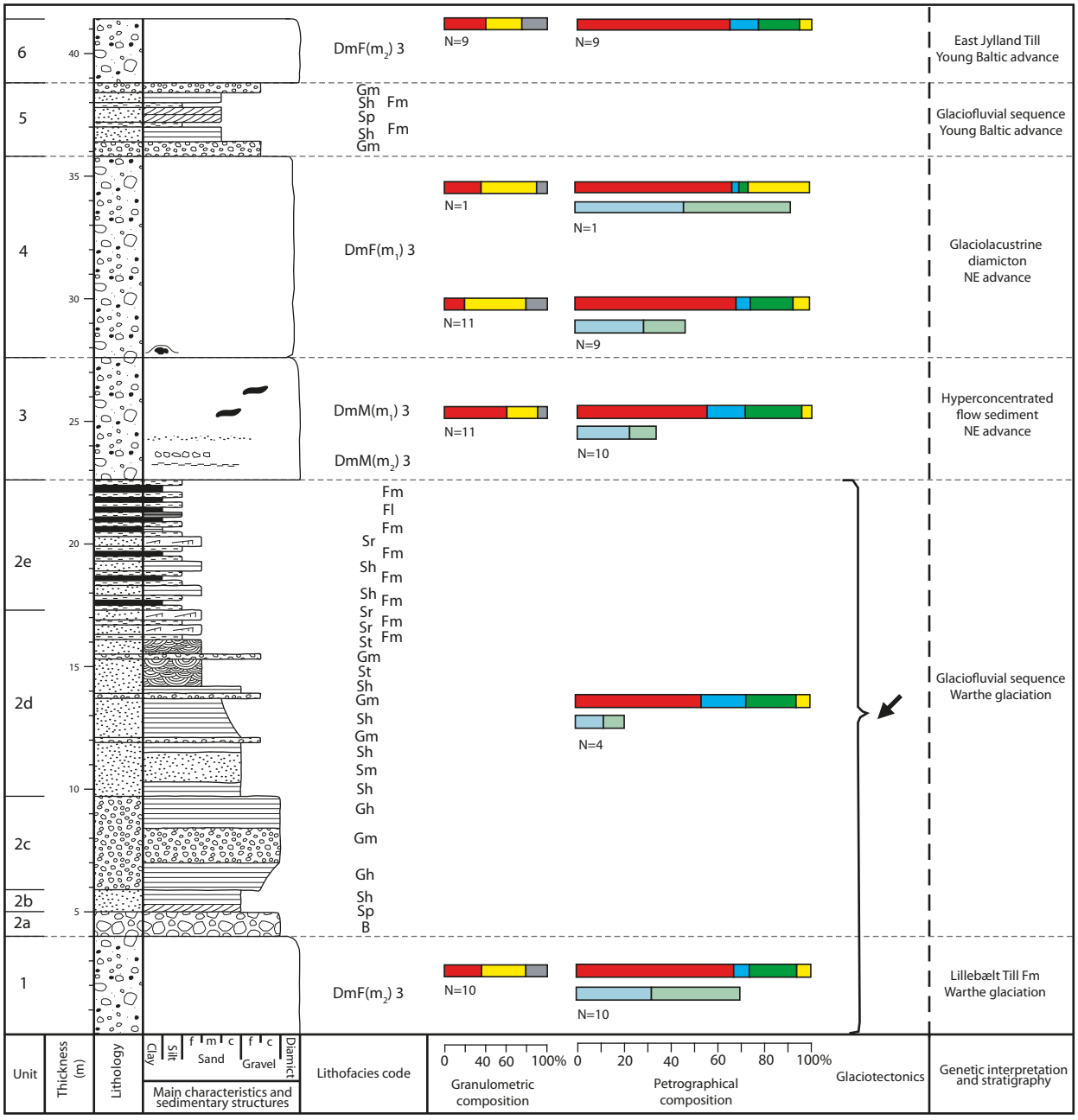

Lithofacies code (Krüger & Kjær 1999)

Diamict sediments

D	Diamict
m	Massive, homogeneous
M	Medium-grained, silty-sandy
F	Fine-grained, clayey-silty
(m_1)	Matrix-supported, clast poor
(m_2)	Matrix-supported, moderate clast content
3	Firm, difficult to excavate

Sorted sediments

B	Boulders
Gm	Gravel, massive
Gh	Gravel, horizontally bedded
Sm	Sand, massive
Sh	Sand, horizontally laminated
St	Sand, trough cross-bedded
Sp	Sand, planar cross-bedded
Sr	Sand, ripple cross laminated
Fm	Fines (silt, clay), massive
Fl	Fines (silt, clay), laminated

Glaciotectonics

Estimated direction of glaciotectonic deformation

Other sedimentary structures

Drop stone draped by lamina

Lenses of sand

Horizon of clay/silt, sand or gravel

Avarage granulometric composition [%]

Sand Silt Clay

N=number of samples

Average petrographical composition [%]

Crystalline rocks
Quartz
Flint
Sedimentary rocks
Limestone (Cretaceous-Danian)
Palaeozoic limestone

N=number of samples

Fig. 3. The glacio-stratigraphic section of Halk Hoved. The diagram shows a lithostratigraphical log accompanied by the average granulometric and petrographical composition for units 1, 3, 4 and 6. The average petrographical composition of unit 2c and 2d is also shown. The sedimentary units are described and classified using lithofacies codes in accordance with the scheme by Krüger & Kjær (1999).

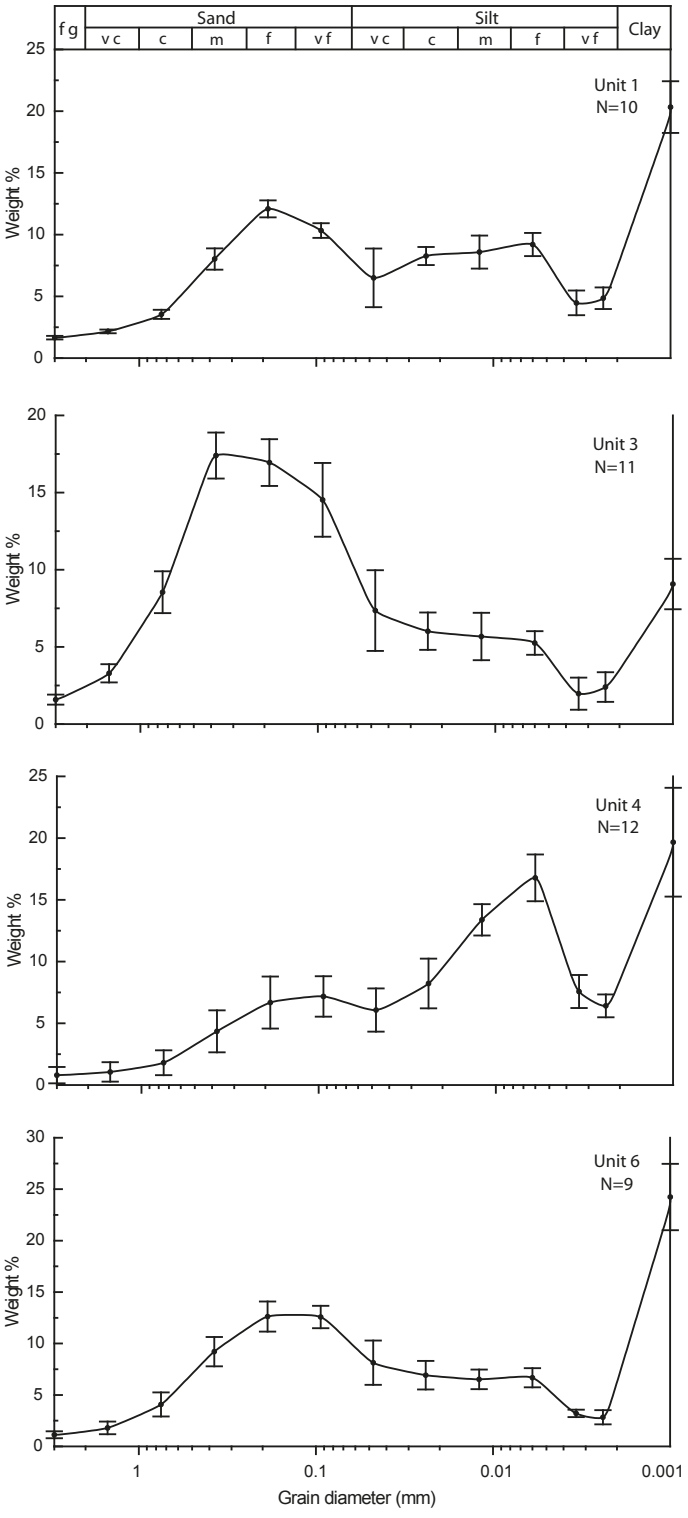

Fig. 4. Grain size distribution with standard deviations (vertical bars are ± 1σ) from units 1, 3, 4 and 6. The abbreviations denote fine gravel (fg), very coarse (vc), coarse (c), medium (m), fine (f) and very fine (vf).

Hyperconcentrated flows occur either due to mass movement or water action eroding and remobilising sediment. With regard to unit 3, the hyperconcentrated flow was likely initiated by the mobilisation of glaciofluvial material (unit 2) down a slope. Presumably, mobilisation was prompted by high pore-water pressures reducing the frictional strength of the sediment, giving the sediment little resistance to downslope movement. The main depositional mechanism would have been frictional freezing from grain-to-grain interaction. This would have triggered rapid dumping of the suspended material, thereby preventing deposition from traction (Bilka & Nemec 1998; Mulder & Alexander 2001) and resulting in the massive structure of unit 3. The few structural elements observed within unit 3 are interpreted to be the result of resedimentation by water, indicating that deposition occurred by the accretion of successive flow surges (Sohn *et al.* 1999).

Unit 4

Unit 4 has been observed in the cliff section at 30–90 m, 250–440 m, and 490–560 m, discordantly overlying deformed sediments (Fig. 2). It is a blackish grey, compact, massive, fine-grained (clayey–silty), matrix-supported diamicton with a low content of clasts ($DmF(m_1)3$) and a small content of dispersed stones (Fig. 5c). The unit has a very variable thickness ranging between 2 and 13 m. The only structural elements observed are a clayey lamina draped over a stone, and layers of sand and gravel. The lower contact is sharp, and in a few places the lowermost 1 m of the sediment is more compact than the rest and has a reddish colour. The matrix of unit 4 consists on average of 21% sand (σ 5.4%), 59% silt (σ 3.9%) and 20% clay (σ 3.3%) (Fig. 3) and is characterised by a bimodal grain-size distribution with a very distinct primary mode in fine silt and a secondary mode in very fine sand (Fig. 4). The fine-gravel composition is 69% crystalline rocks (σ 2.7%), 6% quartz (σ 1.5%), 18% flint (σ 2.5%), 7% sedimentary rocks (σ 1.7%); 32% Cretaceous–Danian limestone (σ 10.5%) and 20% Palaeozoic limestone (σ 1.4%) (Fig. 3).

Towards the upper contact, the matrix of unit 4 becomes slightly more coarse-grained and consists of 36% sand, 54% silt and 10% clay (Fig. 3; sample S4.7 in Fig. 2). Here, the massive sediment has a yellow-brown colour and is interbedded with limestone clasts. Furthermore, the petrographical composition also differs from the rest of unit 4 by having much less flint and a higher content of limestone; the composition is 67% crystalline rocks, 3% quartz, 4% flint, 26% sedimentary rocks; 46% Cretaceous-Danian limestone and 46% Palaeozoic limestone. Due to limited access, it is uncertain whether it is only a localised or a more

widespread phenomenon or even if this sediment represents a similar depositional environment as the rest of unit 4.

Unit 4 is interpreted as a glaciolacustrine diamicton. The deposition of glacial diamicton in an ice-contact lake is often attributed to iceberg calving with a subsequent debris rainout (Domack & Lawson 1985; Dowdeswell *et al.* 1994; Bennett *et al.* 2002) and/or subaqueous sediment gravity flows (Evenson *et al.* 1977; May 1977; Rovey & Borucki 1995) that receive its material from a subglacially deforming bed at the grounding line (Benn 1996; Bennett *et al.* 2002). The massive structure of unit 4 suggests that during deposition the sedimentation rates must have been high in order to suppress structures such as lamination. The very faint clayey lamina draped over a stone represents a period with stagnant water and low sediment supply during which fallout from suspension could occur.

Unit 5

Unit 5 consists of a discontinuous, 1–4 m thick glaciofluvial succession made up of massive gravel (Gm) interbedded with horizontally bedded (Sh) and cross-bedded (Sp) medium- to fine-grained sand with intercalations of silt flasers (Fm). The unit is interpreted to have been deposited in a glaciofluvial environment with massive gravel representing migrating longitudinal bars and the sand representing migrating sandy bedforms (Miall 1985). The massive gravel indicates high-energy water flows that were interrupted by periods of low-energy water flow during which the sandy bedforms were deposited.

Unit 6

The whole cliff is draped by a continuous, brown-coloured, fine-grained (clayey–silty) diamicton with an almost uniform thickness around 1–2 m. The diamicton is massive, firm and matrix-supported with a moderate content of clasts (DmF(m_2)3) . It is characterised by a sharp basal contact and fissile structure with some sand and silt strings. The uppermost 0.5 m is disturbed by post-depositional weathering and modern farming activities.

Unit 6 has a petrographical composition of on average 65% crystalline rocks (σ 2.0%), 12% quartz, (σ 1.5%) 18% flint (σ 2.0%) and 5% sedimentary rocks (σ 0.9%)

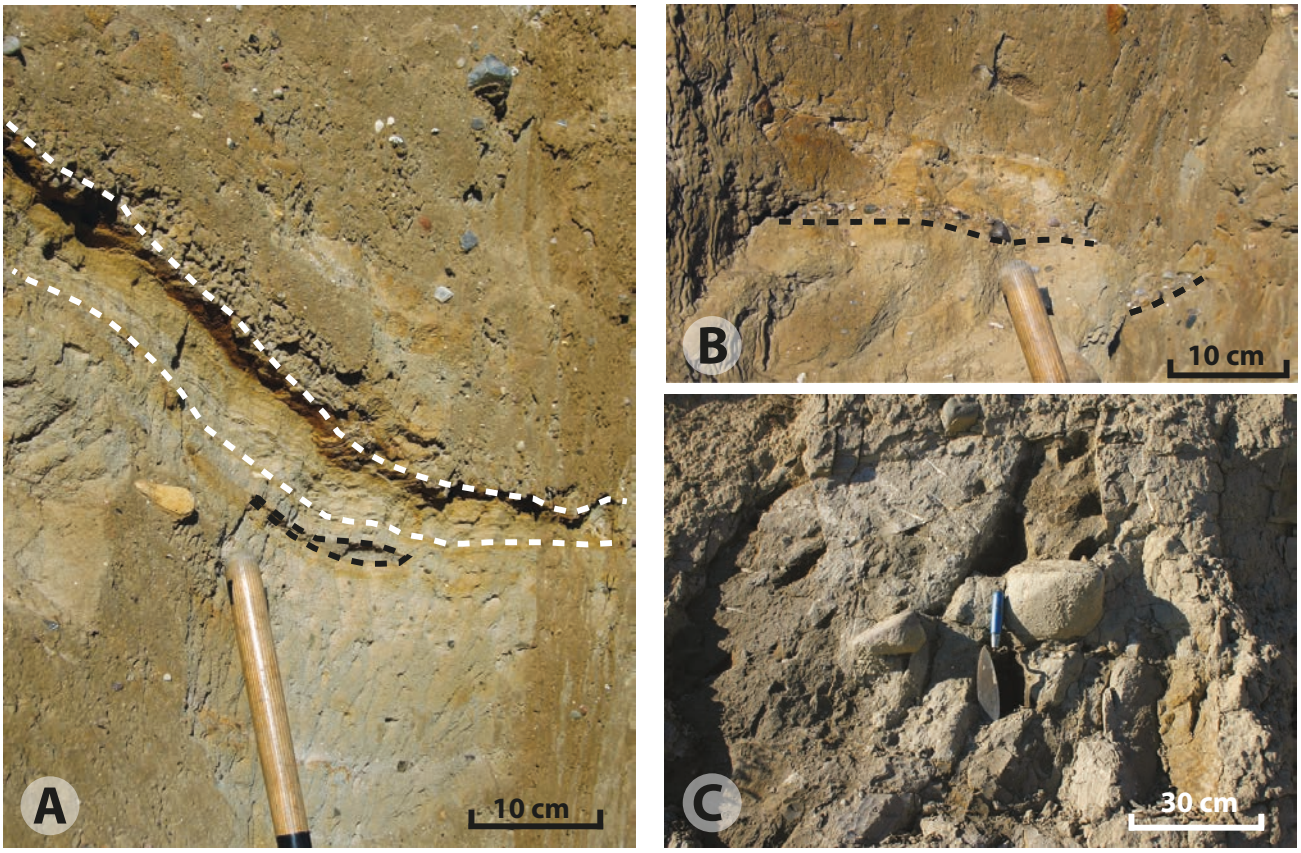

Fig. 5. **A**, Layer of laminated sand and silt interbedded in medium-grained diamicton of unit 3, marked by the white dashed line. Underneath the layer there is a small stretched-out lens of coarse-grained sand indicated by the black dashed line. **B**, Thin layer of gravel resting within medium-grained diamicton of unit 3, underlined by the two black dashed lines. **C**, Blackish grey, compact, massive, clayey silt deposit (unit 4) with two dropstones on both sides of the spatula.

(Fig. 3). The matrix consists of 40% sand (σ 3.6%), 35% silt (σ 3.5%) and 25% clay (σ 3.2%) (Fig. 3), and, like unit 1, the matrix is characterised by a bimodal grain-size distribution with a primary mode in fine sand and a secondary mode in fine silt (Fig. 4). The only difference between the two sedimentary units is that unit 6 is slightly more coarse-grained.

Like unit 1, unit 6 is interpreted as a subglacial traction till (Evans *et al.* 2006). Lodgement was presumably the main depositional process, but subglacial deformation and/or the development of a liquefied till layer would likely also have occurred, particularly in areas where this unit is lying directly over unit 4 and unit 2d, as the low permeability of these sediments would have facilitated high pore-water pressures.

Structural analysis of the glaciotectonic complex

In the following a structural description of the glaciotectonic elements exposed at the Halk Hoved cliff is given with preliminary interpretations to facilitate the understanding of the deformational framework. The macro-scale tectonic structures are described using the terminology associated with thin-skinned thrust-fault tectonics (i.e. footwall, hanging-wall, ramp, and flat). For a detailed description of these terms see Pedersen (2005).

The glaciotectonic complex is divided into two subsections: a distal deformation zone comprising the cliff section at 0–600 m, and a proximal deformation zone comprising the cliff section at 600–920 m. Within the distal deformation zone sixteen thrust sheets are identified, whereas only two thrust sheets are recorded in the proximal zone. In general, the thrust sheets are composed of a diamicton (unit 1) overlain by a varied succession of glaciofluvial sediments (unit 2a–2e). The interpreted architecture of the thrust sheets is shown in Fig. 6.

The exposure in the first 100 m of the southern end of the cliff constitutes the most distal part of the glaciotectonic complex. It is somewhat obscured by vegetation which also covers the contact to the foreland (Fig. 2). Two flat-lying thrust sheets (A and B) are inferred from divergent bedding directions observed within the gravel (unit 2c) and sand (unit 2d) (Fig. 6). Thrust sheet A is about 15 m thick and is composed of unit 1 overlain by a succession of unit 2a–2d. The frontal part of the thrust sheet is defined by a footwall ramp at point 10 m along which thrust sheet A has been displaced for about 1–2 m. During the displacement a fault-propagation fold developed in the hanging-wall of thrust sheet A, causing the bedded gravel (unit 2c) to be folded (Fig. 2). The fold developed because the propagating thrust sheet lost slip towards the tip of the fault, and the lack of slip was then compensated by folding (Brandes & Le Heron 2010). The trailing end of thrust sheet A is truncated by thrust sheet B at point 55 m. Thrust sheet B is approximately 15 m thick and consists of unit 1 with an overlying succession of unit 2c–2b. Unit 4 was deposited on top of the crest of the thrust sheet (Fig. 6). The gravel layer (unit 2c) located between points 40 m and 47 m outlines a hanging-wall anticline at the frontal edge of the thrust sheet. The thrust sheet is estimated to have been displaced approximately 17 m.

Between points 80 m and 90 m, a 1 m thick layer of gravel (unit 2c) is seen up-thrust into the overlying sand (unit 2d), generating divergent bedding directions (Fig. 2). On the basis of the squeezed displacement of the gravel layer it is inferred that the *c.* 7 m thick thrust sheet C was displaced approximately 13 m on top of thrust sheet B (Fig. 6). At its trailing end, thrust sheet C is folded into a footwall syncline, causing the tilting of horizontally bedded sand between points 100 m and 110 m (Fig. 2). The footwall syncline is cut by a thrust fault dipping *c.* 31° NE. The thrust fault forms a footwall ramp along which the *c.* 6 m thick thrust sheet D was displaced about 17 m. The thrust fault is identified in the overlying sand (unit 2d) as a 2–3 cm thick, gravelly clay layer.

Thrust sheet E was displaced about 9 m over the footwall of thrust sheet D. Initially, the two thrust sheets constituted one thrust sheet, which became internally divided by a thrust fault separating it into two individual thrust sheets. During the propagation of thrust sheet E an upper footwall ramp developed, resulting in the formation of a hanging-wall anticline seen at point 135 m (Fig. 6). Within unit 1 several fissures developed during displacement of thrust sheet D and E. Some of the fissures (at point 140 m) show similar orientation as the fault beneath thrust sheet D, while others (at point 118 m) are more or less orientated perpendicular to the strike of the thrust fault (Fig. 2).

▶ Fig. 6. Interpreted large-scale glaciotectonic structures at Halk Hoved. The black dashed line at the top of the cross section represents the glaciotectonic unconformity, whereas the black dashed line between unit 1 and the underlying aquifer indicates the décollement plane. A reconstruction of the top of the thrust-fault complex (prior to erosion) is shown above the glaciotectonic unconformity. The unexposed area below the décollement plane is interpreted to constitute glaciofluvial sand deposits based on wells located inland west of the profile.

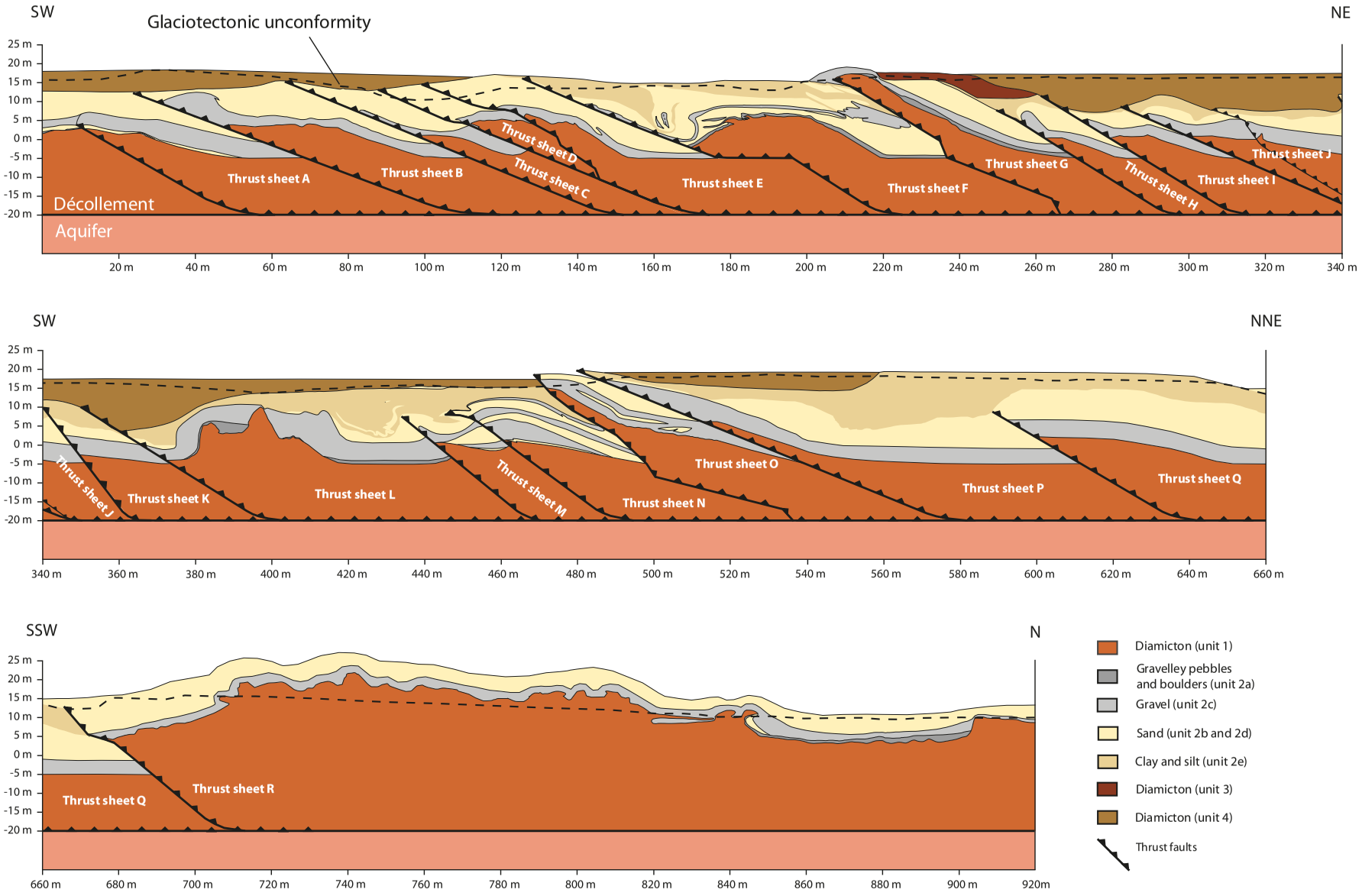
SW
Glaciotectonic unconformity
NE
25 m
20 m
15 m
10 m
5 m
0 m
-5 m
-10 m
-15 m
-20 m
Décollement
Aquifer
Thrust sheet A
Thrust sheet B
Thrust sheet C
Thrust sheet D
Thrust sheet E
Thrust sheet F
Thrust sheet G
Thrust sheet H
Thrust sheet I
Thrust sheet J
20 m
40 m
60 m
80 m
100 m
120 m
140 m
160 m
180 m
200 m
220 m
240 m
260 m
280 m
300 m
320 m
340 m
SW
NNE
Thrust sheet J
Thrust sheet K
Thrust sheet L
Thrust sheet M
Thrust sheet N
Thrust sheet O
Thrust sheet P
Thrust sheet Q
340 m
360 m
380 m
400 m
420 m
440 m
460 m
480 m
500 m
520 m
540 m
560 m
580 m
600 m
620 m
640 m
660 m
SSW
N
Thrust sheet Q
Thrust sheet R
660 m
680 m
700 m
720 m
740 m
760 m
780 m
800 m
820 m
840 m
860 m
880 m
900 m
920m
Diamicton (unit 1)
Gravelley pebbles and boulders (unit 2a)
Gravel (unit 2c)
Sand (unit 2b and 2d)
Clay and silt (unit 2e)
Diamicton (unit 3)
Diamicton (unit 4)
Thrust faults

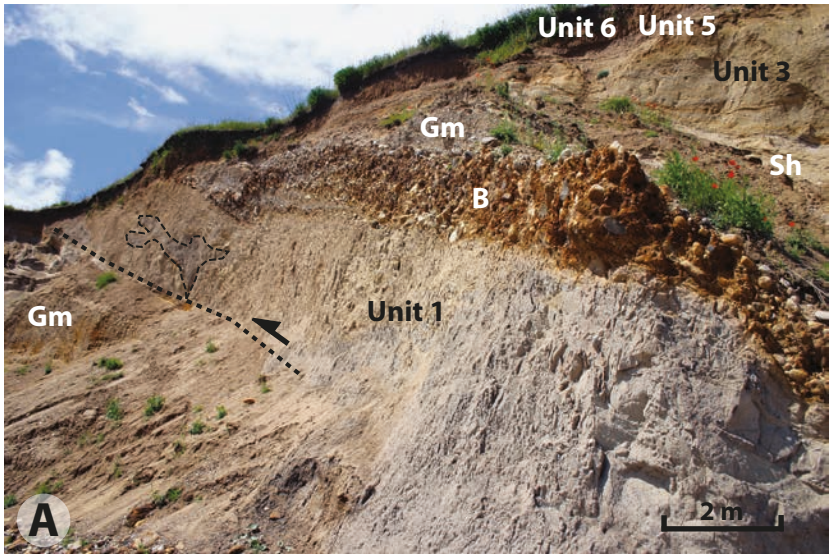

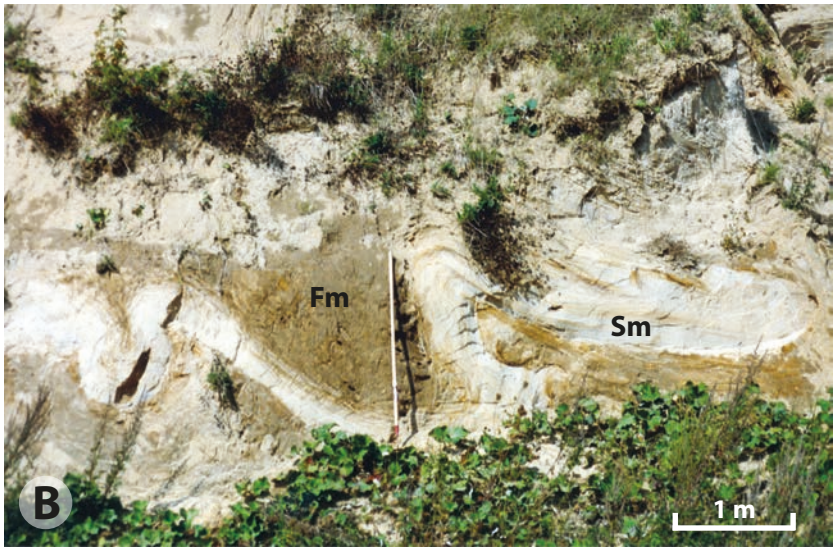

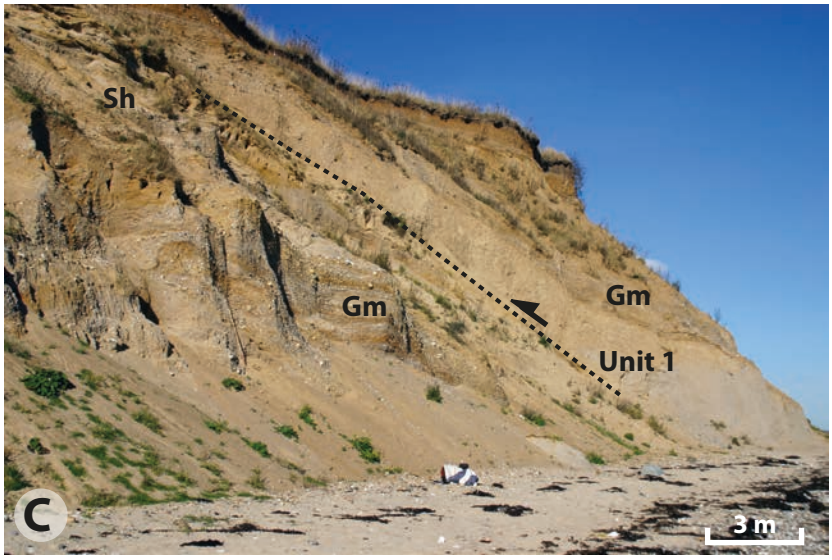

B Boulder
Gm Gravel, massive
Sm Sand, massive
Sh Sand, horizontally laminated
Fm Fines (silt, clay), massive

Fig. 7. **A**, The steeply dipping thrust sheet G composed of a diamicton (unit 1) overlain by a succession of B, Gm and Sh from unit 2. The thrust sheet is discordantly overlain by brown, silty diamicton of unit 3 seen in the upper right corner of the picture. Unconformably overlying thrust sheet G and unit 3 is a layer of gravel and sand (unit 5) followed by the upper diamicton (unit 6). Towards the left a displaced lens of massive gravel is interbedded in unit 1. Around 210–240 m in the profile. **B**, An overturned fold of fine-grained sand within unit 2e located between points 427 m and 433 m. **C**, Thrust sheet O composed of a wedge of diamicton (unit 1) and gravel (Gm, unit 2c), overlying thrust sheet N. In the top of the footwall block below the thrust fault the planar bedded coarse-grained gravel (Gm) is deformed by smaller reverse faults to form an imbricate stack between points 455 and 470 m in the profile.

The hanging-wall anticline of thrust sheet F is exposed at 170–210 m in the cliff section (Fig. 2). The anticline formed as the thrust sheet F was displaced about 30 m up along the footwall ramp and over the flat at the back of thrust sheet E (Fig. 6). Thrust sheet F is *c.* 18 m thick and comprises unit 1 overlain by a succession of unit 2a–2e. Unit 1 is intersected by vertical fissures, and in the foreland-dipping limb of the hanging-wall anticline small-scale thrusts cut the upper contact of unit 1 (Fig. 2). The thrust fault is recognised in the glaciofluvial sediments by a dislocated layer of gravel (unit 2c) between points 140 m and 160 m. During thrusting small decimetre-scale reverse faults formed in the sand (unit 2d) above the gravel layer (Fig. 2). Just above the thrust fault at point 160 m isolated gravel layers (unit 2c) are seen lying almost vertical in the sandy unit (unit 2d) (Fig. 2). The sand and gravel pockets are interpreted to constitute the core of an upright anticline of the glaciofluvial clay and silt (unit 2e) disturbed by hydrodynamic mobilisation due to increased compression during translation (Fig. 6).

The *c.* 14 m thick thrust sheet G consists of unit 1 followed by a glaciofluvial succession of unit 2a and unit 2c–2e. The frontal edge of thrust sheet G is truncated by a glaciotectonic unconformity (Fig. 6). The thrust sheet was displaced at least 25 m on top of the footwall of thrust sheet F. During displacement a small hanging-wall anticline (seen at point 240 m in Fig. 2) formed above a hanging-wall ramp (Fig. 6). Furthermore, a local imbricate fan of gravel with at least four reverse faults formed within the footwall (seen at point 220 m) (Fig. 2). Along the upper hanging-wall flat an intrusion of massive gravel (9 m in length) is observed in unit 1 (Fig. 7a) which, facilitated by high pore-water pressure, was injected during stress propagation. Thrust sheet G is truncated by thrust sheet H whose frontal edge consisting of a glaciofluvial succession of unit 2c–2e is exposed at point 260 m (Fig. 2). It is estimated that thrust sheet H was displaced approximately 8 m, which caused the overturned folding of the horizontally bedded gravel and sand (unit 2c and 2d). An erosional unconformity cuts the tip of the hanging-wall of the thrust sheet upon which unit 3 was deposited (Fig. 6).

In the lower part of the 280–350 m section the cliff exposure is limited. However, based on variation in bedding directions and the presence of unit 1 between points 280 m and 290 m and its recurrence at point 320 m (Fig. 2), it is inferred that this cliff section contains three thrust sheets – thrust sheet I, J and K (Fig. 6). All three thrust sheets are composed of unit 1 succeeded by a succession of unit 2c–2e. Both thrust sheets I and J are estimated to have been displaced about 8 m along the thrust faults, whereas thrust sheet K seems only to have been displaced 2 m. At point 320 m the hanging-wall of thrust sheet J is cut by a reverse fault along which a fault-propagation fold formed within the gravel (unit 2c) (Fig. 6). Displacement along this reverse fault was less than 1 m. The three thrust sheets and thrust sheet L are truncated by an erosional unconformity whereupon unit 4 was deposited (Fig. 6). Both unit 3 and unit 4 are interpreted to have been deposited in a piggyback basin, here designating a local depositional basin wherein sediments are syntectonically accumulated on the back of translating thrust sheets (Pedersen 2005).

Thrust sheet L is composed of unit 1 and a succession of unit 2a and unit 2c–2e. At the frontal edge, the thrust sheet developed into a major diapir (between points 380 m and 410 m in Fig 2.). The diapir formed as the lower part of the till (unit 1) became mobilised and intruded the overlying boulder (unit 2a) and gravel beds (unit 2c), causing the undulation of these layers (Pedersen 2005). The compressional deformation was here released in hydrodynamic brecciation, and displacement along the thrust fault only amounted to 2 m. In the crest of thrust sheet L open, inclined folds as well as recumbent folds are observed within the glaciofluvial succession of clay and silt (unit 2e) between point 420 m and 440 m. A fold axis of 319°/9° was constructed from an overturned fold outlined in a *c.* 0.5 m thick sand layer interbedded in unit 2e (Fig. 7b). This fold axis direction indicates compressive stress from NE. At the trailing end, thrust sheet L is folded into a footwall syncline (Fig. 6).

The approximately 17 m thick thrust sheets M and N consist of unit 1 overlain by unit 2a–2e. Possibly, thrust sheets M and N initially constituted one thrust sheet but became internally divided by the thrust fault at point 460 m at a late stage in the deformation. The tip of the thrust fault separating the two sheets is refracted into parallelism with the bedding in unit 2e, which tends to make thrust sheet M a duplex structure below thrust sheet N (Fig. 6). The two thrust sheets are displaced along a blind thrust fault that terminates beneath the succession of glaciofluvial clay and silt (unit 2e). Thrusting was first initiated by the propagation of thrust sheet M along a fault plane dipping 39° ENE. A hanging-wall anticline (seen between points 450 m and 480 m in Fig. 2) formed as thrust sheet M was displaced about 8 m. As thrust sheet N was displaced about 2 m along the *c.* 30° dipping thrust fault, the underlying sediments were folded into a footwall syncline where the planar sand (unit 2d) was tilted vertically in the northern limb (Fig. 2). In the hanging-wall of thrust sheet N a local imbricate fan formed with more than four reverse faults in the gravel beds of unit 2c and 2d. One of these reverse faults can be traced to continue down into the underlying unit 1

dipping 44° NE (Fig. 2). The reverse faults are therefore interpreted to have been formed by multiple small-scale up-thrusts of unit 1.

Thrust sheet O is *c.* 18 m thick and, judged from the scarce exposure, is interpreted to comprise unit 1 overlain by unit 2c and likely unit 2d. During propagation unit 1 became wedge-shaped because of ramping (Fig. 7c). Furthermore, a small hanging-wall anticline formed above the hanging-wall ramp seen at point 500 m (Fig. 2). The frontal part of the hanging-wall thrust sheet O is truncated by a glaciotectonic unconformity (Fig. 6). Within the hanging-wall divergent bedding directions suggest that a thrust fault developed in the gravel layer, causing a local thickening of the succession. It is estimated that thrust sheet O was displaced at least 30 m.

In the cliff section at 520–680 m only the upper part of the cliff is exposed. The inferred thrust sheets in this section are, therefore, somewhat uncertain. For both thrust sheet P and Q there is no direct evidence of a thrust fault. Thrust sheet P is defined on the basis of divergent bedding directions within the layer of gravel (unit 2c), while thrust sheet Q is determined from the divergent bedding directions within the glaciofluvial sand (unit 2d) and clay/silt (unit 2e) (Fig. 2). In the hanging-wall of thrust sheet Q the horizontally bedded clay and silt of unit 2e seems generally undisturbed, whereas in the footwall of thrust sheet P unit 2d has been subjected to ductile deformation. The folds observed within unit 2e likely formed during propagation of thrust sheet Q. The deformed succession of unit 2e is discordantly overlain by unit 4 (Fig. 2). It is estimated that thrust sheets P and Q are *c.* 30 m thick and were displaced 25 m and 13 m, respectively.

To the north, thrust sheet Q is overlain by thrust sheet R. This thrust sheet comprises unit 1 and a glaciofluvial succession of unit 2c–2d and was displaced *c.* 15 m up along the footwall ramp on thrust sheet Q. Thrust sheet R was presumably affected by diapirism which has caused the trailing end to dip upward (Fig. 6). Diapirism probably dominated the cliff section between point 710 m and 840 m. In the two-dimensional drawing by Jessen (1930, 1935) the northern part of the cliff is dominated by glaciofluvial sediments with only a few traces of the lower till, whereas the drawing by Frederiksen (1976) shows a greater extent of the lower till, which is even greater in the current study. Frederiksen (1975) attributed this change in material to erosion gradually stripping away material from an upright anticline consisting of units 1 and 2. The fold likely formed because of diapirism as the mobilised till (unit 1) intruded into the overlying glaciofluvial succession (unit 2a–2e) and thereby caused the folding of these layers.

Structural framework and balancing of the thrust-fault complex

The cross section of the glaciotectonic complex is approximately 900 m long. The complex contains at least eighteen, generally 15–20 m thick thrust sheets displaced along thrust faults dipping 30–40° NNE. No thrust faults are observed in the northernmost part of the cliff face between points 720 m and 920 m, but the cliff section is partly obscured by scree. Diapirism is, though, interpreted to have played an important role in this part of the complex.

The thrust faults are rooted in a basal décollement plane estimated at around 20 m below sea level (Fig. 6). The upturned ends of the thrust sheets would have formed the ridges of the thrust-fault complex. On the up-glacier side of the ridges depressions formed, resulting in piggyback basins wherein units 3 and 4 were deposited.

The architecture of the glaciotectonic complex is dominated by thrust faults with a ramp-flat geometry whereby a hanging-wall flat is displaced on top of a footwall ramp. Thrust sheet F, however, is inferred to have been displaced along a thrust fault with a ramp-flat-ramp geometry. The hanging-wall of thrust sheet F was thrust up along a lower footwall ramp, translated along the intermediate footwall flat of thrust sheet E and finally displaced up along the upper footwall ramp. During propagation over the lower footwall ramp-hinge the hanging-wall was folded into an anticline with a foreland-dipping forelimb and a hinterland-dipping backlimb. Hanging-wall anticlines have also been observed above the hanging-wall ramps of thrust sheets E, G and O which were likewise formed by the folding of the hanging-wall as it propagated over the ramp-hinge.

At the trailing end of thrust sheets C, L and M, footwall synclines formed beneath the footwall ramps. The synclines formed because the tip of the thrust sheets became folded as the hanging-walls were thrust up along the ramps. Continued propagation resulted in the thrust faults breaking through the folded layers and separating the fold so that a syncline formed below the thrust faults and an anticline above, thereby causing the tilting of the horizontally bedded strata towards the thrust faults.

On the basis of two-dimensional mapping of the cliff section we estimate that the thrust sheets were displaced at least 235 m (the sum of displacement for all the thrust sheets). The restored length of the complex (the lateral extension of deposits prior to deformation) is therefore at least 955 m as the length of the thrust-fault complex is calculated to be 720 m. The

cliff section between points 720 m and 920 m is omitted because the presence of thrust faults in this part of the cliff is unknown. The glaciotectonic shortening of the foreland can be calculated using the formula by Croot (1988) whereby Shortening = (change in length/restored length) ×100. Accordingly, we estimate that the complex has undergone a shortening of least 24% as a result of the deformation.

Glaciodynamic stratigraphy

Based on the glaciodynamic stratigraphy proposed by Pedersen (1996), the sediments and the glaciotectonic deformation in the Halk Hoved cliff section represent three glaciodynamic events which correspond to three glaciodynamic sequences.

The first glaciodynamic sequence is represented by units 1 and 2. In previous studies, Houmark-Nielsen (1987, 2007) correlated unit 1 to the Lillebælt Till Formation deposited during the Warthe glaciation in Late Saalian. The glaciers advanced through the Baltic depression from easterly directions, and the Lillebælt Till Formation is therefore characterised by a pronounced Baltic clast provenance (Houmark-Nielsen 1987, 2007) with a high content of both Cretaceous–Danian limestone and Palaeozoic limestone (Fig. 3).

On top of the Lillebælt Till Formation the fining-upward succession of glaciofluvial sediments (unit 2a–2e) was deposited. In the current investigation, the glaciofluvial sediments are shown to petrographically deviate from the underlying Lillebælt Till Formation by having a lower content of crystalline rocks and a higher content of quartz (Fig. 3). The difference in the petrographical composition could indicate that unit 2 was not deposited by the same ice advance as unit 1. The glaciofluvial sediments were estimated to be of Weichselian age based on studies of similar deposits overlying Eemian material (Houmark-Nielsen 1987). However, OSL (Optically Stimulated Luminescence) dates show ages between 169 and 167 kyr (Houmark-Nielsen 2007), indicating that the glaciofluvial succession, like the Lillebælt Till Formation, most probably was deposited during the Warthe glaciation. If so, then the petrographical deviation must be the result of the difference in the depositional processes as the two units represent two different depositional environments; a subglacial environment and a glaciofluvial environment.

The second glaciodynamic sequence represents the large-scale deformation of units 1 and 2 followed by the syntectonic deposition of units 3 and 4. The structural analysis of the glaciotectonic structures showed that the sediments were primarily deformed by glacial stress from N-NE. The sediments are, therefore, interpreted to be deformed by the NE advance in Late Weichselian, which is consistent with previous studies (Frederiksen 1975; Houmark-Nielsen 1987). During deformation piggyback basins formed, resulting in syntectonic deposition of units 3 and 4. The petrographical composition of unit 3 shows a strong resemblance to that of the underlying glaciofluvial sediments (unit 2) (Fig. 3). Unit 3 is interpreted to have been deposited by a hyperconcentrated flow, which was generated by the mobilisation of water-saturated material down the back of thrust sheet G. The primary source of material would have been the glaciofluvial sediments of unit 2, and unit 3 therefore inherited the petrographical composition of unit 2.

In contrast to units 2 and 3, unit 4 has a high content of crystalline rocks and a low content of quartz (Fig. 3). In previous investigations unit 4 was interpreted as a subglacial till (Jessen 1930; Frederiksen 1976) and petrographically correlated to the Mid Danish Till Formation deposited by the NE advance in Late Weichselian (Houmark-Nielsen 1987, 2007). Although unit 4 in the current study is interpreted as a glaciolacustrine diamicton, it is possible that the Mid Danish Till Formation may be present at Halk Hoved because unit 4 between points 490 m and 560 m was not examined up-close. At point 330 m a sample from the upper part of unit 4 (S4.7; Fig. 2) has a different petrographical composition compared to the rest of the samples from unit 4 (Fig. 3). The sample differs by containing a higher quantity of sedimentary rocks, Cretaceous–Danian limestone and Palaeozoic limestone, while the content of flint is very low. This petrographical deviation could indicate that this part of unit 4 was deposited by another ice advance, possibly the Young Baltic advance, because the high content of sedimentary rocks and Palaeozoic limestone suggests a Baltic origin. However, in the current study it is not possible to ascertain whether this deviating sample represents a different glaciation or depositional environment than the rest of unit 4.

The whole assemblage of units 1–4 constitutes one glaciotectonic unit. The complex is truncated by a glaciotectonic unconformity, formed as the NE advance finally overrode and eroded the upper part of the thrust-fault complex.

The third glaciodynamic sequence is represented by units 5 and 6. The discontinuous glaciofluvial succession (unit 5) was deposited on top of the glaciotectonic unconformity. It is overlain by unit 6 (till) that petrographically correlates to the East Jylland Till Formation (Houmark-Nielsen 1987, 2007) deposited by the Young Baltic advance in Late Weichselian. The Young Baltic advance transgressed through the Baltic depression, and its deposits should therefore be char-

acterised by a high content of Palaeozoic limestone. The fact that no Cretaceous–Danian limestone or Palaeozoic limestone have been observed in unit 6 could presumably be due to weathering. The glaciofluvial sediments (unit 5) were most likely also deposited by the Young Baltic ice sheet, but it is possible that it may also have been deposited by the NE advance during its retreat from the MSL.

Factors controlling the glaciotectonic deformation

In order for proglacial deformation to occur, the compressive stress imposed on the foreland by the ice sheet must exceed the strength of the weakest sediment within the substratum. Several studies of both modern and ancient glaciotectonic complexes (Aber *et al.* 1989; Pedersen 1996, 2005; van der Wateren 1995, 2005) have shown that the presence of fine-grained material (*e.g.* Tertiary marine clay and silts, glacial and interglacial lacustrine fine-grained sediments or marine clay and silts) is often a precondition for the development of large-scale proglacial deformation. At the 1 km long coastal cliff of Ristinge Klint, the décollement plane developed within marine Cyprina Clay which, facilitated the stacking of more than thirty up to 20 m thick thrust sheets (Aber *et al.* 1989; Kristensen *et al.* 2000). Similarly, the formation of multiple thrust sheets and nappes at the 6 km long costal cliff of Rubjerg Knude was facilitated by glaciolacustrine clay (Lønstrup Klint Formation), resulting in a 50% glaciotectonic shortening of the substratum (Pedersen 2005). In both cases the fine-grained layer, assisted by high pore-water pressures, acted as a low-friction plane along which the thrust sheets were easily displaced.

In the investigation by Frederiksen (1975), as well as in the current study, no evidence of such a fine-grained layer acting as a low-friction sliding plane was found at Halk Hoved. In this area the pre-Quaternary surface is situated well below the décollement plane, and Tertiary clay is therefore excluded as a potential contributor to failure.

If the lithology is less favourable to deformation, such as in the absence of a fine-grained layer, then the formation of a décollement plane is strongly dependent upon the hydrogeology of the foreland. Simulations of groundwater flow beneath past ice sheets show that groundwater generally flows downwards beneath the ice sheet and upwards at the ice margin and in the proglacial zone (Boulton & Caban 1995; Piotrowski 1997a, b; Carlson *et al.* 2007; Person 2007). When an aquifer in the proglacial zone is overlain by a low-conductivity layer (*e.g.* till or permafrost), the upward flow will cause water pressures to build up in the aquifer. If such an aquifer is loaded sufficiently rapidly by an ice sheet, preventing gradual pressure dissipation, the elevated pore-water pressures can cause hydrofractures and liquefaction/dilation in the overlying sediments (Boulton & Caban 1995). Liquefaction/dilation occurs as the high water content weakens the electrostatic bonds and increases the distance between the individual grains, thereby reducing the shear strength of the sediment. As shear stress is applied to the liquefied/dilated sediment, the mixture of water and sediment would initiate flow (Evans *et al.* 2006), so that during thrusting the mixture would act as a lubricant creating a plane of low resistance whereupon the thrust sheet is easily displaced (Strayer *et al.* 2001; Philips *et al.* 2008).

In the substratum adjacent to Halk Hoved the Lillebælt Till Formation (unit 1) is estimated to be more than 10–15 m thick (Houmark-Nielsen 2007). In a few well logs approximately 3 km west of Halk Hoved, obtained from the web-based Jupiter well log archive (GEUS 2011a), the thick Lillebælt Till Formation is observed to overlie glaciofluvial sand. Recent TEM (Transient ElectroMagnetic) surveys in the area, obtained from the web-based GERDA geophysical data archive (GEUS 2011b), show the sand layer situated in a more than 100 m deep buried valley extending from Halk Strand northeast of Hejsager and up towards Grarup and Haderslev Fjord (Fig. 1). With the present data, it is not known if the sand layer also extends eastwards into the Halk Hoved area. If it does, the décollement plane likely developed along the lithostratigraphical boundary between the sand and the till. The base of the Lillebælt Till would thus be situated at the décollement plane around 20 m below sea level, which is in accordance with the thickness estimate of Houmark-Nielsen (2007).

The formation of modern glaciotectonic complexes is often associated with the presence of permafrost (Hambrey & Huddart 1995; Boulton *et al.* 1999). As mentioned above, permafrost may be conducive to proglacial deformation as it may facilitate high groundwater pressures. Permafrost, furthermore, hardens the sediments so that the compressive stress applied by the ice sheet can be transmitted horizontally over a large area. However, some authors (Croot 1987, 1988; van der Wateren 2005) emphasise that permafrost is not crucial in the formation of large thrust-fault complexes. In the southern part of Jutland periglacial conditions dominated throughout Weichselian and were only interrupted by the Ristinge ice advance in Middle Weichselian and the NE advance with its successive readvances in Late Weichselian (Houmark-Nielsen 2007). It is possible that prior to deformation permafrost was present as the ice sheet

advanced from NE towards the MSL, but in the current investigation there is no sedimentary evidence of permafrost.

Formation of the thrust-fault complex

The thrust-fault complex was formed by proglacial glaciotectonic deformation caused by the NE advance in Late Weichselian. The foreland would have consisted of a fining-upward glaciofluvial succession (unit 2) overlying a thick till layer (unit 1), which in turn rested on an aquifer. As the ice sheet advanced towards the area, basal meltwater would have been partly drained through the substratum generating glacially driven groundwater flow in the aquifer beneath the till layer. In front of the ice margin the high groundwater pressures beneath the till triggered its oversaturation and drop of shear strength. Thrust faults developed as the lateral stresses within the foreland, generated primarily by the weight of the ice sheet (known as gravity spreading; cf. Huuse & Lykke-Andersen 2000; Bennett 2001), exceeded the shear strength of the till. As a thrust sheet formed it was pushed up along the fault plane facilitated by liquefaction/dilation in the lower part of the till. In some areas the dilation of the till mass resulted in diapirism as seen in thrust sheet K and to a more extensive degree in the northernmost part of the cliff between points 700 m and 920 m (Fig. 6).

A new thrust sheet usually developed in the footwall of an older thrust sheet so that the older thrust sheets would be carried forward on the backs of the younger ones, which is known as piggyback thrusting analogous to thin-skinned tectonics within orogenic belts (cf. Suppe 1985). The sequence of thrust sheets, therefore, started with thrust sheet R and ended with thrust sheet A. However, two of the thrust sheets, E and N, formed in the hanging-wall of pre-existing thrust sheets, D and M, because of the development of internal thrust faults. Thrust sheet propagation along the thrust faults ranged between 1 m and 30 m, which is low compared to other thrust-dominated complexes such as Rubjerg Knude and Ristinge Klint. The reason for this difference may be the fact that the faults developed in till and not in fine-grained material. The till, even though dilated/liquefied, would likely have been more resistant to sliding during propagation because of the higher frictional strength of the till compared to fine-grained sediments such as marine clay and glaciolacustrine clay.

During deformation piggyback basins formed, giving rise to proglacial ponds collecting meltwater and sediment. A larger basin formed between thrust sheets G and O, wherein syntectonic deposition of units 3 and 4 occurred. The tip of thrust sheet G created a ridge with glaciofluvial sediments on the up-glacier side. High pore-water pressures within the glaciofluvial sediments, and gravity, caused the material to slide down the ridge into the piggyback basin generating a hypercontrated flow of predominantly gravel, sand and silt (unit 3). In the water-filled basin glacial diamicton (unit 4) was deposited by debris rainout from floating icebergs. After the piggyback basins became filled by sediment, the NE advance overrode the glaciotectonic complex and truncated its upper part, smoothing the geomorphological expression of the complex.

Conclusions

The history of the glaciotectonic complex at the coastal cliff of Halk Hoved comprises three major ice advances during the late Saalian and late Weichselian glaciations. In Late Saalian, the Warthe ice sheet advanced from easterly directions through the Baltic region and deposited the Lillebælt Till Formation (unit 1). During the retreat, a fining-upward succession of glaciofluvial sediments (unit 2a–2e) was deposited. Following a long ice-free period, the advance of the late Weichselian ice sheet from the northeast triggered prominent proglacial deformation and a thrust-fault complex formed, extending for *c.* 700 m in front of the ice margin. The glaciotectonic complex comprises at least eighteen *c.* 15–20 m thick thrust sheets stacked by piggyback thrusting. Accumulated displacement amounts to at least 235 m, resulting in at least 24% shortening of the complex. Failure is suggested to be due to elevated pore-water pressure in a confined sand aquifer beneath the Lillebælt Till Formation. The high pore-water pressures resulted in dilation/liquefaction which reduced the shear strength of the till and a décollement plane formed along the lithostratigraphical boundary between the Lillebælt Till Formation and the underlying aquifer. The décollement plane is estimated to be situated about 20 m below sea level. During deformation, piggyback basins formed between the thrust sheets, wherein a sediment of hyperconcentrated flow (unit 3) and glaciolacustrine diamicton (unit 4) were syntectonically deposited. The complex is truncated by a glaciotectonic unconformity, formed as the NE advance finally overrode and eroded the upper part of the thrust-fault complex. Following an ice-free phase, a glaciofluvial succession (unit 5) and the East Jylland Till Formation (unit 6) were deposited by the Young Baltic ice stream as it advanced

from southeast through the Baltic region. The Halk Hoved glaciotectonic complex illustrates the nature of the interactions between the Weichselian Ice Sheet and its soft beds, in particular the role of localized sediment deformation triggered by elevated subglacial pore-water pressures close to the ice sheet periphery.

Acknowledgements

We thank the technicians at the Department of Geoscience, Aarhus University for their help with laboratory analyses, Jette Sørensen (VIA University College, Horsens) for discussions and comments on the first draft of this paper, and Rud Friborg (Sønderjylland Amt) for discussions and support. Journal referees Stig A. Schack Pedersen and Michael Houmark-Nielsen are thanked for their thorough and constructive reviews which considerably improved the paper.

Dansk sammendrag

Størstedelen af de kortlagte glacialtektoniske komplekser i Danmark blev dannet under fremrykningen af de store skandinaviske gletschere i Weichsel. Isens fremadrettede tryk på underlaget forårsagede foldning og oppresning af sedimenterne i flager, der blev stablet oven på hinanden. Langs den ca. 900 m lange og 10–20 m høje kystklint Halk Hoved, der er beliggende ca. 12 km sydøst for Haderslev i den sydlige del af Jylland, ses et smukt og velblottet eksempel på et glacialtektonisk kompleks primært opbygget af skråtstillede flager.

I en strukturgeologisk og sedimentologisk undersøgelse af klinten er der udarbejdet et geologisk tværsnit, som viser den overordnede struktur af de glacialtektoniske deformationer samt udbredelsen af de enkelte lithofacies. Lagserien er på baggrund af de sedimentologiske karakteristika samt kornstørrelses- og fingrusanalyser inddelt i seks lithostratigrafiske enheder. Den nederste lithostratigrafiske enhed (unit 1) udgøres af en mindst 4 m tyk, leret till, som henføres til Lillebælt Till Formationen afsat i forbindelse med Warthe fremstødet i Sen Saale. Tillen overlejres af en ca. 6–12 m tyk smeltevandssekvens (unit 2), hvis kornstørrelse aftager opefter. Smeltevandssekvensen tolkes som repræsenterende en ændring i det glaciofluviale miljø fra en proximal til distal flodslette som følge af tilbagesmeltningen af Warthe fremstødet i Sen Saale.

Både Lillebælt Till Formationen og den overliggende smeltevandssekvens blev udsat for proglacial deformation i forbindelse med Nordøst (NØ) fremstødet i Sen Weichsel. Det foreslås, at deformationen skyldes forhøjet porevandstryk i underlaget. Under fremrykningen steg vandtrykket i sandlag under Lillebælt Till Formationen, og gradientforholdene blev opadrettede. Dette førte til et forhøjet porevandstryk i tillens nedre del. Isens fremadrettede tryk på underlaget samt det forhøjede porevandstryk resulterede i dannelsen af forkastninger hældende 30–40° NNØ, forbundet af "et décollementplan" (LML) langs laggrænsen mellem grundvandsmagasinet og tillen. Stedvis førte det forhøjede porevandstryk også til diapirisme, hvori den vandmættede till trængte op i de overliggende sedimenter.

Langs forkastningerne blev mindst 18 ca. 15–20 m tykke flager forskudt i en størrelsesorden af 1–30 m. De blev stablet oven på hinanden via piggyback overskydning, hvori de yngste flager blev forskudt under den samlede vægt af tidligere dannede overskydningsflager. Der har i alt været en samlet forskydning på ca. 240 m svarende til en glacialtektonisk afkortning af landskabet på ca. 24%.

Diskordant over de deformerede sedimenter, ses en 1–5 m tyk, siltet–sandet diamicton (unit 3) med enkelte indslag af sorteret materiale. Enheden tolkes at være aflejret af en hyperkoncentreret sedimentstrøm, der opstod ved en mobilisering af smeltevandssedimenterne (unit 2) ned langs ryggen af en glacialtektonisk flage. Enhed 3 er overlejret af en 2–13 m tyk, siltet–leret diamicton (unit 4) tolket som aflejret i en issø foran NØ fremstødet. Både enhed 3 og 4 tolkes som syntektonisk aflejret i et piggyback bassin, dvs. et bassin beliggende ovenpå og mellem de glacialtektoniske flager.

Hele sekvensen af sedimenter er afskåret af en glacialtektonisk inkonformitet og diskordant overlejret af en diskontinuert, 1–4 m tyk smeltevandssekvens. Toppen af klinten er dækket af en 1–2 m tyk, leret till, der tilhører East Jylland Till Formationen. Begge enheder er afsat af det Ungbaltiske fremstød i Sen Weichsel.

References

Aber, J.S., Croot, D.G. & Fenton, M.M. 1989: Glaciotectonic landforms and structures. Kluwer Academic Publisher, Dordrecht, Netherlands, 200 pp.

Benn, D.I. 1996: Subglacial and subaqueous processes near a glacier grounding line: sedimentological evidence from a former ice-dammed lake, Achnasheen, Scotland. Boreas 25, 23–36.

Bennett, M.R. 2001: The morphology, structural evolution and significance of push moraines. Earth-Science Reviews 53, 197–236.

Bennett, M.R., Huddart, D. & Thomas, G.S.P. 2002: Facies architecture within a regional glaciolacustrine basin: Copper River, Alaska. Quaternary Science Reviews 21, 2237–2279.

Beverage, J.P. & Culbertson, J.K. 1964: Hyperconcentrations of suspended sediment. Proceedings of the American Society of Civil Engineers, Journal of the Hydraulics Division 90, 117–128.

Bilka, L.H. & Nemec, W. 1998: Postglacial colluvium in western Norway: depositional processes, facies and Palaeoclimatic record. Sedimentology 45, 909–959.

Boulton, G.S. 1978: Boulder shapes and grain-size distributions of debris as indicators of transport paths through a glacier and till genesis. Sedimentology 25, 773–799.

Boulton, G.S. & Caban, P. 1995: Groundwater flow beneath ice sheets: part II – its impact on glacier tectonic structures and moraine formation. Quaternary Science Reviews 14, 563–587.

Boulton, G.S., van der Meer, J.J.M., Beets, D.J., Hart, J.K. & Ruegg, G.H.J. 1999: The sedimentary and structural evolution of a recent push moraine complex: Holmstrømbreen, Spitsbergen. Quaternary Science Reviews 18, 339–371.

Brandes, C. & Le Heron, D. 2010: The glaciotectonic deformation of Quaternary sediments by fault-propagation folding. Proceedings of the Geologists' Association 121, 270–280.

Carlson, A.E., Jenson, J.W. & Clark, P.U. 2007: Modeling the subglacial hydrology of the James Lobe of the Laurentide Ice Sheet. Quaternary Science Reviews 26, 1384–1397.

Croot, D.G. 1987: Glacio-tectonic structures: a mesoscale model of thin-skinned thrust sheets? Journal of Structural Geology 9, 797–808.

Croot, D.G. 1988: Morphological, structural and mechanical analysis of neoglacial ice-pushed ridges in Iceland. In Croot, D.G. (ed.): Glaciotectonics: forms and processes, 33–47. A.A. Balkema, Rotterdam, Netherlands.

Domack, E.W. & Lawson, D.E. 1985: Pebble fabric in an ice-rafted diamicton. Journal of Geology 93, 577–591.

Dowdeswell, J.A., Whittington, R.J. & Marienfeld, P. 1994: The origin of massive diamicton facies by iceberg rafting and scouring, Scoresby Sund, East Greenland. Sedimentology 41, 21–35.

Dreimanis, A. & Vagners, U.J. 1971: Bimodal distribution of rock and mineral fragments in basal tills. In: Goldthwait (ed.): Till, a Symposium, 237–250. Ohio State University Press.

Ehlers, J. 1979: Fine gravel analyses after the Dutch method as tested out on Ristinge Klint, Denmark. Bulletin of the Geological Society of Denmark 27, 157–165.

Evans, D.J.A., Philips, E.R., Hiemstra, J.F. & Auton, C.A. 2006: Subglacial till: Formation, sedimentary characteristics and classification. Earth-Science Reviews 78, 115–176.

Evenson, E.B., Dreimanis, A. & Newsome, J.W. 1977: Subaquatic flow tills: a new interpretation for the genesis of some laminated till deposits. Boreas 6, 115–133.

Frederiksen, J.K. 1975: Glacialtektoniske og -stratigrafiske undersøgelser i udvalgte områder i det sydlige Danmark. Prisopgave, University of Copenhagen, 170 pp.

Frederiksen, J.K. 1976: Hvad de Sønderjyske klinter fortæller. VARV 2, 35–45.

GEUS 2011a: Danmarks og Grønlands Geologiske Undersøgelse, Jupiter boredatabase. http://Jupiter.geus.dk.

GEUS 2011b: Danmarks og Grønlands Geologiske Undersøgelse, Jupiter geofysiske database. http://gerda.geus.dk/Gerda/.

Haldorsen, S. 1981: Grain-size distribution of subglacial till and its relation to glacial crushing and abrasion. Boreas 10, 91–107.

Haldorsen, S. 1983: Mineralogy and geochemistry of basal till and their relationship to till-forming processes. Geografisk Tidsskrift 63, 15–25.

Hambrey, M.J. & Huddart, D. 1995: Englacial and proglacial glaciotectonic processes at the snout of a thermally complex glacier in Svalbard. Journal of Quaternary Science 10, 313–326.

Houmark-Nielsen, M. 1987: Pleistocene stratigraphy and glacial history of the central part of Denmark. Bulletin of the Geological Society of Denmark 36, 1–189.

Houmark-Nielsen, M. 2007: Extent and age of Middle and Late Pleistocene glaciations and periglacial episodes in southern Jylland, Denmark. Bulletin of the Geological Society of Denmark 55, 9–35.

Huuse, M. & Lykke-Andersen, H. 2000: Large-scale glaciotectonic thrust structures in the eastern Danish North Sea. Geological Society, London, Special Publications 176, 293–305.

ICS, International Commission on Stratigraphy 2010: Regional chronostratigraphical correlation table for the last 270,000 years, Europe north of the Mediterranean. http://www.stratigraphy.org/upload/Quaternary_last270ka.pdf.

Jakobsen, P.R. 1996: Distribution and intensity of glaciotectonic deformation in Denmark. Bulletin of the Geological Society of Denmark 42, 175–185.

Jakobsen, P.R. 2003: GIS based map of glaciotectonic phenomena in Denmark. Geological Quarterly 47, 331–338.

Jessen, A. 1930: Klinten ved Halk Hoved. Danmark Geologiske Undersøgelse, VI Række 8, 26 pp.

Jessen, A. 1935: Beskrivelse til geologisk kort over Danmark. Kortbladet Haderslev. Danmark Geologiske Undersøgelse, I Række 17, 95 pp.

Kjær, K.H., Houmark-Nielsen, M. & Richardt, N. 2003: Ice-flow patterns and dispersal of erratics at the southwestern margin of the last Scandinavian Ice Sheet: signature of palaeo-ice streams. Boreas 32, 130–148.

Kristensen, P., Gibbard, P., Knudsen, K.L. & Ehlers, J. 2000: Last Interglacial stratigraphy at Ristinge Klint, South Denmark. Boreas 29, 103–116.

Kronborg, C. 1986: Fine-gravel content of tills. In: Møller, J.T. (ed.), Twentyfive Years of Geology in Aarhus. Aarhus University, Geoskrifter 24, 189–210.

Kronborg, C., Bender, H., Bjerre, R., Friborg, R., Jacobsen, H.O., Kristiansen, L., Rasmussen, P., Sørensen, P.R. & Larsen, G. 1990: Glacial stratigraphy of East and Central Jutland. Boreas 19, 273–287.

Krüger, J. & Kjær, K.H. 1999: A data chart for field description and genetic interpretation of glacial diamicts and associated sediments – with examples from Greenland, Iceland and Denmark. Boreas 28, 386–403.

Larsen, N.K., Piotrowski, J.A. & Kronborg, C. 2004: A multi-proxy study of a basal till: a time-transgressive accretion and deformation hypothesis. Journal of Quaternary Science 19, 9–21.

May, R.W. 1977: Facies model for sedimentation in the glacio-lacustrine environment. Boreas 6, 175–180.

Miall, A.D. 1985: Architectural-element analysis: a new method of facies analysis applied to fluvial deposits. Earth-Science Reviews 22, 261–308.

Mulder, T. & Alexander, J. 2001: The physical character of subaqueous sedimentary density flows and their deposits. Sedimentology 48, 269–299.

Pedersen, S.A.S. 1996: Progressive glaciotectonic deformation in Weichselian and Palaeogene deposits at Feggeklit, northern Denmark. Bulletin of the Geological Society of Denmark 42, 153–174.

Pedersen, S.A.S. 2005: Structural analysis of the Rubjerg Knude Glaciotectonic Complex, Vendsyssel, northern Denmark. Geological Survey of Denmark and Greenland Bulletin 8, 192 pp.

Person, M., McIntosh, J., Bense, V. & Remenda, V.H. 2007: Pleistocene hydrology of North America: The role of ice sheets in reorganizing groundwater flow systems. Reviews of Geophysics 45, RG3007, doi: 10.1029/2006RG000206.

Phillips, E., Lee, J.R. & Burke, H. 2008: Progressive proglacial to subglacial deformation and syntectonic sedimentation at the margins of the Mid-Pleistocene British Ice Sheet: evidence from north Norfolk, UK. Quaternary Science Reviews 27, 1848–1871.

Piotrowski, J.A. 1992: Till facies and depositional environments of the upper sedimentary complex from the Stohler Cliff, Schleswig-Holstein, North Germany. Zeitschrift für Geomorphologie Neue Folge 84, 37–54.

Piotrowski, J.A. 1997a: Subglacial hydrology in northwestern Germany during the last glaciation: groundwater flow, tunnel valleys, and hydrological cycles. Quaternary Science Reviews 16, 169–185.

Piotrowski, J.A. 1997b: Subglacial groundwater flow during the last glaciation in northwestern Germany. Sedimentary Geology 111, 217–224.

Piotrowski, J.A., Larsen, N.K., Menzies, J. & Wysota, W. 2006: Formation of subglacial till under transient bed conditions: deposition, deformation, and basal decoupling under a Weichselian ice sheet lobe, central Poland. Sedimentology 53, 83–106.

Rovey, C.W. & Borucki, M.K. 1995: Subglacial to Proglacial sediment transition in a shallow ice-contact lake. Boreas 24, 117–128.

Smed, P. 1981: Landskabskort over Danmark, Blad 2, Midtjylland. Geografforlaget, Brenderup, Danmark.

Sohn, Y.K., Rhee, C.W. & Kim, B.C. 1999: Debris flow and hyperconcentrated flood-flow deposits in an alluvial fan, northwestern part of the Cretaceous Yongdong Basin, Central Korea. Journal of Geology 107, 111–132.

Strayer, L.M., Hudleston, P.J. & Lorig, L.J. 2001: A numerical model of deformation and fluid-flow in an evolving thrust wedge. Tectonophysics 335, 121–145.

Suppe, J. 1985: Principles of Structural Geology. Englewood Cliffs, Prentice Hall, New Jersey, 537 pp.

van der Wateren, D.F.M. 1995: Structural geology and sedimentology of push moraines: processes of soft sediment deformation in a glacial environment and the distribution of glaciotectonic styles. Mededelingen Rijks Geologische Dienst 54, 168 pp.

van der Wateren, D.F.M. 2005: Ice-marginal terrestrial landsystems: southern Scandinavian Ice Sheet margin. In Evans, D.J.A. (ed.): Glacial landsystems,166–203. Arnold, London.

Instructions to authors

The Bulletin publishes articles normally not exceeding 16 printed pages, notes not longer than 4 pages, and short contributions of maximum 1 printed page. Longer articles may be published at the discretion of the editor, but it is advisable to consult the editor before submitting long manuscripts. Short contributions may be comments on previously published articles, presentation of current scientific activities, short scientific notes, or book reviews.

Manuscripts with complete sets of illustrations, tables, captions, etc., should be submitted electronically to the chief editor (lml@geus.dk). The **main text** with references and figure captions should be either in Word or pdf format, **figures** should be in either pdf, jpeg, or tiff format, and **tables** should be in Word text format, i.e. written in lines with tab spacing between table columns. "Word tables" are discouraged because they are not re-formatted easily. Consult the editor before submitting other formats.

Manuscripts will be reviewed by two referees; suggestions of referees are welcome. Articles will be published approximately in the order in which they are accepted for publication. The final decision on whether or not a manuscript will be accepted for publication rests with the chief editor, acting on the advice of the scientific editors.

Manuscript

Language – Manuscripts should be in English. Authors who are not proficient in English should ask an English-speaking colleague for assistance before submission of the manuscript.

Title – Titles should be short and concise, with emphasis on words useful for indexing and information retrieval. An abbreviated title to be used as running head must also be submitted.

Abstract – An abstract in English must accompany all papers. It should be short (no longer than 250 words), factual, and stress new information and conclusions rather than describing the contents of the manuscript. Conclude the abstract with a list of key words.

Main text – Use 1.5 or double spacing throughout, and leave wide margins. Italics should be used only in generic and species names and in some Latin abbreviations (*e.g. c., et al., ibid., op. cit*).

Spelling – Geological units named after localities in Greenland, formal lithostratigraphical units and intrusions named after localities in Greenland remain unchanged even if the eponymous locality names have since been changed in accordance with modern Greenlandic orthography.

References to figures, tables and papers – References to figures and tables in the text should have the form: Fig. 1, Figs 1–3, Table 3 or as (Smith 1969, fig. 3) when the reference is to a figure in a cited paper.

References to papers are given in the form Smith (1969) or (Smith 1969). Combined citations by different authors are separated by a semicolon; two or more papers by same author(s) are separated by commas. Citations are mentioned chronologically and then alphabetically. Use '*et al.*' for three or more authors, e.g. Smith *et al.* (1985).

Reference list

Use the following style:

Smith, A.A. 1989: Geology of the Bulbjerg Formation. Bulletin of the Geological Society of Denmark 38, 119–144. [Note that name of journal is given in full].

Smith, A.A., Jensen, B.B. & MacStuff, C.C. 1987: Sandstones of Denmark, 2nd edition, 533 pp. New York: Springer Verlag. [For more than 10 authors, use first author followed by *et al.*].

Smith, A.A., Jensen, B.B. & MacStuff, C.C. 1992: Characterization of Archean volcanic rocks. In: Hansen, D.D. *et al.* (eds): Geology of Greenland. Geological Survey of Denmark and Greenland Bulletin 40, 1397–1438. [More than three editors – therefore *et al.* form is used].

Sorting – Danish letters æ, ø and å (aa) are treated as ae, o and a (aa), respectively.

References are sorted by:

1: Alphabetically by the first author's surname
2: Papers by one author: two or more papers are arranged chronologically
3: Papers by two authors: alphabetically after second author's name. Two or more papers by the same two authors: chronologically.
4: Papers by three or more authors: chronologically. Papers from the same year are arranged alphabetically after second, third, etc.author's name.

Authors themselves are responsible for the accuracy and completeness of their references. If incorrect references are found, the manuscript will be returned to the author for complete rechecking. The reference list must include all, and only, the references cited in the paper (including figures, tables etc).

Illustrations

May be prepared in either black and white or colour. There is no colour charge. Horizontal illustrations are much to be preferred. Size of smallest letters in illustrations should not be less than 5.5 pt. Remember scale.

All figures (including photographs) should be submitted in electronic form ready for direct reproduction, i.e. having the dimensions of the final figure with a standard resolution of 300 dpi for photographs. Preferred formats are pdf, tiff and jpg.

Size – The width of figures must be 82 mm, 125 mm or 171 mm. Maximum height is 223 mm.

Captions – Captions to figures, tables and plates must be delivered on separate pages.

Proofs

Proofs – Authors receive page proofs of the article after technical set-up. The cost of any alterations against the final manuscript will be charged to the author.

Content, vol. 60

ISSN 1350-0150